DEVELOPMENT OF AND APPLICATION OF PLASMONIC NANOMATERIALS FOR MASS SPECTROMETRY BASED BIOSENSING

A Dissertation

by

ROBERTO CARLOS GAMEZ

Submitted to the Office of Graduate and Professional Studies of
Texas A&M University
in partial fulfillment of the requirements for the degree of

DOCTOR OF PHILOSOPHY

Chair of Committee,	David H. Russell
Committee Members,	James D. Batteas
	Jean-Philippe Pellois
	Emile A. Schweikert
Head of Department,	David H. Russell

May 2014

Major Subject: Chemistry

ABSTRACT

The use of nanomaterials for sensing and biological applications has recently gained interest owing to the unique physical, chemical and optical properties that arise when materials are reduced to the nanoscale. The unique optical properties exhibited by gold (Au) and silver (Ag) nanomaterials have made for versatile platforms in a wide range of applications including surface plasmon biosensing techniques and laser desorption/ionization mass spectrometry (LDI-MS). A primary driver for this work is the relative ease performing surface modifications to nanoparticles (NPs), which can be used to enhance the selectivity of ionization and/or facilitate analyte capture. The research presented here focuses on the development of AuNP and AgNP based biosensors for selective capture and ionization of low abundance compounds from complex mixtures and subsequent detection by LDI-MS and Matrix Assisted Laser Desorption Ionization-Mass Spectrometry (MALDI-MS).

First, a 'strategy' for selective capture and ionization of specific compound classes based on chemical derivatization of gold nanorods (AuNRs) and infrared laser desorption ionization (IR-LDI) is described. LDI is performed at near infrared wavelengths (1064 nm) that overlap with the longitudinal surface plasmon resonance (LSPR) mode of AuNRs which allows absorbed energy from the laser to facilitate the desorption and ionization of the analyte. Capture of hydrophobic species using surfactant coated AuNRs and subsequent detection by IR-LDI-MS was also demonstrated in these experiments.

Second, the fabrication of a label-free MS and optical detection based biosensor platform consisting of a phospholipid layer partially tethered to the surface of a gold nanorod for the detection of low abundance lipophilic analytes from complex mixtures is described. In these experiments, stable phospholipid capped AuNRs are produced by tethering some of the phospholipids to the surface of the AuNRs though a covalent, gold-thiol linkage. The effectiveness of the biosensor is demonstrated for the label-free detection of a membrane active lipophilic drug from aqueous solution and of a lipopeptide from fetal bovine serum.

Lastly, porous AgNP embedded thin films were fabricated by the sol-gel method and utilized as matrix-free LDI-MS biosensors applicable to several chemical classes. In these experiments, UV laser irradiation (337 nm) of the AgNP facilitates desorption and ionization of a number of peptides, triglycerides, and phospholipids. Preferential ionization of sterols from vesicles composed of olefinic phosphosphatidylcholines is also demonstrated.

DEDICATION

I would like to dedicate this dissertation to my family and friends who have supported me during my time away from home.

ACKNOWLEDGEMENTS

I would like to thank my committee chair, Dr. David H. Russell for giving me the opportunity to be a member of his research group, and for his support and guidance throughout my graduate studies. I would like to also thank my committee members, Dr. James D. Batteas, Dr. Jean-Philippe Pellois, and Dr. Emile A. Schweikert, for their useful discussions and insight which helped to significantly advance my research projects. I also thank Dr. Paul S. Cremer for many useful conversations and for allowing me to have access to his laboratory and instruments, without which, would have made completion of my research more difficult.

Thanks to past and current members of the Russell Research Group who helped to guide me in the right direction, namely, Dr. Edward T. Castellana, and Dr. Stephanie M. Cologna. Thanks also go to my friends and colleagues and the Chemistry department staff for their help with completing all the steps in the program. I also want to extend my gratitude to the Louis Stokes Alliances for Minority Participation Bridge to Doctorate program and the Texas A&M Graduate Diversity Fellowship program, which provided funding and support for a majority of my graduate career.

NOMENCLATURE

Au	Gold
Ag	Silver
NP(s)	Nanoparticle(s)
AgNP(s)	Silver Nanoparticle(s)
AuNP(s)	Gold Nanoparticle(s)
AuNR(s)	Gold Nanorod(s)
MS	Mass Spectrometry
LDI	Laser Desorption Ionization
MALDI	Matrix Assisted Laser Desorption Ionization
TEM	Transmission Electron Microscopy
FE-SEM	Field Emission Scanning Electron Microscopy
Uv-Vis	Ultraviolet Visible Spectroscopy
SPR	Surface Plasmon Resonance
LSPR	Longitudinal Surface Plasmon Resonance
m/z	Mass to charge ratio
CTAB	Cetyltrimethylammonium Bromide
SAM	Self Assembled Monolayer
AmB	Amphotericin B
XPS	X-ray Photoelectron Spectroscopy
TAG(s)	Triacylglyceride(s)

DIOS	Desorption Ionization On Porous Silicon
CHCA	α-Cyano-4-hydroxycinnamic acid
DHB	2,5-dihydroxybenzoic acid
DABA	Diaminobenzoic acid
DOPC	1-2,-dioleoyl-sn-glycero-3-phosphocholine
POPC	1-palmitoyl-2-oleoyl-sn-glycero-3-phosphocholine
DPPC	1,2-dipalmitoyl-sn-glycero-3-phosphocholine
DMPC	1,2-dimyristoyl-sn-glycero-3-phosphocholine
TEOS	tetraethyl orthosilicate
POPG	1-palmitoyl-2-oleoyl-sn-glycero-3-phosphoglycerol

TABLE OF CONTENTS

Page

LIST OF FIGURES

FIGURE Page

FIGURE Page

FIGURE Page

LIST OF TABLES

CHAPTER I

INTRODUCTION

Matrix-assisted laser desorption ionization mass spectrometry (MALDI-MS) has evolved as one of the most important "soft" ionization techniques for mass spectrometric analysis of polar, thermally labile molecules, especially peptides and proteins.[1-4] In these experiments, first described by Karas and Hillenkamp, an organic matrix facilitates desorption and ionization of non-volatile biomolecules resulting in analyte ions with low internal energies and thus less fragmentation during analysis.[2,5,6] A distinct analytical figure of merit associated with MALDI is its ability to ionize a broad range of compound classes present in chemical mixtures; however, there are cases where "ion suppression" limits the application of MALDI. Additionally, there are specific analyses where the general requirements of MALDI restrict its applications. Specifically, the matrix and analyte must (i) be miscible and (ii) must co-crystallize-, a process that is oftentimes achieved by trial and error.[7] Uniform co-crystallization of the analyte and the matrix within the dried spot is also a concern given that uneven crystallization leads to the formation of "hot spots" in the matrix film yielding inconsistent spectral reproducibility.[7,8] In addition, analysis of lower molecular weight compounds (<1000 *m/z*) is often complicated by significant background noise in the form of matrix clusters, which congest the low mass region of the spectra.[4,7] In an attempt to address some of these issues, alternative matrices for mass spectrometric analysis were investigated shortly after the initial description of the MALDI method. One of the most notable

methods was described by Tanaka *et al.* which employed cobalt nanoparticles suspended in glycerol to desorb and ionize large proteins and polymers up to mass-to-charge (*m/z*) of 100,000.[9] Sunner, *et al.* went on to demonstrate the effectiveness of graphite particles (2-150 μm) suspended in glycerol to produce signal for a number of peptides and proteins by laser desorption ionization.[10] The development of techniques stemming from MALDI has continued to progress and has evolved into the investigation of "matrix-free" platforms for laser desorption ionization mass spectrometry (LDI-MS). Suizdak and coworkers introduced a matrix free method, desorption ionization on porous silicon (DIOS) which employs chemical etching of a silicon wafer for production of a porous surface which analytes are spotted directly on for signal production. Significant advantages of DIOS include, low sensitivity, minimized sample preparation, and applicability for the analysis of small molecules since the platform produces little to no background noise in the low *m/z* region.[11-13] Derivatization of this porous silicon surface with a hydrophobic coating was also demonstrated to be useful for on-plate analyte enrichment of hydrophobic peptides.[14,15]

Recently, there has been a growing interest in the use of nanoparticles (NPs) and other novel "materials" as sensors for various classes of biomolecules. A primary driver for this work is the relative ease for performing surface modifications to NPs, which can be used to enhance the selectivity of ionization and/or facilitate analyte capture. Such modifications generally have minimal impact on the unique optical and physical properties of the NPs that are so well-suited for a number of biosensing techniques, including LDI-MS.[16-18] Recent applications utilizing gold (Au) and silver (Ag) NPs have

focused on monitoring shifts in the optical absorption spectra that occur upon changes in the local environment of the nanoparticles or for producing significant signal enhancements in Raman spectroscopy.[19-23] Biofunctionalized plasmonic nanoparticles have also been used to target and destroy cancer cells by a photothermal process. In these experiments, the NPs absorb laser irradiation, which results in significant temperature rises and ultimately cell death by disruption of the plasma membrane of the diseased cell.[24-29] It is this unique optical absorption and rapid temperature rise that makes NPs appealing for use as mass spectrometry platforms; as such properties could be exploited to desorb analytes coupled directly to the NP surface.

Several investigations in our lab have focused on the use of plasmonic NPs for a number of MS-based studies. Previously we showed that LDI ion yields from citrate-capped AuNP varied with NP size, and subsequent experiments demonstrated that the presence of both anions and cations also influenced the laser induced ion signals.[30,31] Surface modification of AuNPs with a self-assembled monolayer of 4-aminothiophenol (4-ATP) also proved useful in increasing ion yields, reducing the number of alkali metal adducts, and extending the useful analyte mass range.[18] By changing the composition of the NPs from Au to Ag, preferential ionization of olefins from mixtures was demonstrated owing to the unique coordination of Ag ions with double bonds of olefins.[32] The studies described here outline a number experiments aimed at further developing the use of nanoparticle based methods for utilization as mass spectrometry platforms. Specifically, the investigation of gold nanorods (AuNRs) as energy absorbers of near infrared laser irradiation (1064 nm) for LDI-MS is discussed.[16] Derivatization of

the AuNRs with stable lipid coatings for enrichment of membrane active and low abundance components in complex mixtures is also investigated.[17] Development of a silver nanoparticle embedded thin film platform for matrix free analysis of a number of biological compounds is also discussed herein.

Optical Absorption and Electronic Properties of Noble Metal Nanoparticles

The reduction of bulk noble metals to the nanoscale results in the emergence of unique physical, electronic and optical properties. For centuries, colloidal solutions of noble metal nanoparticles such as silver and gold have been used as colorants in glass and ceramic owing to the strong colors exhibited by the small metallic nanoparticles in solution. These colors are primarily caused by the surface plasmon resonances which result when coherent oscillations of the free electrons within the conduction band interact with an electromagnetic field. A schematic of this oscillation is demonstrated for a spherical nanoparticle in **Figure 1**, where the electric field from incoming light induces polarization of the free conduction electrons of the nanoparticle creating a charge separation between the free electrons and the ionic metal core. The electrons oscillate back and forth owing to a restoring Coloumbic force on the nanoparticle boundaries (surface) resulting in a dipole oscillation for a spherical nanoparticle in the simplest case.[33,34]

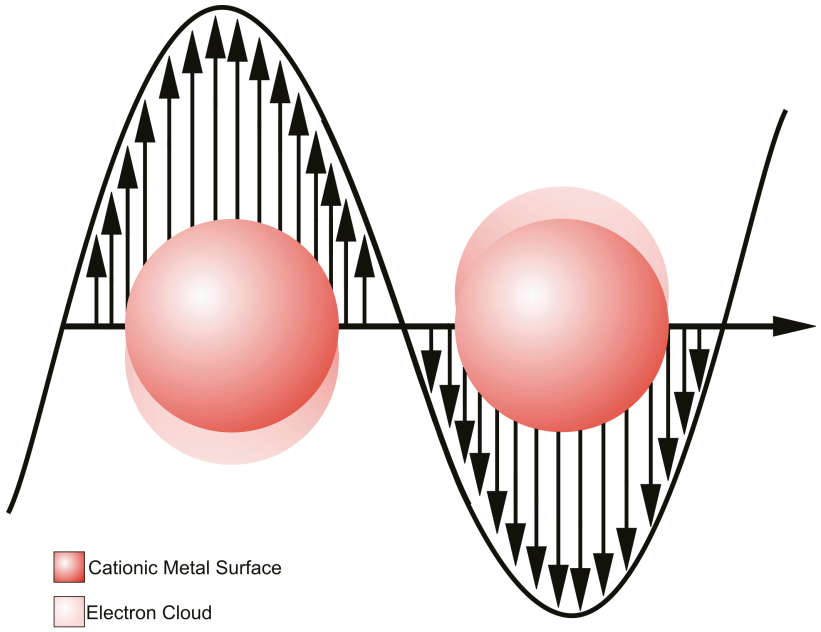

Figure 1. Schematic representation of polarized light interacting with a spherical gold nanoparticle and the resulting electron cloud displacement from the metallic core and subsequent oscillation.

Resonance of the frequency of the electromagnetic radiation with the electron motion results in a strong absorption band in the electromagnetic spectrum, which is around 520 nm in the case of spherical gold nanoparticles. In the case of gold nanorods, there are two directions along which polarization of the incident light can induce electron oscillation; the short and long axes of the nanorod, respectively. Excitation of the short axis, known as the transverse surface plasmon resonance, induces an oscillation similar to that of a spherical gold nanoparticle and gives rise to an absorption band around 520 nm which is not dependent on the aspect ratio of the nanorods. The aspect ratio is defined as the value of the long axis (length) divided by the short axis (width). Excitation along the long axis, known as longitudinal surface plasmon resonance, gives

rise to another lower energy absorption band which is dependent on the nanorod aspect ratio, and increases linearly to longer wavelengths with increasing aspect ratio. Schematics of the longitudinal and transverse surface plasmon resonances are demonstrated in **Figure 2**.

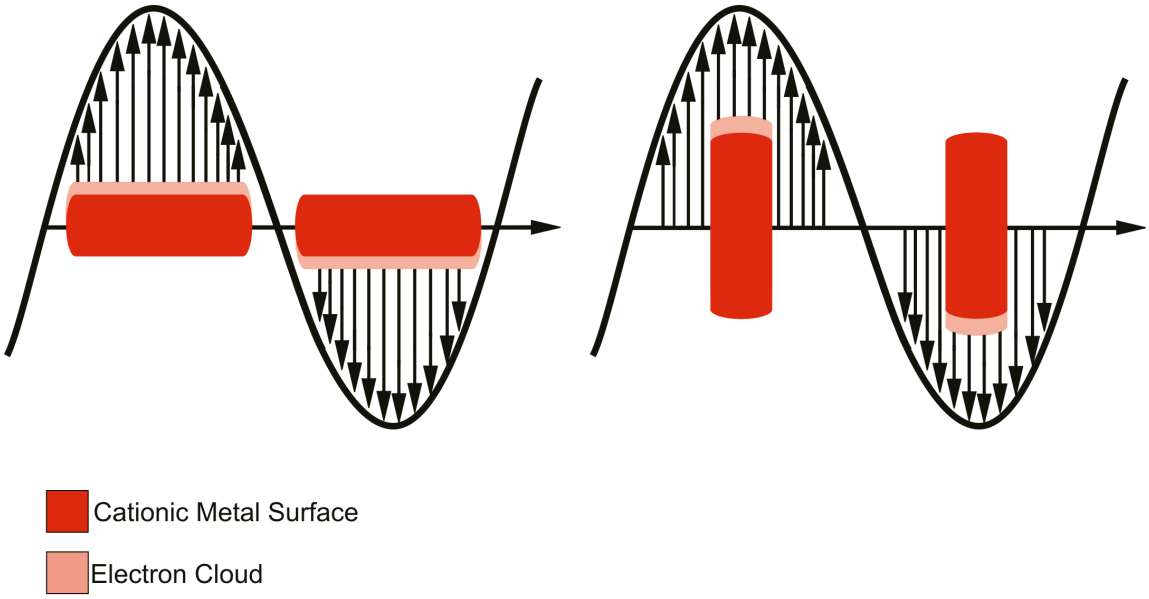

Figure 2. Schematic representation of polarized light interacting with the long axis (left) and short axis (right) of a gold nanorod and the resulting electronic cloud displacement and oscillation from the metallic core.

The description of the origin of the optical properties for spherical metal nanoparticles was first theorized by Mie in 1908 when he solved Maxwell's equations for the interaction of electromagnetic field with small spheres.[33] In order to explain the optical properties of gold nanorods, an extension of Mie theory was necessary and is described by Gans theory, which treats the nanorods as ellipsoids and predicts the

longitudinal absorption band.[35] Gans formula for randomly oriented ellipsoids in the dipole approximation follows:

$$\frac{\gamma}{N_p V} = \frac{2\pi\varepsilon_\alpha^{3/2}}{3\lambda}\sum_{j=A}^{C}\frac{\left(\frac{1}{P_j^2}\right)\varepsilon^2}{\left[\varepsilon_1 + \left(\frac{1-P_j}{P_j}\right)\varepsilon_\alpha\right]^2 + \varepsilon_2^2}$$

Where N represents the number of particles, V is the single particle volume, λ is the wavelength of light in a vacuum, ε_α is the dielectric constant of the surrounding medium, ε_1 is the real and ε_2 is the imaginary component of the refractive index of the nanoparticles. The geometrical factors of the ellipsoid are represented by P_j, and consider elongation along the three axes of the nanorod where A > B = C:

$$P_A = \frac{1-e^2}{e^2}\left[\frac{1}{2e}\ln\left(\frac{1+e}{1-e}\right) - 1\right]$$

$$P_B = P_C = \left(\frac{1-P_A}{2}\right)$$

$$e = \left(\frac{L^2 - d^2}{L^2}\right)^{1/2}$$

Using these equations and a fixed value of 4 for the medium dielectric constant, it was determined that the maximum of the longitudinal band red-shifted 150 nm when the aspect ratio was increased from 2.6 to 3.6 and continued to increase linearly with increasing aspect ratio. The longitudinal band is also sensitive to the medium dielectric constant, and has been the focus of biosensing applications since changes in the local of

the environment of induce a shift of the SPR wavelength.[36-38] Based on the tunability of the longitudinal band of gold nanorods to near IR wavelengths, we developed a method for utilization of gold nanorods as a mass spectrometry based platform.

Time of Flight Mass Spectrometry

One of the most common types of mass analyzers for MALDI applications is the Time of Flight (TOF) mass spectrometer.[39-41] In a typical TOF analysis, ions are first produced and accelerated by a potential difference *U*, between the sample plate and a grid or electrode to a given kinetic energy, *KE*. Thus, for an ion of a given charge state, *z*, and elementary charge, *e*:

$$KE = zeU$$

The ions, now with the same *KE*, then travel down a field free drift tube region where they will be separated based on their mass, *m*, due to their different velocities, *v*, based on the following equation:

$$\text{KE} = \tfrac{1}{2}\, mv^2, \text{ or } v = \sqrt{\frac{2E_k}{m}} = \sqrt{\frac{2zeU}{m}}$$

For a given flight time, t, and flight tube length, L:

$$t = L\sqrt{\frac{m}{2E_k}} = L\sqrt{\frac{m}{2zeU}}$$

This equation can then be inverted to find the mass to charge ratio:

$$\frac{m}{z} = 2eU\left(\frac{t}{L}\right)^2$$

One of the main sources of error involved in TOF instruments which can result in degrading the mass resolution, if not corrected, arises when ions of the same particular mass have different initial velocity distributions when extracted from the MALDI desorption plume.[42] A method known as delayed extraction was developed in order to account for this difference in initial velocities. In this method, the electric field between the sample and the first electrode is initially kept field-free and after a short delay (nanoseconds) is triggered to extract the ions into the flight tube. During the initial field-free delay time, ions traveling at a faster velocity will move closer to the first electrode than ions traveling at a slower velocity. Thus, when the electrode is turned on, the faster ions will experience less of a potential difference from the electric field and have less energy transferred to them than the slower ions. This results in the slower ions receiving more kinetic energy and eventually reaching the faster ions in the flight tube and eventually the detector.[41,43-46] A schematic for a delayed extraction time of flight mass spectrometer is displayed in **Figure 3**.

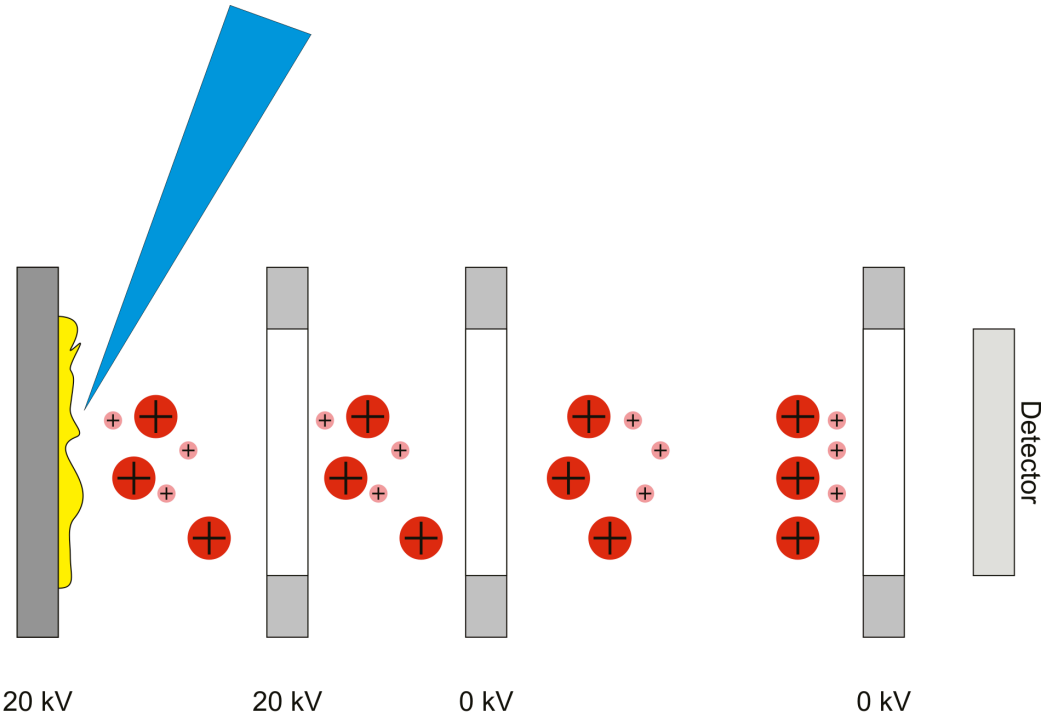

Figure 3. Delayed extraction set up. Laser pulses (blue) ionize analytes and after a short time delay are pulsed into a field free flight tube.

Another method to compensate for the initial energy distribution of ions is the electrostatic ion reflector, also known as a reflectron, which was initially proposed by Mamyrin in 1973.[47,48] The basic design of a reflectron time of flight instrument is shown in **Figure 4**.

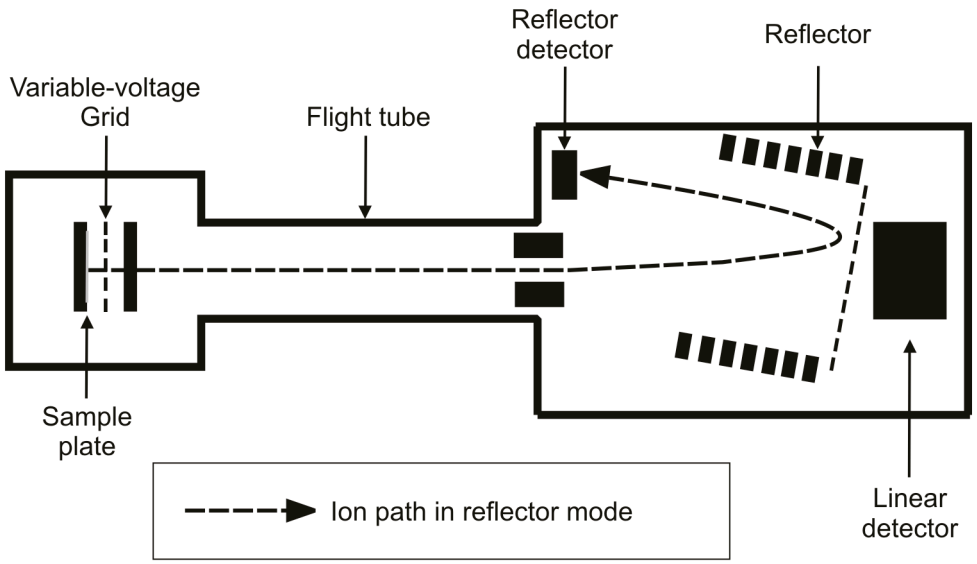

Figure 4. Schematic of a basic reflectron time of flight mass spectrometry instrument, showing the ion path in reflector mode.

In these instruments, the reflector is a series of ring electrodes, which serve to create an electric field, intended to slow down ions and deflect them back towards a detector. A common analogy used to portray the mechanism by which a reflectron operates is to compare it to a ball rolling up a hill. For example, if two ions of the same *m/z* had different initial kinetic energy distributions, those ions with a higher initial kinetic energy will arrive at the reflectron at an earlier time than the slower ions with lower initial kinetic energy. The higher energy ions will "roll higher up the hill" or penetrate the reflectron more deeply than the lower energy ions, thus increasing the amount of time spent in the reflectron. Through tuning of the reflectron voltages the higher energy and low energy ions can be focused to reach the detector at the same time, improving the resolving power of the instrument. While reflectron time of flight mass

spectrometry can improve mass resolution, it is not without disadvantages; sensitivity and mass range are limited in these instruments.

Sol-Gel Chemistry and Processing

The use of the sol-gel method for the production of materials has recently gained considerable interest owing to the versatility and simplicity of the method. As the name would imply, the sol-gel process is divided into two main components. In the most basic definition, a sol is a colloidal suspension of solid particles in a liquid and gelation is the process in which a free flowing solution is converted into a solid network; both of which are observed in some form during sol-gel processing. A typical sol-gel protocol for the production of materials is based on a series of reactions with a metal alkoxide precursor, which in the case of the experiments described in this dissertation, is strictly limited to the silicon based alkoxide, Tetraethyl orthosilicate (TEOS). In these experiments, by combining TEOS with 2-ethoxyethanol as a solvent, water to promote hydrolysis, and nitric acid as a catalyst, uniform colloidal particles comprising the sol, are formed by a series of hydrolysis and condensation reactions. Allowing the rate of condensation to continue promotes the eventual gelation of the sol, and the formation of a porous semi-solid network of small cross-linked solid particles enclosing the liquid solvent. Generally, the point of gelation can be controlled by modifying reaction conditions such as pH and can be marked by an increase in viscosity and elasticity of the solution.[49,50] As briefly mentioned before, there are two main reactions that occur for the formation of the

sol, hydrolysis and condensation of the TEOS precursor.[51-54] The following reactions occur with TEOS for the formation of the silica network:

Hydrolysis.

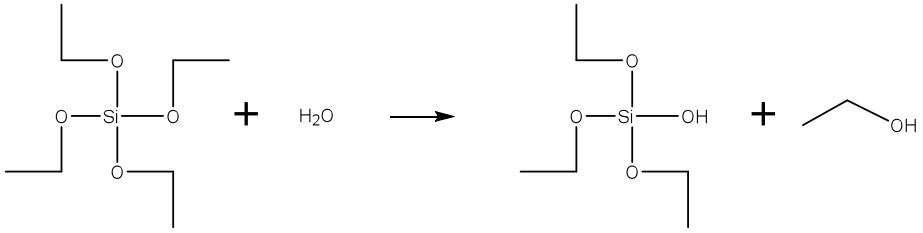

Condensation.

Water forming condensation:

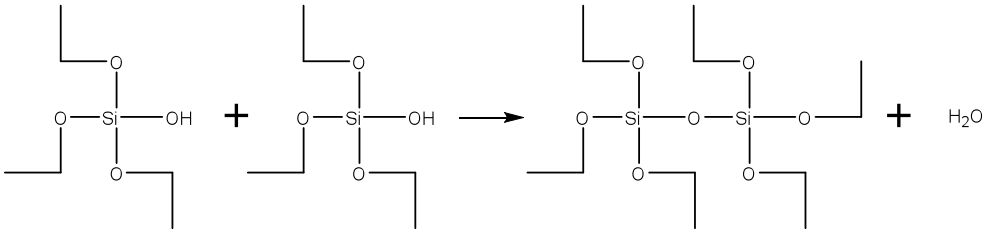

Alcohol forming condensation:

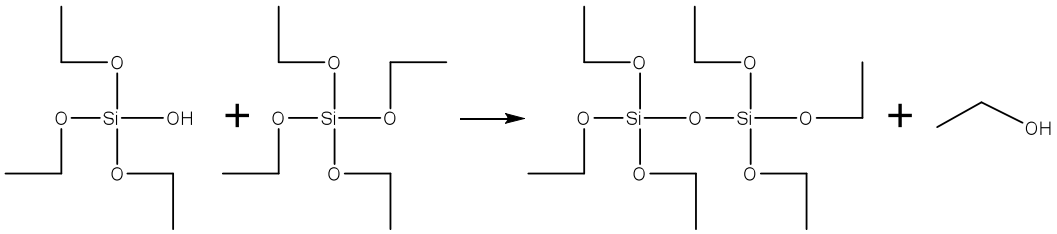

Hydrolysis in TEOS is significantly different from other metal based alkoxides, such as Zr and Ti, and requires for the addition of an acid or a base to catalyze the reaction. Whereas $Zr(OCH_2CH_3)_4$ and $Ti(OCH_2CH_3)_4$ carry a considerable partial

positive charge, ~0.65 and ~0.63, respectively; $Si(OCH_2CH_3)_4$ carries a reduced partial positive charge of ~0.32. For Zr and Ti alkoxides, nucleophilic attack by the oxygen atom of water, which carries a partial negative charge, occurs relatively quickly for hydrolysis.[54] TEOS, with its reduced partial charge on the Si atom hinders this nucleophilic attack, thus reducing the reaction kinetics and ultimately requiring an acid or a base catalyst for hydrolysis to occur in a moderate timeframe (minutes to hours). Although the final form of the hydrolyzed silica is greatly influenced by which type of catalyst is used, in these experiments, the sol-gel is processed solely by an acid based catalysis; hence the focus of this dissertation will be aimed towards discussion of the acid based catalysis of TEOS. In acid catalyzed reactions, protonation of an oxygen atom on the alkoxide group occurs to withdraw the electron density around the Si atom making it more electrophilic, thus making the Si atom more susceptible to attack by water. As a result, the positive charge of the protonated alkoxide group is slightly reduced making the alcohol (ethanol) a better leaving group.[53] The hydrolysis step in this system is a fast process and generally proceeds to completion before any significant amount of condensation occurs, making the condensation the rate-determining step. During condensation, a Si-O-Si network is formed and can follow two different mechanisms, (i) water forming condensation or (ii) alcohol forming condensation as demonstrated above. In water forming condensation, reaction occurs between two hydrolyzed TEOS molecules and a water molecule is formed as a result. The resulting water molecule can be used for further hydrolysis of another alkoxy group on a TEOS molecule, thus theoretically only a 2:1 mole ratio of water to TEOS are required for the

complete hydrolysis and condensation. In alcohol forming condensation, reaction occurs between a hydrolyzed TEOS molecule and an unhydrolyzed molecule, resulting in the formation of an ethanol molecule. These reactions continue and eventually give rise to the final form the three-dimensional silica network. Generally, it has been found that in acid catalyzed reactions, the silica particles tend to from linear chains with a low crosslink density whereas under basic conditions, more branching and a higher crosslink density is observed. While the pH of the sol-gel solution can greatly influence the final form of the sol-gel reaction, other factors such as polarity of the solvent, reaction molar ratios, and temperature can also be used to manipulate the final structure. In these experiments, the addition of a silver nitrate is incorporated into the sol-gel reaction for the eventual production of a silver nanoparticle impregnated thin film. Although the exact mechanism for the incorporation of the silver ions into the silica network is relatively unknown, previous researchers have considered that the silver ions are involved in complexes with the network and are reduced thermally after heat treating. Additionally, the polarizability of the Ag^+ ion has also been considered for the formation of a Si-O-Ag network produced by a cation exchange process with a hydrolyzed non-bridging oxygen atom as follows:

$$\equiv Si\text{-}OH + Ag^+ \rightarrow \equiv Si\text{-}O\text{-}Ag + H^+$$

The details of silver incorporation into the sol-gel system and characterization of the subsequent thin film are discussed in further detail in Chapter 4.[55,56]

CHAPTER II

LONGITUDINAL SURFACE PLASMON RESONANCE BASED GOLD NANOROD BIOSENSORS FOR MASS SPECTROMETRY·

Introduction

Nanomaterials are of great interest because their behavior differs from that of both bulk materials and individual atoms or molecules. For example, the optical, chemical, and physical properties of nanomaterials are governed by size, composition, and their assembly into structures on the nano- and micro- scale. It is the unique chemical and optical properties that make nanomaterials attractive for a wide array of applications such as surface enhanced vibrations spectroscopies,[57-61] targeted nanomedicines,[25,62,63] and laser desorption ionization mass spectrometry (LDI-MS).[64-75] Additionally, nanomaterials offer several distinct advantages over traditional platforms for LDI-MS including; simplified sample preparation, relatively uncomplicated low mass spectra (less noise from matrix clusters), and greater flexibility in the sample deposition conditions (e.g., pH, solvents, etc.). We have recently reported on the use of size-selected AuNPs for UV LDI-MS analysis of biomolecules,[31] functionalized AuNPs for increased analyte ionization efficiency as well as the useful analyte mass-to-charge (*m/z*) range,[18] and AgNPs for the selective desorption/ionization of olefins.[32] We have also published a detailed study exploring the effects of anions on analyte ion yields in

· Reprinted with permission from Castellana, E. T.; Gamez, R. C.; Gomez, M. E.; Russell, D. H. Longitudinal Surface Plasmon Resonance Based Gold Nanorod Biosensors For Mass Spectrometry *Langmuir* **2010**, 26, 6066.

LDI-MS from AuNPs.[30] Here, the optical properties of AuNRs in designing a versatile biosensor platform capable of producing analyte ions under near-IR laser irradiation are exploited.

The optical properties of AuNRs are one aspect that makes them ideal candidates for the development of biosensing and nano-medicine platforms. Such applications often make use of the longitudinal surface plasmon resonance (LSPR) adsorption mode of AuNRs, for either optical detection[20,21,76-78] or absorption-induced heating effects.[26,63,79-86] For nanomaterials, it is well established that the SPR absorption characteristics are highly dependent on particle size, shape, composition, and the dielectric constant of the surrounding medium.[34] Illumination of NPs with electromagnetic radiation at or near the SPR absorption band has been demonstrated to cause elevated temperatures and changes in particle size.[79,87,88] In fact, irradiation at the SPR wavelength has been used as a means of desorbing and ionizing metal atoms and clusters from the surface of thin metal films and other assemblies of nanomaterials.[89-92]

Recently, there have been several reports utilizing the SPR absorption of nanomaterials as a means to facilitate LDI of small molecules, peptides, polymers, and small proteins. These reports all focus on utilizing the SPR mode that occurs in the visible region of the electromagnetic spectra (~520 nm for Au). Visible SPR-LDI-MS has been demonstrated from thin metal films,[93-95] AuNPs,[96] Au-coated porous silicon,[70,97] and AuNR arrays.[70] Additionally, by mixing AuNPs with UV-absorbing organic matrices and irradiating sample spots at 532 nm, SPR induced MALDI-MS is possible.[98] In the case of AuNRs, the absorption mode at ~520 nm is referred to as the

transverse SPR mode; however, AuNRs also exhibit a LSPR absorption band. The LSPR absorption maximum is dependent on the aspect ratio of the AuNRs and can vary from visible wavelengths well into the IR region.

The primary goal of the study reported here has been to investigate the effectiveness of AuNRs as a LSPR active mass spectrometry based biosensor. Herein two methods are presented. In the first, analyte is mixed with 4-aminothiophenol-capped AuNRs, spotted onto a stainless steel sample plate, and dried under vacuum prior to LSPR-LDI-MS analysis. By irradiating gold nanorods near their LSPR absorbance wavelength does facilitate the LSPR-LDI of surface adsorbed biomolecules. The second method utilizes the surfactant, Cetyltrimethylammonium bromide (CTAB), which coats the AuNR as a capping layer as a result of the synthesis of the nanomaterial. The CTAB-capped AuNRs are incubated with an analyte capable of inserting itself into the CTAB layer surrounding the AuNRs. After centrifugal separation and rinsing, analytes adsorbed to the surface of the AuNRs are detected by irradiating the AuNRs near their LSPR absorbance wavelength.

Materials and Methods

The CTAB used in this study was purchased from Alpha Asar, product #A15235, Lot 10123898. The peptide Angiotensin II was acquired from American Peptide Company, Inc. (Sunnyvale, CA). All other chemicals used in this study were purchased from Sigma Aldrich, Inc. (St. Louis, MO), and all aqueous solutions were prepared using 18.2 MΩ/cm^2 water (NANOpure Ultrapure Water System, Barnstead, Dubuque, IA). To

synthesize the AuNRs, both a seed solution and a growth solution were prepared in 40 mL dram vials. All glassware was cleaned with aqua regia, extensively rinsed, and baked at 150ºC for 2 hours prior to use. *When working with aqua regia always wear protective clothing, goggles, gloves, lab coat and work in a clean well ventilated fume hood.* The seed solution consisted of 5.0 mL of 0.00050 M chloroauric acid ($HAuCl_4$) and 5.0 mL of 0.20 M CTAB. This solution was placed in a 27º C water bath and stirred at 1000 rpm. The seed particles were formed by the rapid addition of 0.60 mL of ice-cold 0.010 M sodium borohydride ($NaBH_4$). The resulting seed solution was stirred for 2 minutes and allowed to age for an additional 10 minutes prior to use. The growth solution was made by mixing: 25 μL of 0.040 M silver nitrate ($AgNO_3$), 5.0 mL of 0.20 M CTAB, 20 μL of 0.5 M sulfuric acid (H_2SO_4), 5.0 mL of 0.0010 M $HAuCl_4$, and 70 μL of 0.0788 M ascorbic acid. The resulting growth solution was gently mixed until the color changed from dark yellow to colorless. A 12 μL aliquot of the seed solution was added; the solution was gently mixed again, and incubated at 27º C. The final growth solution was aged for a minimum of 2 hours. During this time the color of the solution changed from clear to light peach. The AuNRs were characterized by Transmission Electron Microscopy (TEM) and UV-Vis spectroscopy.

For preparation of 4-aminothiophenol (4-ATP) functionalized AuNRs, a surface exchange protocol was developed. After synthesis of the AuNRs, excess CTAB was removed from 5.0 mL of the as prepared solution by two cycles of centrifugation at 4500 g for 30 minutes, removal of the supernatant and subsequent resuspension of the AuNRs. After the first centrifugation, the AuNRs were resuspended in 5.0 mL of water and after

the second centrifugation the AuNRs were resuspended in 5.0 mL of a 10 mM 4-ATP solution containing 0.1% trifluoroacetic acid (TFA). The resulting solution was sonicated at 50ºC for 30 minutes (VWR, bath sonicator, model B3500A-DTH). The AuNR/4-ATP mixture was then centrifuged at 4500 g, resuspended in 5.0 mL of 10 mM 4-ATP in 0.1% TFA and sonicated again at 50º C for 30 minutes. The excess 4-ATP and remaining CTAB was removed from the AuNR solution by two cycles of centrifugation at 4500 g. The final 4-ATP capped AuNR solution was prepared by removal of the supernatant, and resuspension in 2.5 mL of 0.1% TFA.

Exchange of CTAB with mPEG-thiol followed a similar exchange protocol as 4-ATP. Excess CTAB was removed from 5.0 mL of the as prepared AuNR solution by two cycles of centrifugation at 4500 g for 30 minutes, removal of the supernatant and subsequent resuspension of the AuNRs. After the first centrifugation, the AuNRs were resuspended in 5.0 mL of water and after the second centrifugation the AuNRs were resuspended in 5.0 mL of a 10 mM mPEG-thiol solution. The resulting solution was sonicated at 50ºC for 30 minutes (VWR, bath sonicator, model B3500A-DTH). The AuNR/mPEG-thiol mixture was then centrifuged at 4500 g, resuspended in 5.0 mL of 10 mM mPEG-thiol and sonicated again at 50º C for 30 minutes. The excess mPEG-thiol and remaining CTAB was removed from the AuNR solution by two cycles of centrifugation at 4500 g. The final mPEG-thiol capped AuNR solution was prepared by removal of the supernatant, and resuspension in 2.5 mL of 10mM mPEG-thiol solution.

The AuNRs were characterized by Transmission Electron Microscopy (TEM) and UV-Vis spectroscopy. All TEM images were obtained using a JEOL JEM-2010

TEM (Tokyo, Japan). Mass spectrometry data was acquired with a Voyager DE-STR MALDI-TOF-MS (Applied Biosystems, Foster City, CA). LSPR-LDI-MS was obtained using a Nd:YAG laser (1064 nm, Tempest-20, New Wave Research, Fremont, CA). UV LDI-MS (337 nm) was obtained using a nitrogen laser (model VSL-337ND-S, Thermo Laser Science, Franklin, MA). The laser energy was measured using a thermopile detector (model PS-310WB, Gentec Electro-Optics, Quebec, QC, Canada), a 200 Ohm DB-15 BNC adaptor (Gentec Electro-Optics), and a multimeter (model 8840A, Fluke, Everett, WA).

To demonstrate the use of AuNRs for the LSPR-LDI-MS of biologically relevant analytes, 4-ATP- or CTAB-capped AuNRs were mixed with the peptide Angiotensin II in ~1:500 molar ratio, and 2.0 μL aliquots of the mixture were spotted directly onto a stainless steel sample plate and dried under vacuum. LSPR-LDI-MS was carried out by irradiating the sample spot with 5-30 μJ/pulse of 1064 nm laser light.

Results and Discussion

We hypothesized that for a given AuNR aspect ratio, analytes adsorbed on the surface of the rods can be desorbed and ionized (e.g., proton capture, proton loss) under irradiation corresponding to the nanorods LSPR absorption wavelength. AuNRs are prepared using a modified version of the surfactant directed seed-mediated growth process.[99,100] Using this method, it is possible to synthesize AuNRs with a variety of aspect ratios simply by varying the reaction conditions (i.e., ratios of Au, Ag, or CTAB). The λ_{max} of the LSPR absorption in the AuNRs is directly proportional to the aspect ratio

of the AuNRs. By growing AuNRs to an aspect ratio of ~5:1 and replacing the CTAB with a self assembled monolayer (SAM), we were able to increase the wavelength of the LSPR absorption mode of the AuNRs so that they would absorb the 1064 nm emission of a Nd:YAG laser when dried in a sample spot. **Figure 5** contains UV-vis and TEM data of the AuNRs before and after replacing the CTAB with 4-ATP.

To demonstrate the use of gold nanorods for the LSPR-LDI-MS of biologically relevant analytes, 4-ATP- or CTAB-capped AuNRs were mixed with the peptide Angiotensin II in ~1:500 molar ratio, and 2.0 μL aliquots of the mixture were spotted directly onto a stainless steel sample plate and dried under vacuum. LSPR-LDI-MS was carried out by irradiating the sample spot with 5-30 μJ/pulse of 1064 nm laser light **(Figure 6)**. The laser beam was focused to a diameter of ~50 μm with an average laser energy of ~15 μJ/pulse; thus, the resulting laser fluence was estimated to be ~0.76 J/cm^2. From these values we estimate a rapid rise in AuNR temperature of at least several hundred degrees. Because the volume of the AuNRs will remain almost constant, this energy will be channeled internally into the reshaping and fragmentation of the AuNRs and externally into the LDI of analytes present at the surface of the AuNRs.[79,101,102] The LSPR-LDI mass spectra of the peptide Angiotensin II acquired using AuNRs and 1064 nm laser irradiation are shown in **Figure 7**.

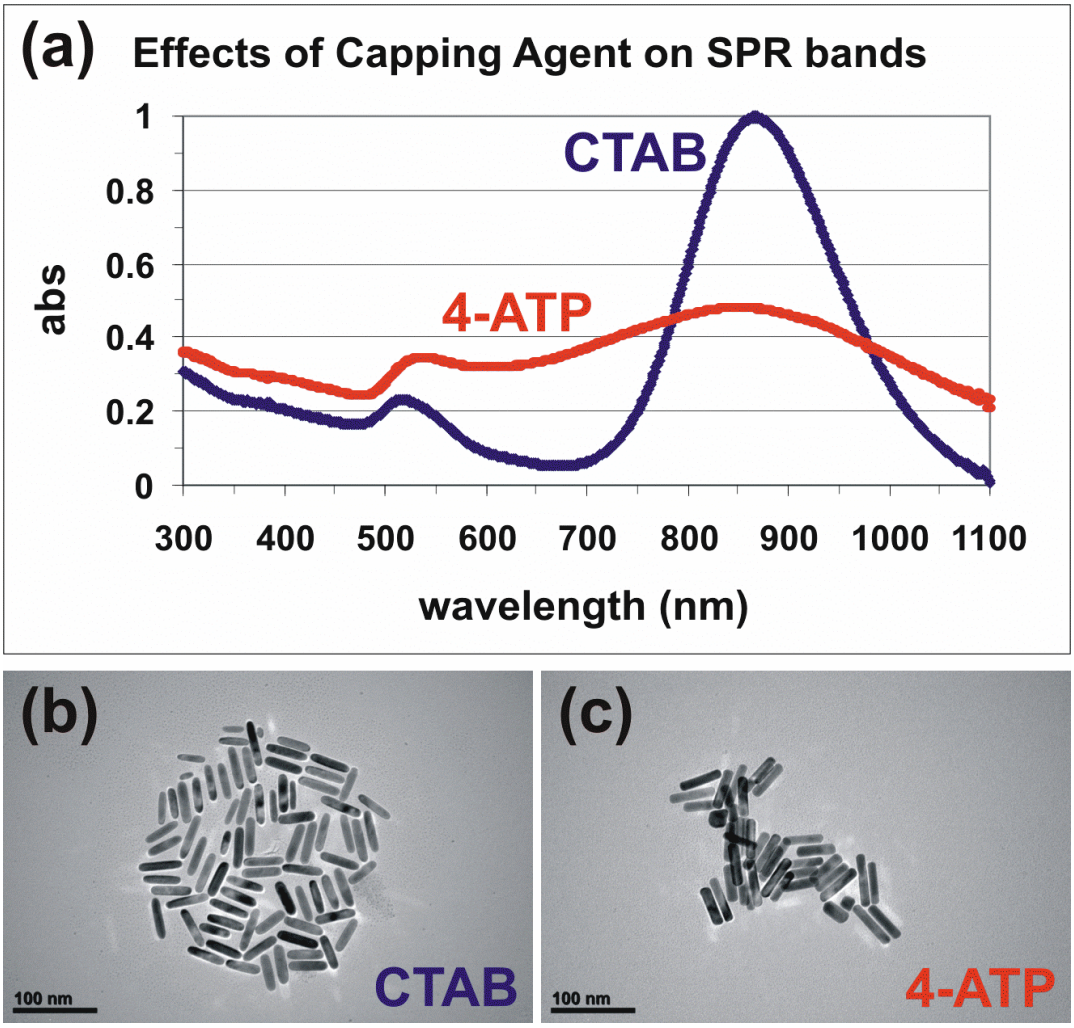

Figure 5. Absorbance spectra of (a) CTAB-capped AuNRs (blue) and 4-ATP-capped AuNRs (red) and TEM images of (b) CTAB-capped AuNRs and (c) 4-ATP-capped AuNRs.

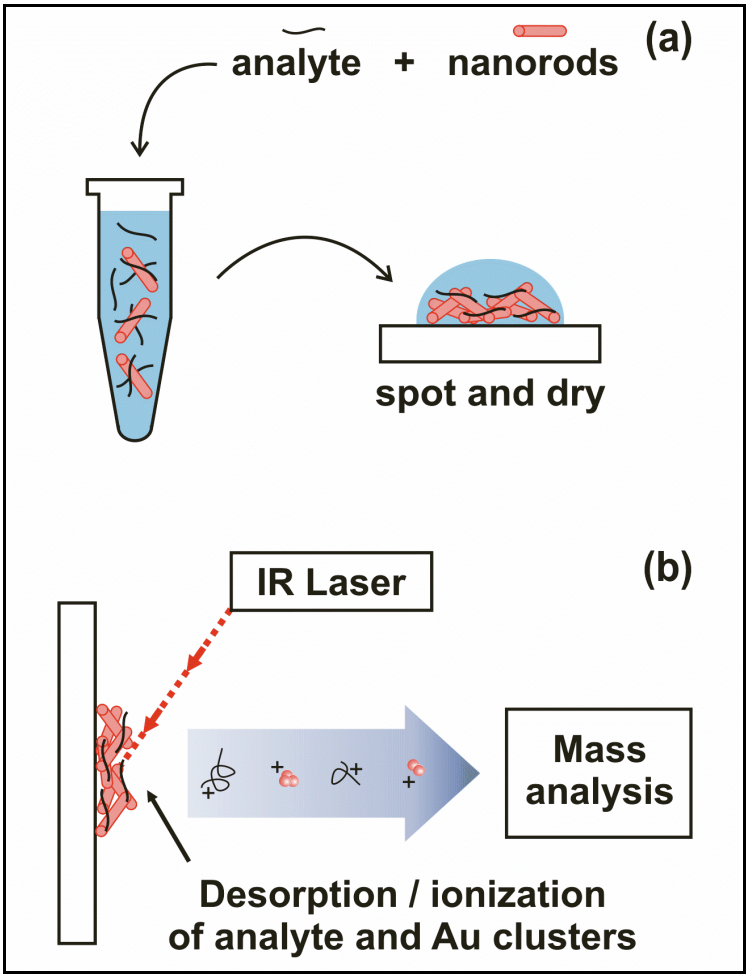

Figure 6. A schematic representation illustrating the use of AuNRs for LSPR-LDI-MS utilizing infrared laser irradiation. (a) Analyte is mixed with AuNRs in solution, spotted onto the sample plate, and dried prior to analysis. (b) Ions are produced by 1064 nm irradiation of a sample spot containing a mixture of AuNRs and analyte.

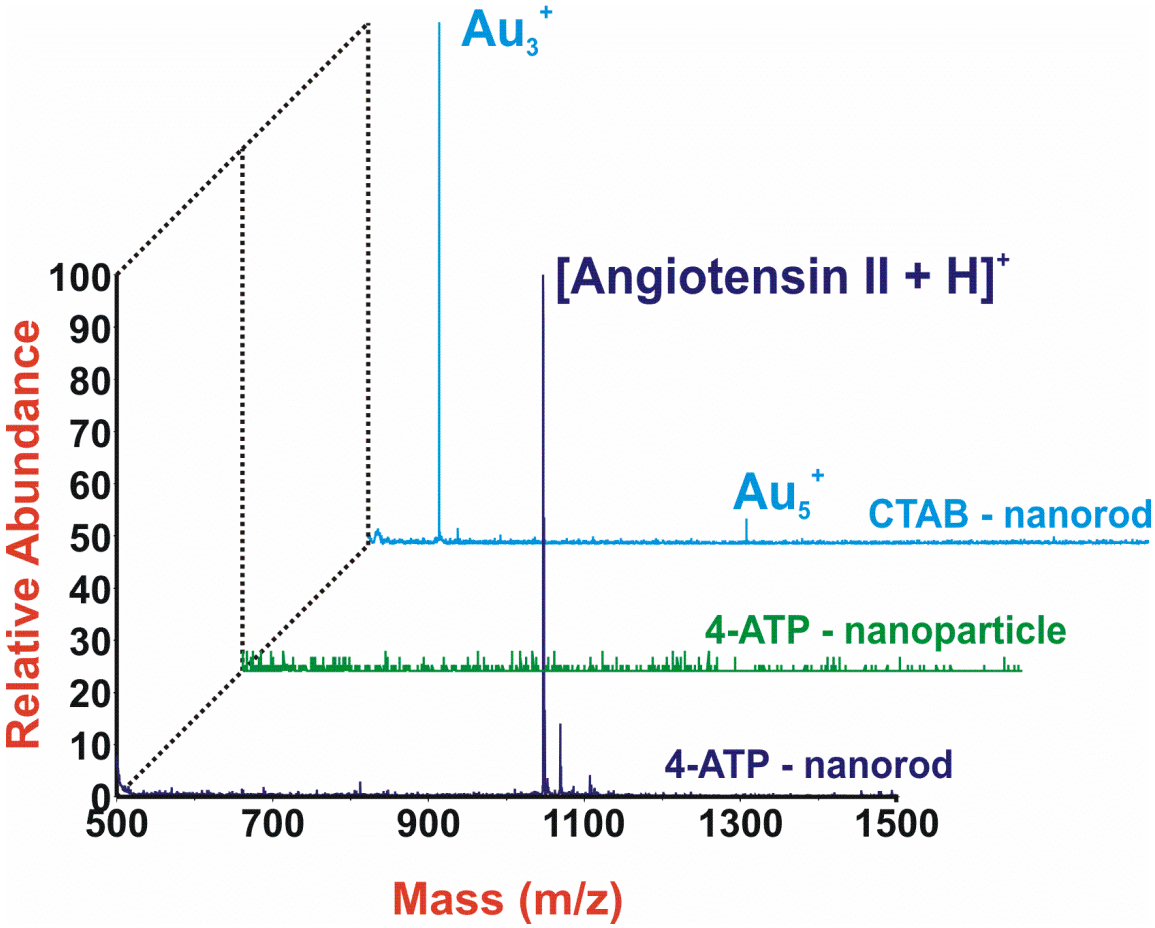

Figure 7. LSPR-LDI mass spectra of Angiotensin II (*m/z* = 1046.5) using 4-ATP capped AuNRs (dark blue), 4-ATP capped AuNPs (green), and CTAB-capped AuNRs (light blue).

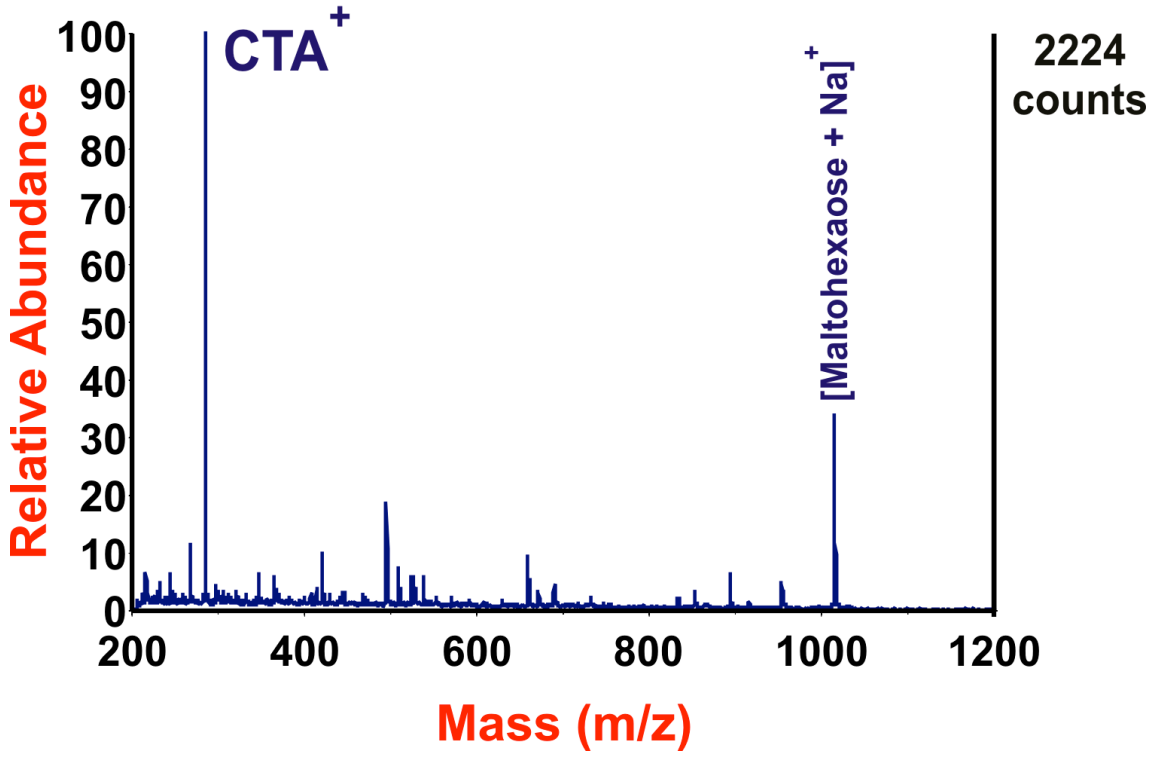

Figure 8. LSPR-LDI mass spectra of [Maltohexaose + Na]$^+$ (*m/z* = 1013.3) using 4-ATP capped AuNRs.

Note that peptide ions are only observed when the CTAB is replaced with a SAM of 4-ATP. Analyte ions are not observed from sample spots containing mixtures of 4-ATP-capped AuNP (no LSPR absorption) and peptide or from CTAB coated AuNRs (**Figure 7)**. Similar results are observed for the oligosaccharide maltohexaose **(Figure 8)**. The presence of CTAB on the surface of the nanorods can inhibit desorption and ionization of analyte by numerous mechanisms. We speculate that (i) the CTAB does not provide a sufficient proton source to ionize the peptide and (ii) the positively charged CTAB bilayer inhibits the peptide from adsorbing to the AuNR surface. Decoupling the peptide from the AuNR surface diminishes energy transfer from the AuNRs to the

peptide during the LDI event. In support of this argument note that previous work has demonstrated that when in solution the CTAB bilayer on the surface of AuNRs is a good thermal insulator relative to biopolymers.[103] If the thermal energy generated by the relaxation of the surface plasmons is confined to the AuNRs rather then being consumed by the process of analyte desorption and ionization, then we would expect to produce more gold cluster ions and less analyte ions during the LDI event. This result is readily observed in the mass spectrum **(Figure 7, light blue trace)** of CTAB capped AuNRs as $[Au_3]^+$ and $[Au_5]^+$ ions are the dominant signals. Additionally, cetyltrimethylammonium ions $[CTA]^+$ are observed in the low mass region of the spectrum of CTAB capped AuNRs, presumably because the $[CTA]^+$ exists as a preformed ion and is in direct contact with the surface of the AuNRs. We hypothesize that the laser energy being absorbed by the surface plasmons is transferred from the AuNRs to their surroundings is used for desorption of $[CTA]^+$ ions rather then the production and desorption of analyte ions.

The presence of a 4-ATP monolayer has the opposite effect. Under the mildly acidic conditions employed, the 4-ATP monolayer will be partially protonated. This allows the peptide to interact with the surface of the monolayer through hydrogen bonding and also provides a proton source to facilitate peptide ionization. We suspect that the shared proton can easily be transferred to the peptide during laser irradiation enhancing the peptide ion yield in this experiment. Since the peptide is adsorbed in close proximity to the AuNR surface, there will be sufficient energy transfer from the AuNRs to the peptide/4-ATP complex for desorption and ionization to occur. As shown in

Figure 7 (dark blue trace), abundant protonated peptide ions are observed, whereas gold cluster ions are not observed. This indicates that the 4-ATP monolayer allows energy transfer to the peptide rather than the formation of gold cluster ions. In the case of the spherical gold nanoparticles capped with 4-ATP, we would expect similar analyte-surface interactions and a sufficient proton source, however the spherical nanoparticles do not absorb at 1064 nm; thus, peptide ion signal is not observed (**Figure 7, green trace)**. It is apparent from the data shown in **Figure 7** that analytes can be desorbed and ionized using the LSPR absorption of gold nanorods when (i) there is sufficient optical absorption of the laser energy, (ii) the analyte is present at or very close to the surface of the AuNR, and (iii) sufficient energy is transferred from the AuNRs to the analyte, resulting in desorption and ionization.

Despite the fact that the CTAB bilayer surrounding the AuNRs inhibits the production of analyte ions in LSPR-LDI-MS, we set out to make use of the amphoteric nature of the surfactant. Previous studies have shown that hydrophobic molecules will partition into the CTAB bilayer surrounding AuNRs. On the basis of these experiments, we hypothesized that it should be possible to capture a hydrophobic analyte within the CTAB bilayer and subsequently detect it by LSPR-LDI-MS. To test our hypothesis, we demonstrate the capture of benzyldimethylhexadecylammonium chloride (BDAC). In the first, 1.0 mL of CTAB-capped AuNRs was centrifuged at 4500g and resuspended in 300 μL of water twice. A 100 μL aliquot of the twice resuspended AuNR solution was incubated in 1.0 mL of 5 μM BDAC for 30 minutes. Following incubation, the AuNRs were separated from the BDAC solution by centrifugation at 4500g, removal of the

supernatant, and resuspension in 1 mL of water. After a second centrifugation (4500g) and supernatant removal, the AuNRs were resuspended in 60 µL of water. A 1.0 µL aliquot of this solution was spotted onto a sample plate and dried under vacuum. Analysis reveals the successful capture of BDAC in the CTAB bilayer surrounding the nanorods and subsequent detection by LSPR-LDI-MS **(Figure 9)**. Control experiments attempting to capture BDAC with mPEG-capped AuNRs produced no discernible $[BDA]^+$ signals above the background **(Figure 10)** owing to the minimization of hydrophobic interactions between the AuNR surface and the target analyte.

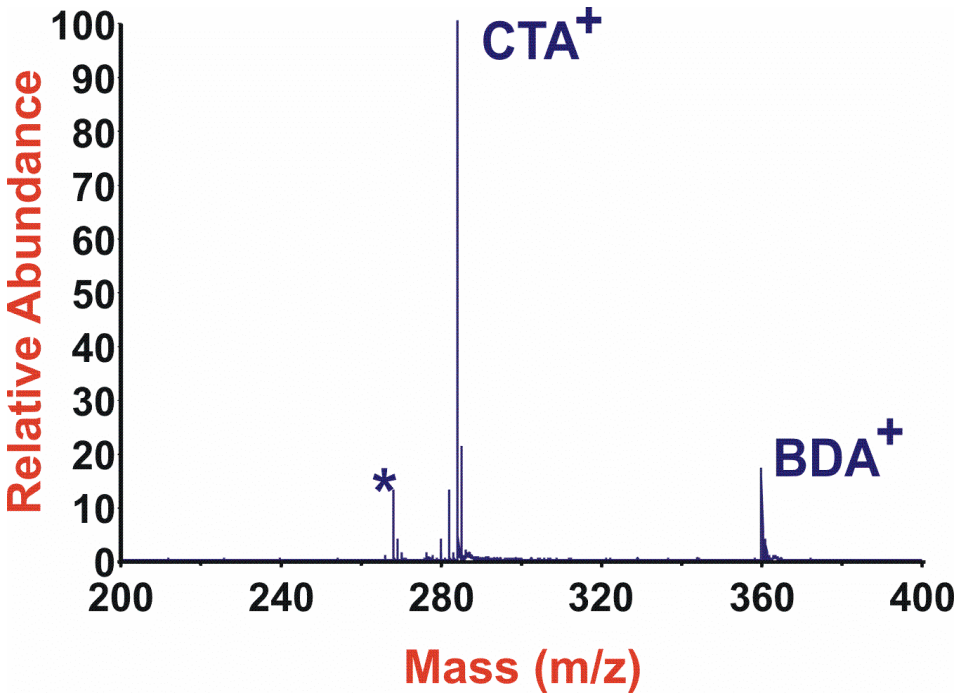

Figure 9. LSPR-LDI mass spectrum of benzyldimethylhexadecylammonium ion $[BDA]^+$ (*m/z* = 360.36) captured in the CTAB bilayer capping of the AuNRs. The peak labeled with an asterisk corresponds to a $[CTA]^+$ fragment ion.

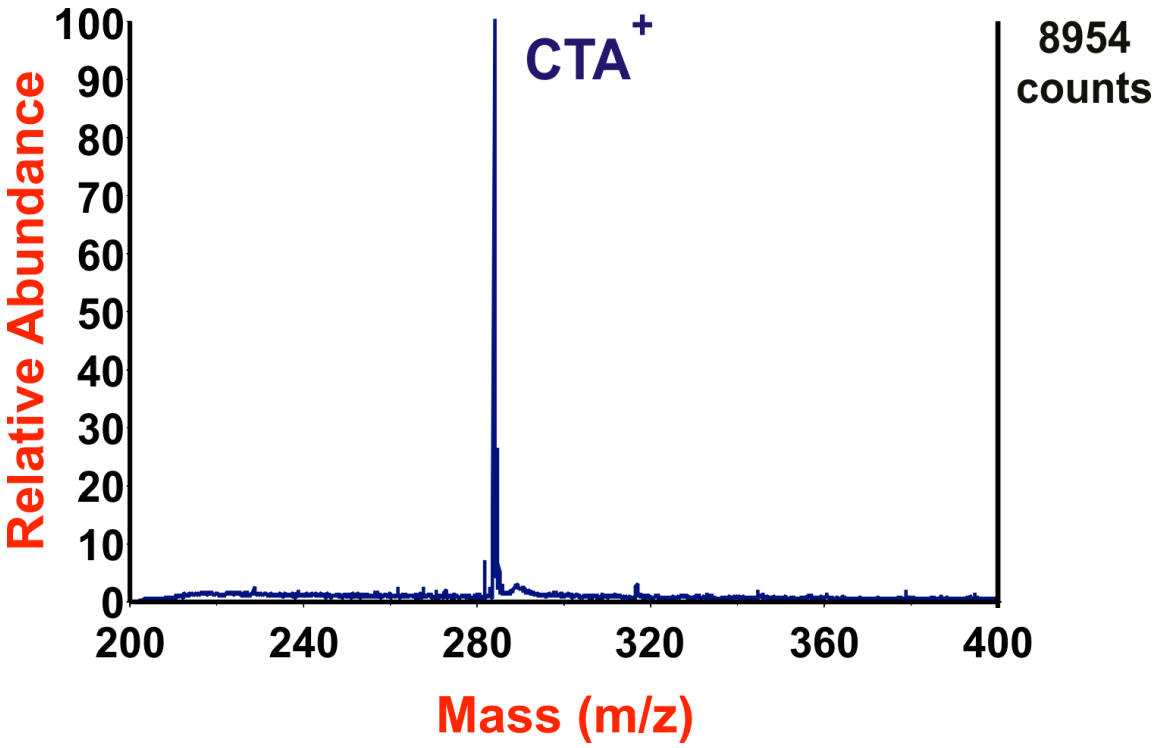

Figure 10. LSPR-LDI mass spectrum of an attempt to capture $[BDA]^+$ utilizing mPEG-thiol functionalized AuNR. Note: There is no signal at m/z = 360.36 corresponding to the $[BDA]^+$ owing to the absence of hydrophobic interaction between the target analyte and AuNR surface. $[CTA]^+$ exists as residual coating, however, its presence is not sufficient enough to warrant analyte capture.

Conclusions

The first examples of laser desorption/ionization of biomolecules using AuNRs irradiated with 1064 nm laser pulses are demonstrated. The laser energy deposited via the LSPR mode of the AuNRs is then used to desorb and ionize the analyte. LDI of synthesized AuNRs yields ions exclusively from the CTAB capping agent used in the NR synthesis thus, the CTAB must be replaced with a SAM in order for this method to produce detectable amounts of analyte ions. Because the analyte does not readily desorb and ionize without the use of an organic or nanomaterial matrix, even at 337 nm, we

conclude that the SAM is necessary to facilitate the LDI process for non "preformed" ion analytes. The SAM helps to facilitate LDI by assisting in the transfer of a proton to the analyte and/or sequestering the analyte in close proximity of the AuNR surface. Conversely, the CTAB capping agent has little or no ability to transfer a proton and may insulate the analyte from the energy transfer process from the AuNRs during LDI. We are currently designing experiments to further investigate our model for analyte LDI from the surface of AuNRs and nanomaterials in general.

The utility of AuNRs as an analyte capture platform is also investigated. Making use of the readily prepared nanorods, we have demonstrated the capture of an analyte that exists as a "preformed ion" and has an affinity for the CTAB on the surface of the nanorods. The analyte BDAC was sequestered and concentrated by the CTAB-capped AuNRs and subsequently detected by LSPR-LDI-MS. Conversely, AuNRs that were functionalized with a SAM of mPEG thiol exhibited no capture capabilities. These experiments demonstrate the feasibility of tailoring the surface chemistry of the AuNR platform to afford analyte capture and MS detection from complex samples. This strategy has potential for applications in biomarker screening to capture and identify unknown analytes present in low abundances from complex biological fluids.

CHAPTER III

LABEL-FREE BIOSENSING WITH LIPID FUNCTIONALIZED GOLD NANORODS[·]

Introduction

Nanomaterials offer versatile platforms for development of analyte capture and bioanalytical sensor platforms owing to their unique optical and physical properties.[104-107] Additionally, the high surface area combined with the capacity to precisely control the surface chemistry gives nanomaterials an inherent advantage when employed in capture or separation techniques. Identification of lipophilic analytes is important in a wide range of fields including: pharmacokinetics,[108] food safety,[109] lipidomics,[110,111] and biomarker screening.[112,113] Therefore, a biosensor platform capable of selectively targeting lipophilic analytes from complex solutions for rapid detection would be widely applicable. Gold nanorods (AuNRs) have rapidly become powerful base platforms for development of optical biosensors,[37,112,114-116] nanomedicines,[26,117] and gene delivery.[118-120] In previous work we demonstrated the unique capabilities of AuNRs for the infrared laser desorption/ionization (IR-LDI-MS) of various biomolecules for MS analysis.[16] Recently, several reports have focused on the combination of lipids and nanomaterials for a handful of bioanalytical applications. To date there are limited numbers of methods for producing lipid capped AuNRs.[118,121-123] The general procedure involves replacing

[·] Reprinted with permission from Castellana, E. T.; Gamez, R. C.; Russell, D. H. Label-Free Biosensing with Lipid-Functionalized Gold Nanorods. *Journal of the American Chemical Society* **2011**, *133*, 4182. Copyright 2011 American Chemical Society.

the cationic surfactant cetrimonium bromide (CTAB), which is necessary to grow the AuNRs, with lipids. The majority of these methods rely on the interaction of the quaternary amine of phosphatidylcholine headgroup, which is similar to CTAB, with the surface of the AuNRs. This weak interaction allows for a lipid bilayer to form around the AuNR through a self-assembly process.[121] However, for utility in our experiments, the weak interaction of the chemisorbed lipids is not strong enough to form a stable lipid bilayer that can withstand multiple cycles of centrifugation. That is, once excess lipid is removed from solution the lipid capped AuNRs begin to aggregate; a trend that also occurs when excess CTAB is removed from solution of CTAB capped AuNRs. To circumvent this problem, we have developed a method of producing stable lipid capped AuNRs by tethering some of the lipids to the AuNR through a thiol gold linkage. Here, we report a label-free mass spectrometry (MS) based biosensor platform for the detection of low abundance lipophilic analytes from complex mixtures.

Materials and Methods

The CTAB used in this study was purchased from Alpha Asar, product #A15235, Lot #10123898. Chloroauric acid, sodium borohydride, ascorbic acid, and silver nitrate were purchased from Sigma Aldrich, Inc. (USA), and all aqueous solutions were made using 18.2 MΩ/cm^2 water (NANOpure Ultrapure Water System, Barnstead, Dubuque, IA). 1,2-dipalmitoyl-sn-glycero-3-phosphocholine (DPPC), 1-palmitoyl-2-oleoyl-sn-glycero-3-phosphoglycerol (POPG) and 1,2-Dipalmitoyl-sn-Glycero-3-Phosphothioethanol (DPPTE) in chloroform were purchased from Avanti Polar Lipids.

Lipopeptide (Myristoyl-Lys-Arg-Thr-Leu-Arg) was purchased from American Peptide Co., Inc. (Sunnyvale, CA) and fetal bovine serum was purchased from Sigma Aldrich, Inc. (USA).

To synthesize the AuNRs, both a seed solution and a growth solution were prepared in 40 mL dram vials. All glassware was cleaned with aqua regia, extensively rinsed, and baked at 150ºC for 2 hours prior to use. *When working with aqua regia always wear protective clothing, goggles, gloves, lab coat and work in a clean well ventilated fume hood.* The seed solution consisted of 5.0 mL of 0.00050 M Chloroauric acid ($HAuCl_4$) and 5.0 mL of 0.20 M CTAB. This solution was placed in a 27º C water bath and stirred at 1000 rpm. The seed particles were formed by the rapid addition of 0.60 mL of ice-cold 0.010 M sodium borohydride ($NaBH_4$). The resulting seed solution was stirred for 2 minutes and allowed to age for an additional 10 minutes prior to use. The growth solution was made by mixing: 25 μL of 0.040 M silver nitrate ($AgNO_3$), 5.0 mL of 0.20 M CTAB, 20 μL of 0.5 M sulfuric acid (H_2SO_4), 5.0 mL of 0.0010 M $HAuCl_4$, and 70 μL of 0.0788 M ascorbic acid. The resulting growth solution was gently mixed until the color changed from dark yellow to colorless. A 12 μL aliquot of the seed solution was added; the solution was gently mixed again, and incubated at 27º C. The final growth solution was aged for a minimum of 2 hours. During this time the color of the solution changed from clear to light peach. The AuNRs were characterized by Transmission Electron Microscopy (TEM) and UV-Vis spectroscopy.

To prepare the vesicles, appropriate amounts of lipids ($3.07x10^{-5}$ mol DPPC and $3.42x10^{-6}$ mol DPPTE) or ($2.92\ 07x10^{-6}$ mol POPG and $3.42x10^{-6}$ mol DPPTE) were

mixed, dried under a stream of nitrogen, and desiccated under vacuum for ~3 hours. After desiccation, lipids were rehydrated in 5.0 mL of water and sonicated for ~20 minutes to ensure the lipids were fully dissolved. The solution was then subjected to 10 freeze thaw cycles by alternating between immersions in liquid nitrogen followed by immersion in a 25ºC water bath. Next, the lipid solution was extruded 10 times through 100 nm polycarbonate pore size filters.

After synthesis of the gold nanorods, excess CTAB was removed from 10 mL of the as prepared solution by two cycles of centrifugation at 4500 g for 20 minutes, removal of the supernatant and subsequent resuspension of the nanorods. Following the first centrifugation, the nanorods were resuspended in 5.0 mL of a 10-fold dilution of the lipid vesicle preparation. After a second centrifugation and resuspension in an additional 5.0 mL of a 10-fold dilution of the lipid vesicles, the resulting solution was sonicated at 50º C for 30 minutes (VWR, bath sonicator, model B3500A-DTH). The lipid nanorod mixture was then centrifuged at 4500 g for 20 minutes, resuspended in 5.0 mL of 10-fold dilution of lipid vesicles and sonicated again at 50º C for 70 minutes. This lipid nanorod mixture was then allowed to cool to room temperature then stored at 4º C.

For the capture experiment, 1.0 mL of the prepared lipid nanorods was used. The excess lipid vesicles were removed from the nanorod solution by two cycles of centrifugation at 3000 g, removal of the supernatant and resuspension in water. After the second cycle of centrifugation, the solution was concentrated to 200 μL. A 100 μL aliquot of the twice-centrifuged lipid nanorod solution was incubated with 500 μL of a 1.0 μM Amphotericin B (AmB) solution for 30 minutes at room temperature. Following

incubation, the nanorods were separated from the AmB solution by centrifugation at 3000 g, removal of the supernatant and resuspension in 600 μL of water. After a second centrifugation (3000 g), and removal of the supernatant, the nanorods were resuspended in 40 μL of water. This capture solution was mixed with 2,5-dihydroxybenzoic acid (DHB), and a 1.0 mg/mL sodium chloride (NaCl) solution, in a 4:2:1 ratio, respectively. A 1.0 μL aliquot was spotted onto the sample plate and dried under vacuum for MS analysis. MALDI-MS was acquired at laser fluence just above the threshold required for desorption-ionization.

For capture of a target lipopeptide from a complex mixture, fetal bovine serum, lipid capped nanorods were prepared for the capture experiment in an identical method as previously stated. A 100 μL aliquot of the twice-centrifuged nanorod solution was incubated with 500 μL of an 11 nM lipopeptide in a 3.0 mg/mL fetal bovine serum solution for 20 minutes at room temperature. Following incubation, the nanorods were separated from the serum solution by centrifugation at 3000 g, removal of the supernatant and resuspension in 600 μL of water. After a second centrifugation (3000 g), and removal of the supernatant, the nanorods were resuspended in 40 μL of water. For MALDI analysis, a 1.0 μL aliquot of the capture solution containing the lipid capped AuNRs was spotted onto a stainless steel MALDI plate and dried under vacuum. This process was repeated until a total of 5.0 μL was deposited in the same spot. Finally, 1.0 μL of α-Cyano-4-hydroxycinnamic acid (CHCA) was spotted over the dried sample spot and MALDI-MS data was acquired. MALDI-MS was acquired at laser fluence just above the threshold required for desorption-ionization.

Results and Discussion

The lipid capped AuNRs were characterized by UV-visible spectroscopy **(Figure 11)**, MALDI-MS **(Figure 12)**, and transmission electron microscopy **(Figure 13)**. Analysis of TEM images provides evidence that the lipid capping layer protects the AuNRs during production of the biosensor and after multiple cycles of centrifugation and resuspension. TEM images also reveal that the lipids protect the integrity of the AuNRs and prevent aggregation during deployment in analyte capture experiments. Additionally, the longitudinal surface plasmon resonance peak (~850 nm) and the MALDI mass spectra of the lipid capped AuNRs remains unchanged after several cycles of centrifugation and resuspension **(Figure 14)**. This suggests that the tethered lipid capping is both stable and provides ample protection of the AuNRs against aggregation during processing.

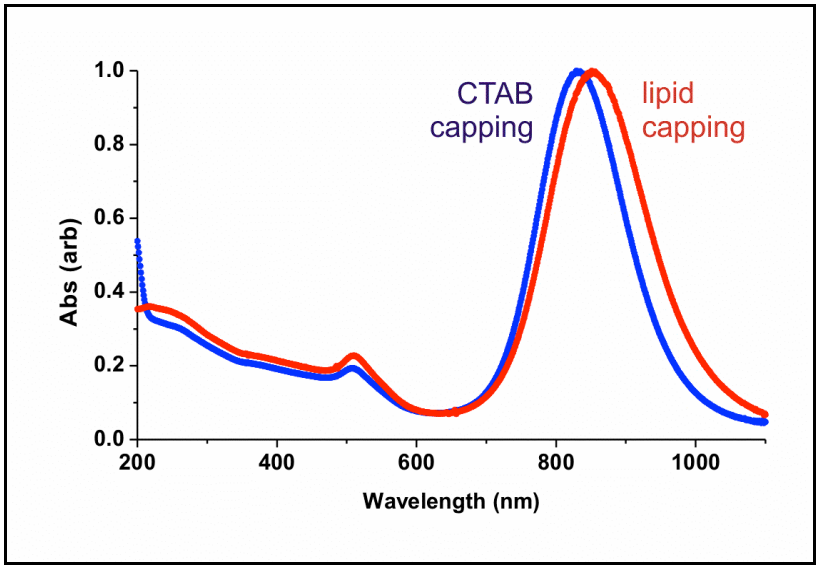

Figure 11. UV-vis spectra of CTAB capped AuNRs (blue) and lipid capped AuNRs (red).

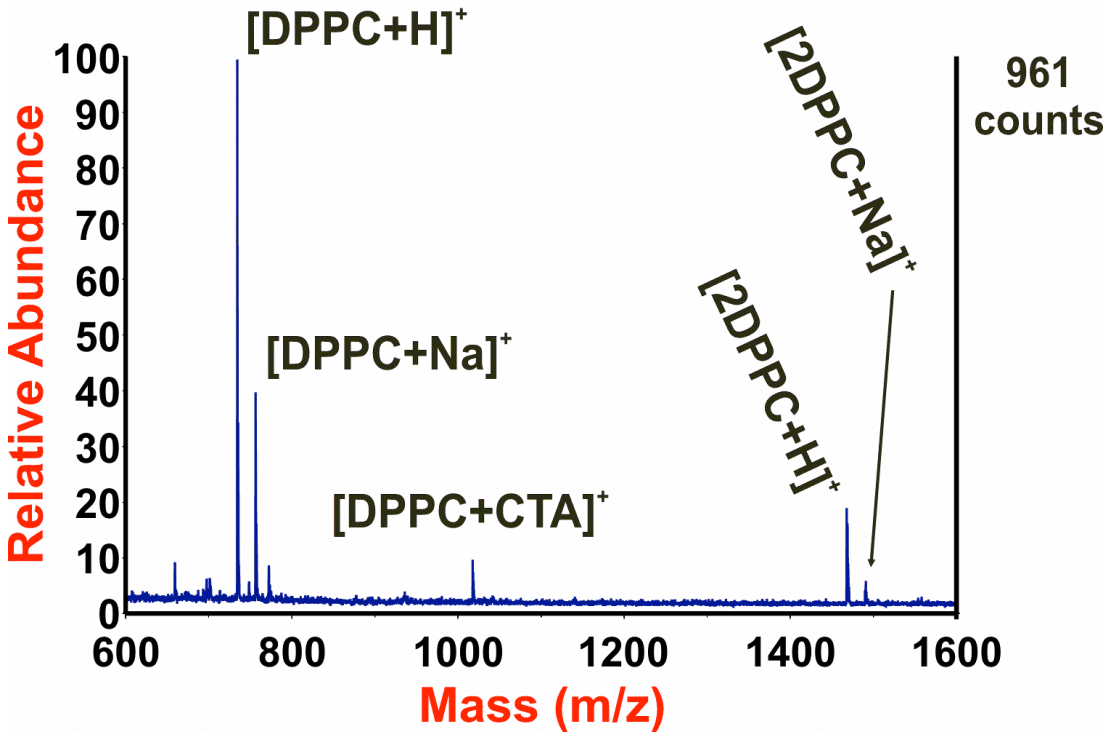

Figure 12. MALDI mass spectrum of lipid capped AuNRs before employment as affinity probes for capture experimental.

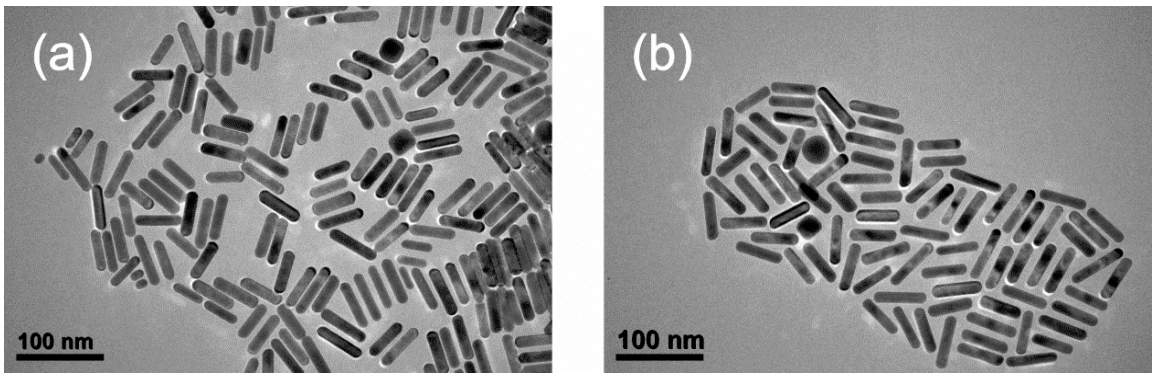

Figure 13. TEM images of (a) CTAB functionalized AuNRs and (b) lipid functionalized AuNRs.

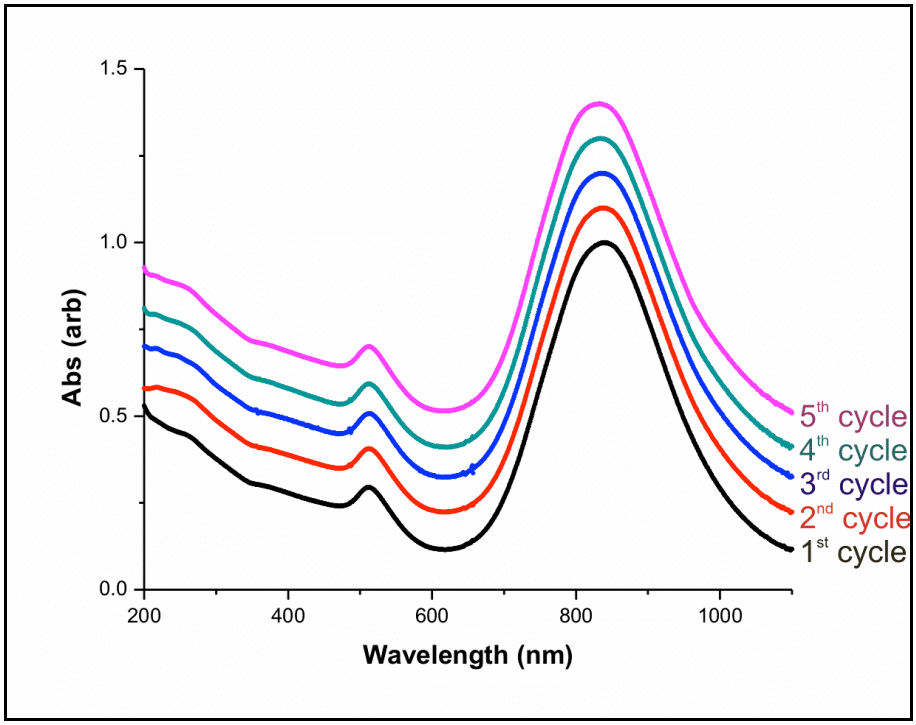

Figure 14. UV-vis spectra after multiple cycles of centrifugation and resuspension of the lipid capped AuNRs in water. Note: each data set is normalized to 1.0 and offset by 0.1 on the y-axis for clarity.

Many drugs function through interactions with cellular membranes. These interactions include processes such as targeting cell surface receptors,[124,125] disrupting cell membranes,[126-128] and traversing the cell membrane. Amphotericin B (AmB), an antifungal drug, whose mechanism of action involves formation of pores by inserting into and disrupting cellular membranes, makes it an ideal candidate to demonstrate capture of cell membrane active drugs in the lipid capped AuNRs. Additionally, AmB exhibits optical absorption in the UV-visible region owing to its highly conjugated structure, thus allowing optical confirmation of its capture by the lipid capped AuNRs.

Capture experiments were performed by incubating lipid capped AuNRs in 0.5 mL of an aqueous 1.0 μM AmB solution for 20 minutes. Following incubation, the AmB-lipid capped AuNR complex was separated from the solution by centrifugation, washed twice with water and resuspended. The final AmB-lipid capped AuNR complex was concentrated to 40 μL prior to analysis by MALDI-MS and an aliquot was re-diluted for UV-vis spectroscopy. **Figure 15** contains the optical absorption spectra of the lipid capped AuNRs (red trace), a 10 μM AmB solution (green trace), and of the AmB lipid capped AuNR complex (blue trace) spectra. Successful capture of the AmB by the lipid capped AuNRs is confirmed by the presence of AmB's optical signature observed in the 300-500 nm region of the absorption spectrum. Owing to the sensitivity of the SPR band to the dielectric constant of the surrounding medium, the local environment change resulting from the insertion of the AmB into the lipid coating of the AuNRs induces a perturbation in the longitudinal surface plasmon resonance band of the capture experiment which is also observed in the absorption spectrum.

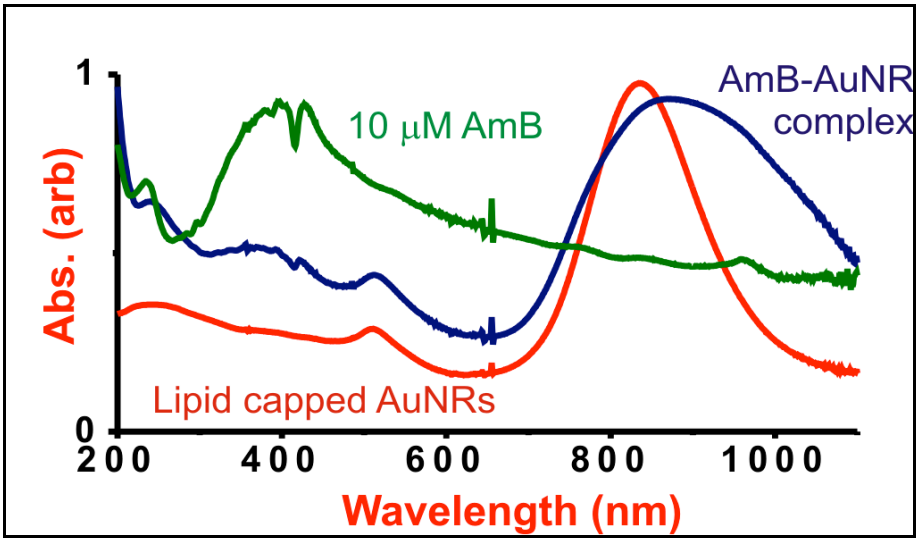

Figure 15. UV-vis spectra of the lipid capped AuNRs (red), a 10 μM solution of AmB (green) and lipid capped AuNRs after capture of AmB from solution (dark blue). Distinct UV-vis spectra are observed for both the lipid capped AuNRs, and the AmB. In the procedure where the AmB is captured by the AuNRs, a combination of each of the individual spectra is observed.

The concentrated AmB-lipid capped AuNR complex was mixed with the organic matrix 2,5-dihydroxybenzoic acid (DHB) prior to MALDI-MS analysis. As a control, a mixture of the capture solution (1.0 μM AmB) and lipid capped AuNRs was mixed together with DHB without incubation or centrifugation. By MALDI-MS, we are only able to observe the AmB following its capture and concentration by the lipid capped AuNRs **(Figure 16)**. No AmB signal is observed from the control experiment **(Figure 17)**. Also observed in both mass spectra **(Figures 16 and 17)** are peaks corresponding to the lipid 1,2-dipalmitoyl-sn-glycero-3-phosphocholine (DPPC), a DPPC dimer, and a complex between a DPPC molecule and a CTAB molecule. It is also important to note

that AmB was not detected by direct MALDI-MS analysis of the 1.0 μM AmB capture solution **(Figure 18)**.

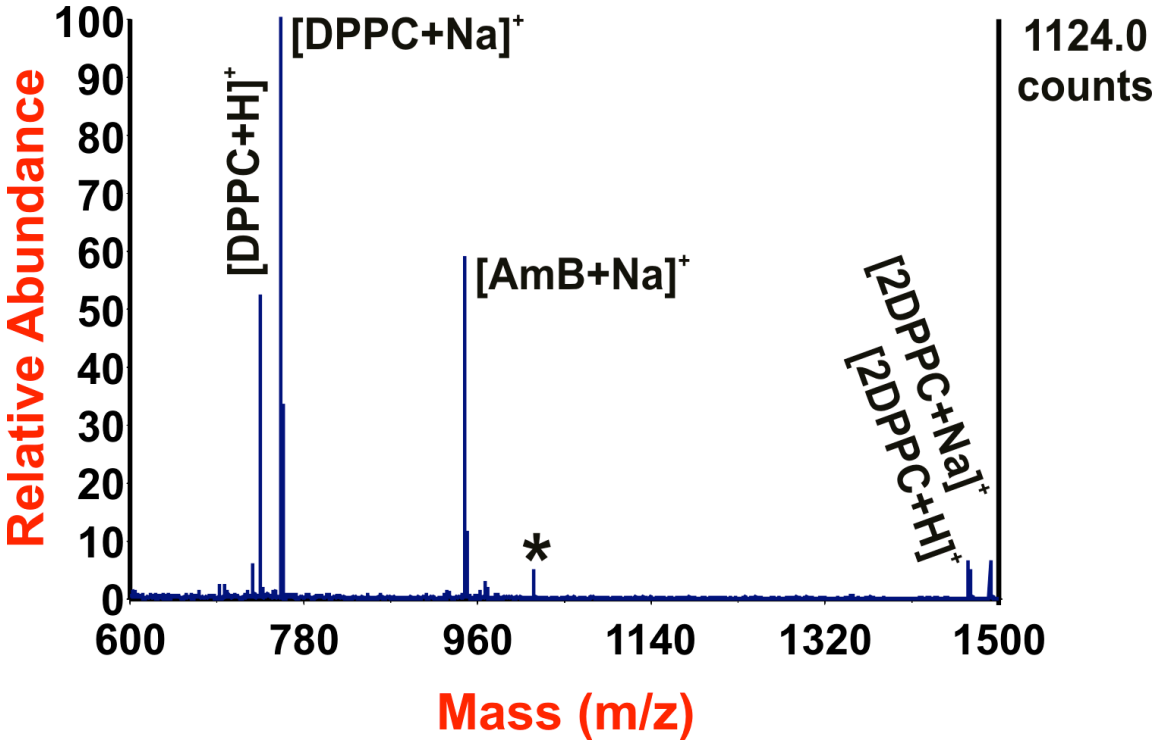

Figure 16. MALDI mass spectrum of AmB-AuNR complex after AmB was captured from an aqueous 1.0 μM AmB solution. The peak labeled with an asterisk (*) was identified as a CTAB-DPPC complex by MS/MS.

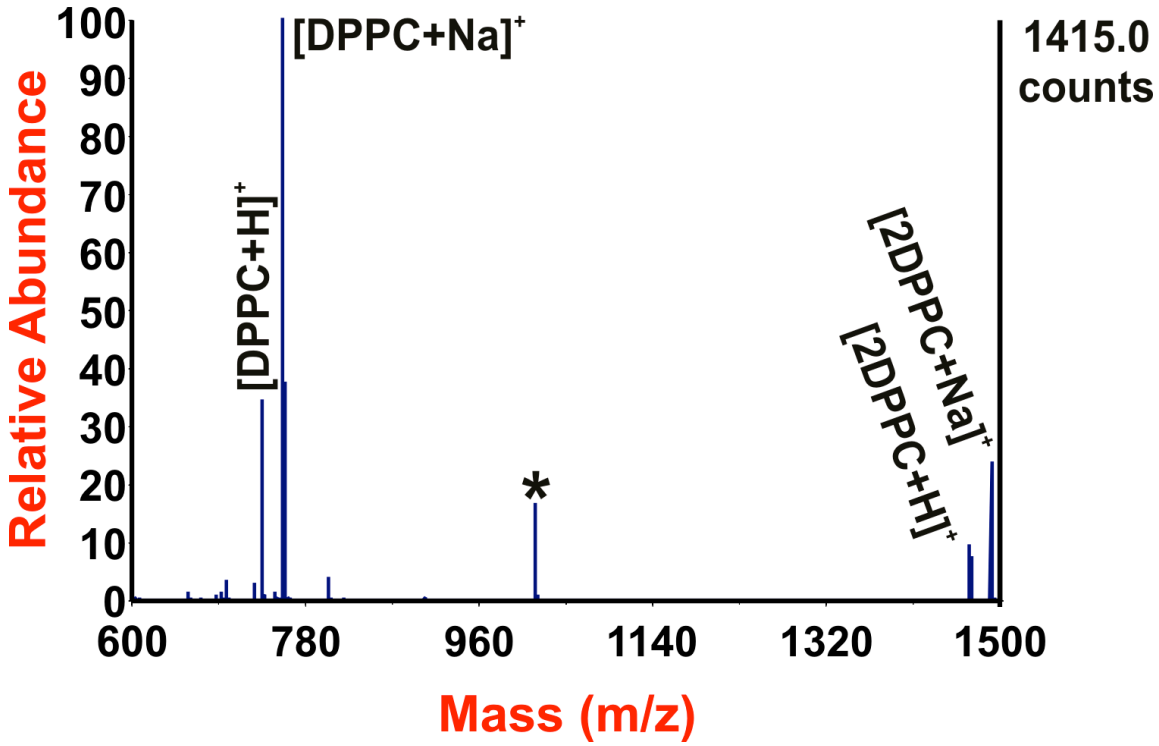

Figure 17. MALDI mass spectrum of control experiment which includes a mixture of AmB and lipid capped AuNRs without incubation. This demonstrates that the presence of the lipid capped AuNRs alone is not enough to facilitate interaction and that the incubation period is necessary for partition of AmB into the bilayer surrounding the AuNRs. The peak labeled with an asterisk (*) was identified as a CTAB-DPPC complex by MS/MS.

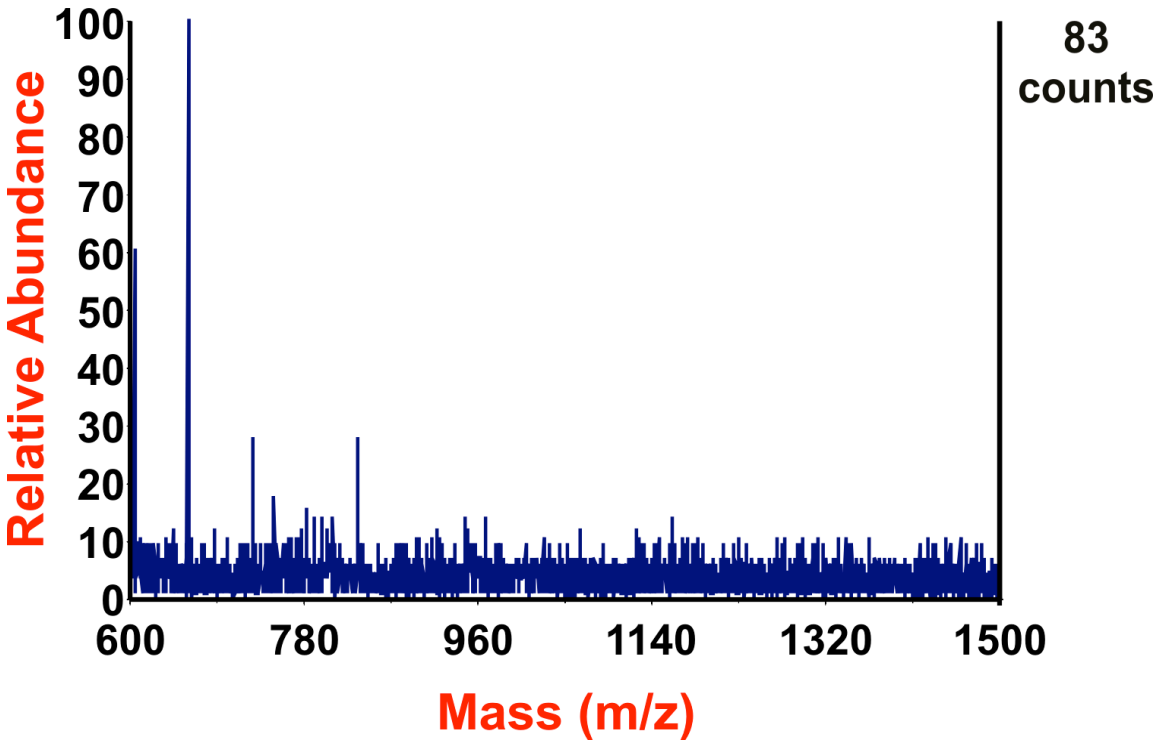

Figure 18. MALDI mass spectrum of a 1.0 μM AmB capture solution. Signal for the analyte is not observed before enrichment by the lipid capped AuNRs.

Modification of the lipid vesicles to incorporate a negatively charged headgroup was also investigated and proved equally as successful for the capture of low abundance analytes from aqueous solutions. By changing the bulk composition of the lipid vesicles from the phosphatidylcholine, DPPC, to a phosphatidylglycerol, POPG, the AuNRs were able to be successfully functionalized with the POPG. An identical capture experiment as outlined above was employed for the capture of Valinomycin and Melittin from dilute aqueous solutions. Valinomycin, a cyclic peptide and potassium specific ionophore used to transport metal ions across lipid membranes contains a hydrophobic region allowing for it to partition into lipid bilayers[126]. **Figure 19** demonstrates the analysis of a dilute

solution (100 nM) of Valinomycin, which did result in signal for the analyte, however, it was buried in the background noise and an isotopic distribution for the analyte was barely discernable. After a capture experiment from a 500 µl aliquot of a 100 nM solution using the POPG functionalized AuNRs, analyte signal corresponding to $[M+Na]^+$ was readily observable for Valinomycin (**Figure 20**). An additional analyte which has been extensively studied and is known to interact and associate with lipid bilayers, Melittin, a 26 amino acid residue peptide was also demonstrated to be successfully enriched after employing the POPG functionalized AuNRs. Similar to the previous analytes, MALDI-MS of the melittin solution (100nM) gives rise to no signal for the target analyte (**Figure 21**) and it is only after enrichment utilizing the POPG functionalized AuNRs that signal is obtained at *m/z* = 2846.4 corresponding to $[M+H]^+$ for the analyte. **Figure 22** demonstrates the resulting spectrum after enrichment in which the inset contains the mass range corresponding to the analyte signal; revealing a clearly resolved isotopic distribution and a good signal to noise against the background.

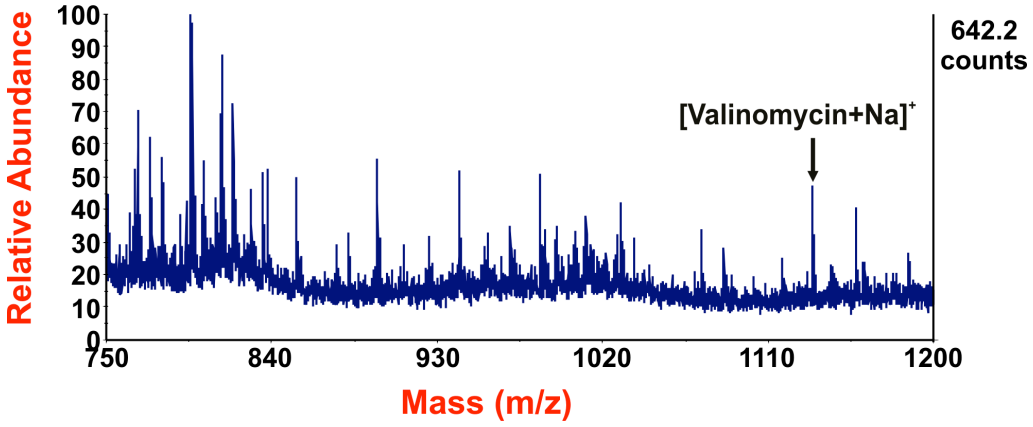

Figure 19. MALDI mass spectrum of a 100 nM Valinomycin solution. The analyte signal is present, however, prevalent background noise complicates the spectrum.

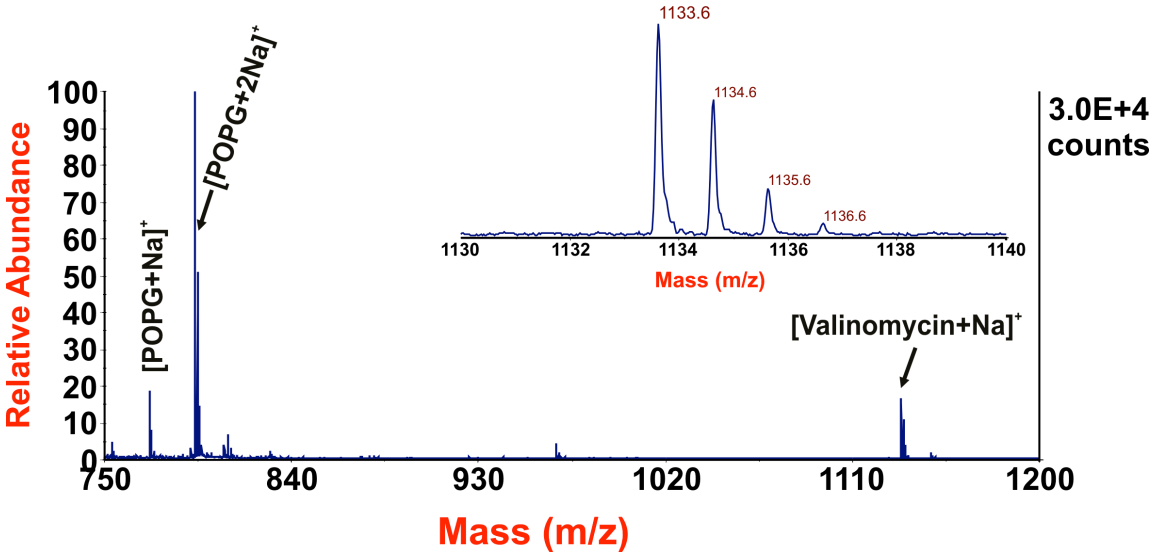

Figure 20. MALDI mass spectrum of the capture experiment from a 100 nM Valinomycin solution utilizing POPG functionalized AuNRs. The inset contains the mass range corresponding to the analyte signal, demonstrating the reduced background signal and improvement in signal-to-noise.

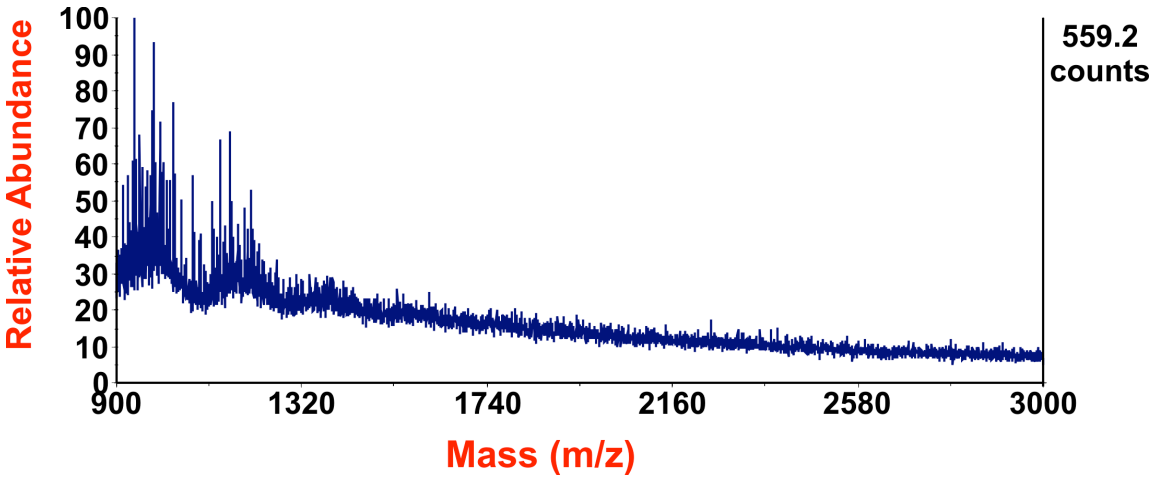

Figure 21. MALDI mass spectrum of a 100 nM Melittin solution which gave rise to no discernable analyte signal.

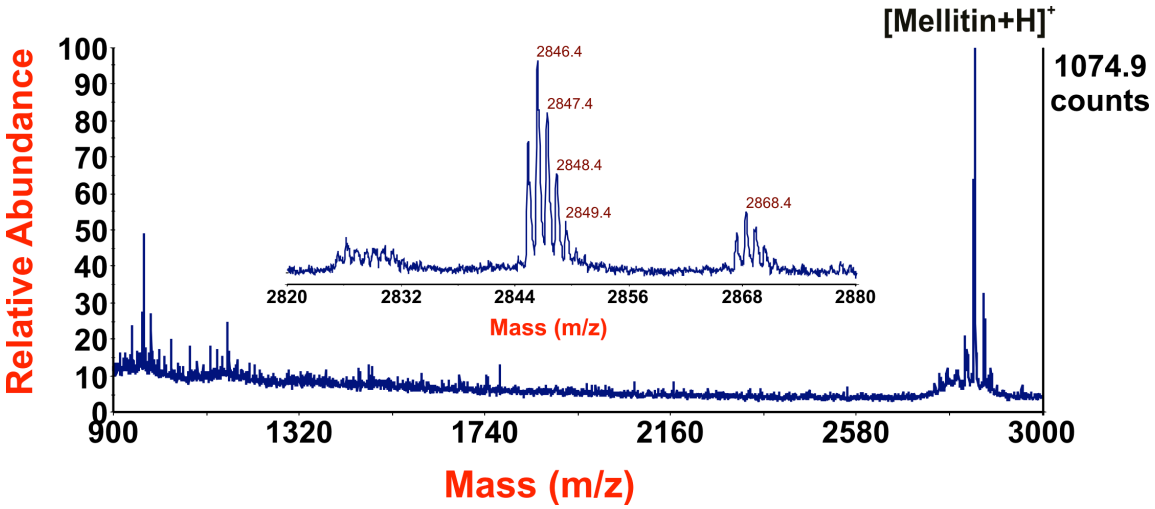

Figure 22. MALDI mass spectrum of the capture experiment from a 100 nM Melittin solution utilizing POPG functionalized AuNRs. The inset contains the mass range corresponding to the analyte signal, demonstrating the reduced background signal and improvement in signal-to-noise.

These results demonstrate, for the first time, the successful application of a hybrid lipid capped AuNR biosensor for the capture and label-free detection of a membrane active drug by MS. Although the unique optical absorption of AmB would be sufficient to detect its presence, many analytes will not elicit such an obvious change in the absorbance profile. In fact, if the analyte does not strongly absorb in the ultraviolet or visible region of the electromagnetic spectrum, then only a small change in the absorbance profile of the lipid capped AuNRs would be observed. On the other hand, if multiple species are present, any change observed in the optical spectra could not be confidently assigned to an individual analyte. Ultimately, for the analysis of complex samples, where it is desired to capture multiple analytes simultaneously and/or identify unknown analytes, MALDI-MS is one of the best detection methods available. This is

particularly important in the development of point-of-care molecular diagnostic assays where multiplexed high throughput analysis of body fluids is the key to success.[129]

The applicability of the lipid capped AuNR as a label-free biosensing platform, was tested by capturing a lipophilic analyte present at low concentration (11 nM) from a complex biological matrix, fetal bovine serum. To prepare the mixture, a stock solution of the target lipopeptide was diluted to a final concentration of 11 nM in 3.0 mg/mL fetal bovine serum. Capture of the lipopeptide, myristoyl-Lys-Arg-Thr-Leu-Arg, was performed using a similar method as outlined above for the AmB capture. After removing the unbound species by centrifugation and resuspension in water, a 1.0 μL aliquot the lipid capped AuNRs containing the captured lipopeptide was spotted onto a stainless steel MALDI plate and dried under vacuum. This process was repeated until 5.0 μL of solution was deposited on the sample plate and then 1.0 μL of 1.0 mg/mL solution of α-Cyano-4-hydroxycinnamic acid (CHCA) was spotted over the dried sample spot. The sample was then analyzed by MALDI-MS **(Figure 23)**. MALDI-MS analysis of the solution following the selective capture and concentration of the lipopeptide by the lipid capped AuNRs reveals a drastic improvement in our ability to detect the lipopeptide. The dominant signal in the spectra for the capture experiment corresponds to the lipopeptide $[M+H]^+$ ion at *m/z* = 883.6. In fact, the s/n ratio of the lipopeptide $[M+H]^+$ peak has increased to ~550 and it is now the most abundant signal. The spectra labeled with numbers represent unidentified species present the serum.

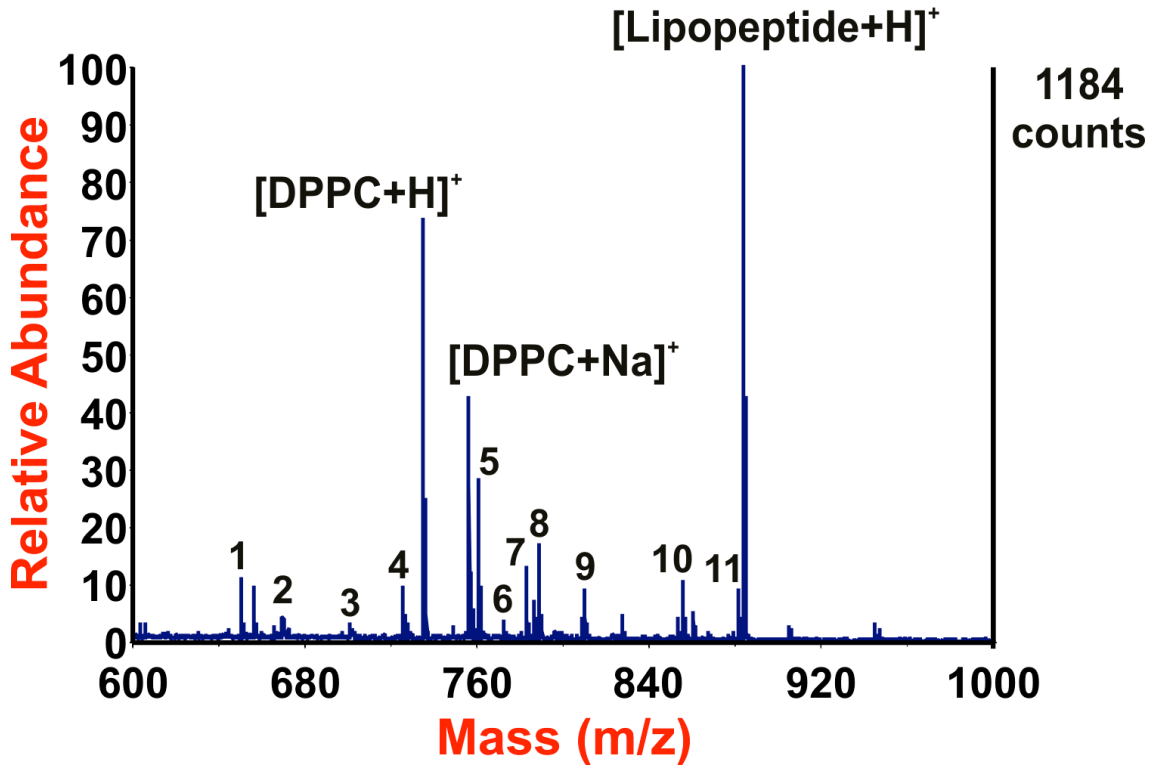

Figure 23. MALDI mass spectrum of the lipopeptide lipid capped AuNR complex after the lipopeptide was captured from an 11 nM solution of lipopeptide in 3.0 mg/mL fetal bovine serum solution. The peaks labeled with numbers correspond to unidentified species present in the calf serum.

As a control experiment, an identical sample preparation procedure was repeated for the lipopeptide/serum solution without the addition of lipid capped AuNRs **(Figure 24)**. Here, the most abundant peaks in the spectra correspond to serum components (peaks labeled 4, 7, and 9). More importantly, the lipopeptide is barely discernable in the spectra (S/N < 3).

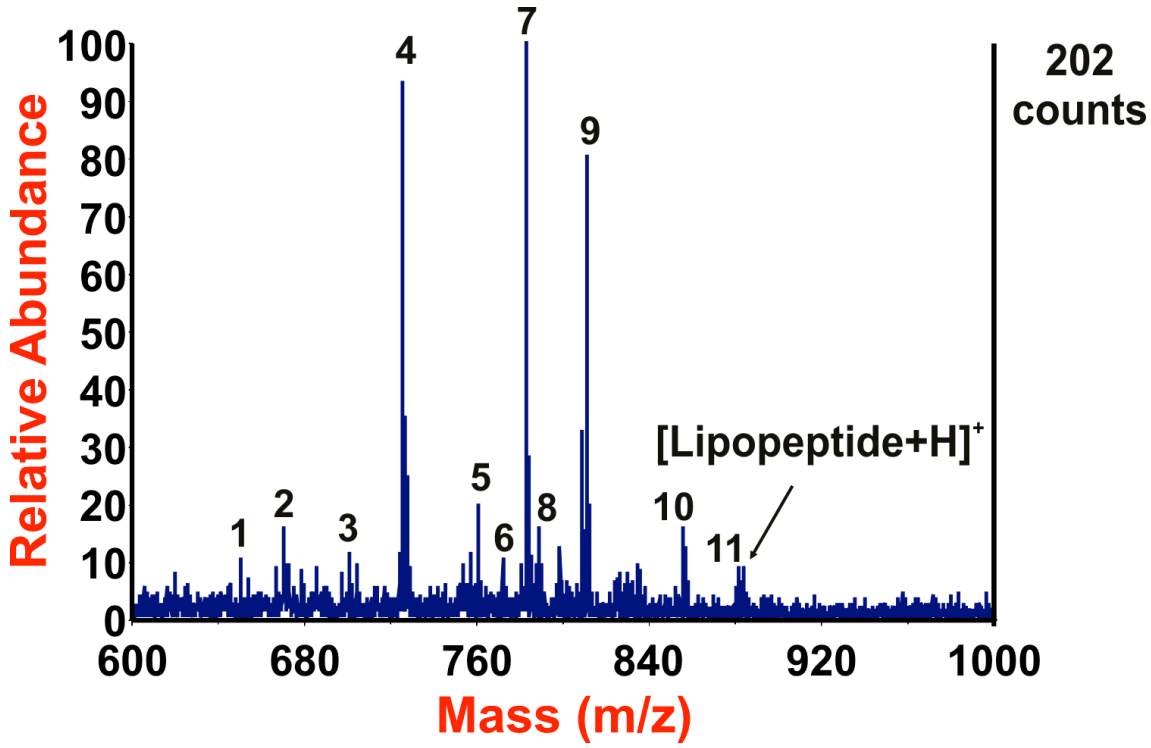

Figure 24. MALDI mass spectrum of 11 nM lipopeptide solution in 3.0 mg/mL fetal bovine serum. The peaks labeled with numbers correspond to unidentified species present in the serum.

To further verify that selective capture of the lipopeptide is occurring due to the presence of the lipid capping, the AuNRs, control experiments were performed in which non-lipophilic capping agents were employed (mPEG-thiol or 4-aminothiophenol).[18] In order to eliminate any effect or possible interferences from components of the serum, these control experiments were carried out with aqueous lipopeptide solutions and were performed using an identical capture protocol and sample preparation parameters as with the lipid-capped AuNR. An additional control experiment utilizing CTAB capped AuNR was performed, however, as previously noted, the CTAB functionalized AuNR were unable to withstand multiple washing steps and no analyte signals were observed by

MALDI-MS due to AuNR aggregation. MALDI-MS spectrum of the capture experiments utilizing mPEG-thiol capped AuNR **(Figure 25)** or 4-aminothiophenol capped AuNRs **(Figure 26)** contained no discernable lipopeptide signal above the background. It is important to note that incubation is essential for analyte capture. For example, when the lipid-AuNR were mixed with the serum solution and analyzed immediately, there was no significant increase in the lipopeptide signal **(Figure 27)** in comparison to the capture experiment, which was allowed to incubate at room temperature for 20 minutes before analysis.

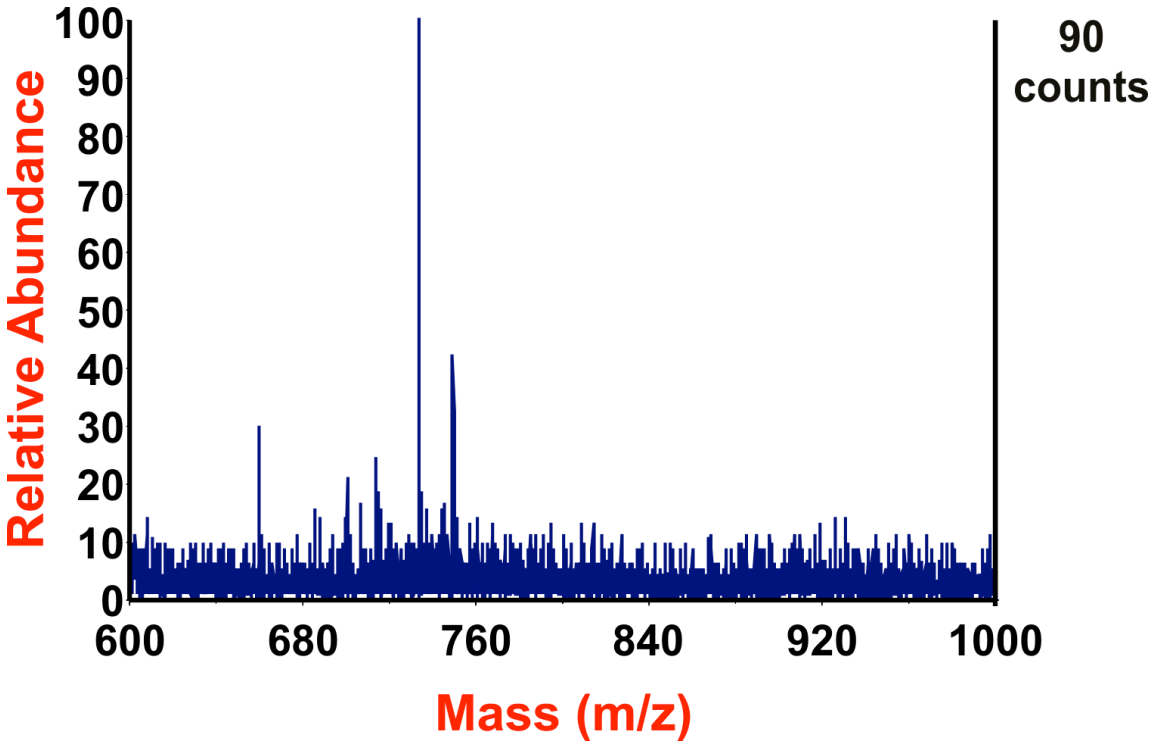

Figure 25. MALDI mass spectrum of the attempted capture of the lipopeptide using mPEG-thiol capped AuNRs. The lipopeptide was present at a concentration of 11 nM in water; however, there is no discernable signal for the target analyte using mPEG-thiol capped AuNRs as the affinity platform.

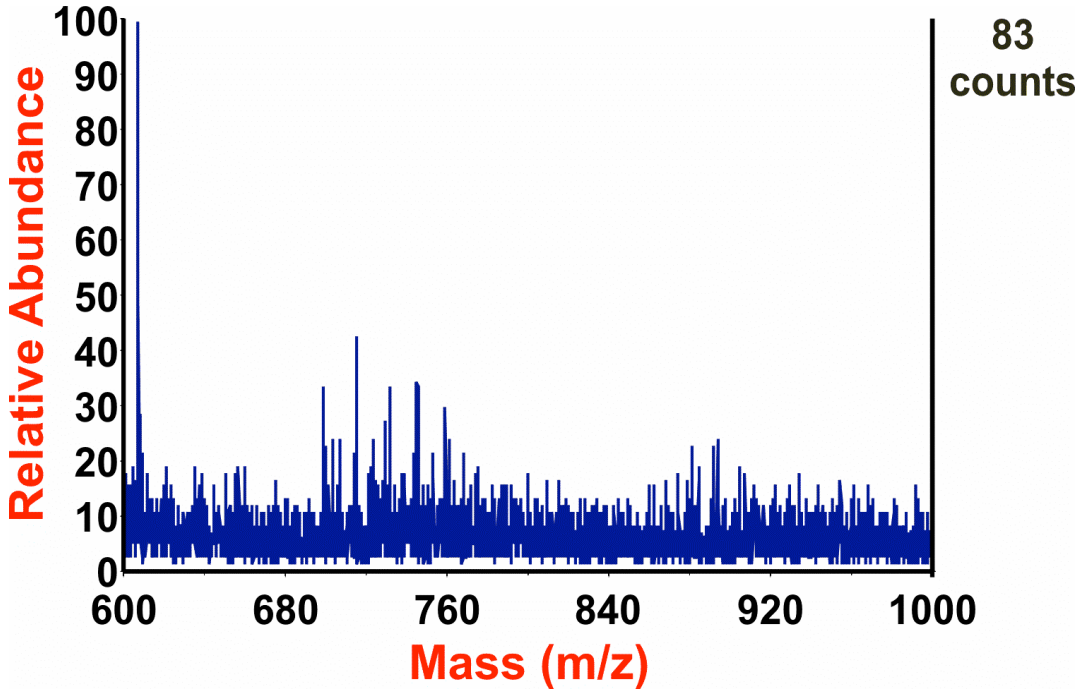

Figure 26. MALDI mass spectrum of the attempted capture of the lipopeptide using 4-aminothiophenol capped AuNRs. The lipopeptide was present at a concentration of 11 nM in water; however, there is no discernable signal for the target analyte using 4-aminothiophenol capped AuNRs.

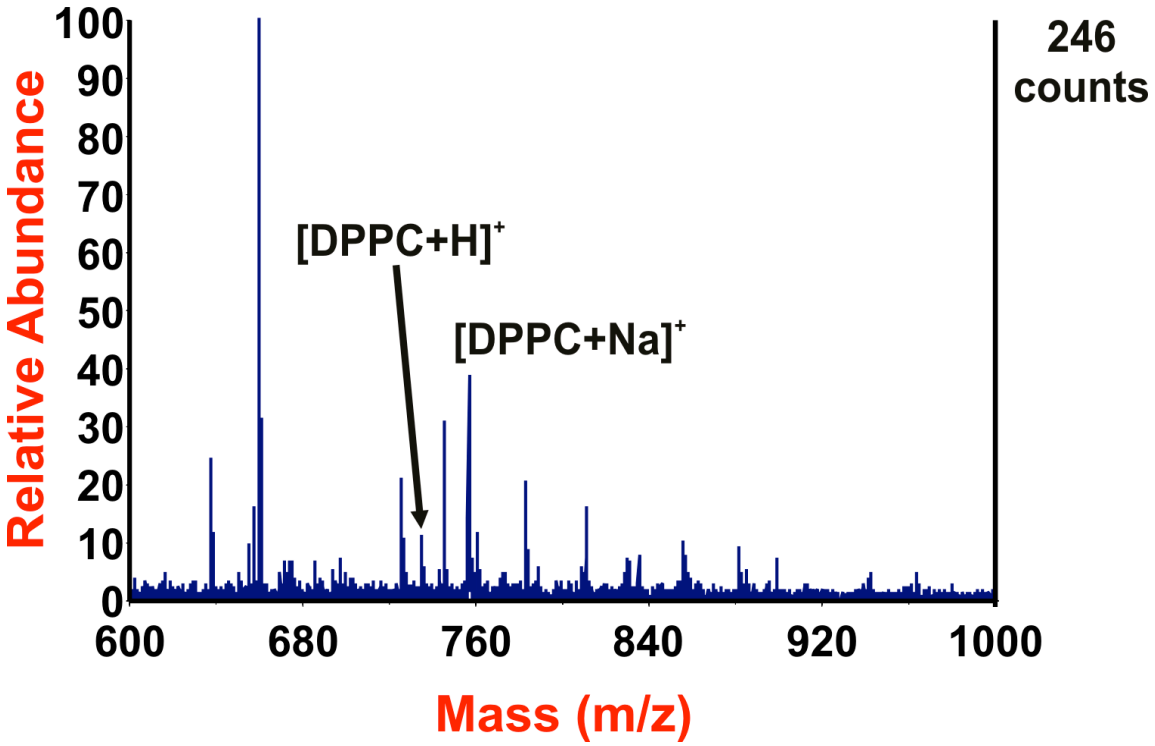

Figure 27. MALDI mass spectrum of lipid capped AuNRs mixed with an 11 nM lipopeptide solution in fetal bovine serum and analyzed immediately.

Conclusions

The data presented here illustrate the utility and applicability of lipid capped AuNRs as label-free biosensor platforms for both optical and mass spectrometry based detection. Previous studies addressed the importance of lipid bilayers for stabilization of AuNRs, and tethering of lipid bilayers to the surface of the AuNRs also provides an effective medium for the capture of lipophilic analytes from solution.[77,130] The AmB and lipopeptide capture data clearly illustrate the utility of the lipid-AuNR biosensor for the selective capture, detection, and identification of lipophilic analytes. This work underscores the potential of lipid-capped AuNRs for biosensor applications; however, lipid-capped AuNR may provide avenues for developing powerful multiplexed label-free sensor platforms. For example, tailoring the chemical and physical properties by altering the composition of the lipids or by attaching targeting molecules to the headgroups of the lipids would allow for additional degrees of selectivity to be incorporated into the biosensor platform. Such approaches would significantly enhance the selectivity of the lipid-AuNR platform, thereby extending the capability of the biosensor to target different types of analytes. For example, it should be possible to develop a multiplexing system that incorporates an array of lipid capped AuNR biosensors, which would serve to simultaneously target a variety of analytes in solution. Mass spectrometry then becomes an essential component of the label-free detection of the multiple targeted analytes owing to the low specificity of optical detection methods.

CHAPTER IV

A SOL-GEL DERIVED SILVER NANOPARTICLE EMBEDDED THIN FILM FOR MASS SPECTROMETRY-BASED BIOSENSING·

Introduction

Owing to their biological significance, the rapid detection of peptides, proteins and lipids has become the basis for the development of numerous biosensing techniques over the past several years. Among these techniques, matrix assisted laser desorption ionization mass spectrometry (MALDI-MS) has been proven to be invaluable for the analysis of a number of high molecular weight compounds;[1-3,6] however its utility for analysis of small molecules (<1000 *m/z*) such as steroids and lipids has been limited due to significant background noise from matrix clusters that congest the low mass region of the spectra.[4,7] A number of matrix free platforms have since been developed to probe lower mass region analytes with considerable success. One such method, desorption ionization on porous silicon (DIOS), utilizes etched silicon wafers to fabricate a porous nanostructure that can be used for directly desorbing and ionizing analytes from the surface.[11-13,64] While this method has been proven successful in both minimizing background noise and detecting several low molecular weight compounds including peptides and organic compounds, the technique has been generally limited to basic analytes.[131] Additionally, the shelf life of the DIOS platform is relatively short, owing to

· Reprinted with permission from Gamez, R. C., Castellana, E. T., Russell, D. H. A Sol-Gel-Derived Silver-Nanoparticle-Embedded Thin Film for Mass Spectrometry-Based Biosensing. *Langmuir* **2013**, 29, 6502-6507. Copyright 2013 American Chemical Society.

its susceptibility to surface oxidation which results in decreased performance and reproducibility.[11,131]

Alternatively, the sol-gel method has recently gained considerable attention as a simple means for producing effective MS platforms via incorporation of organic matrices and optically active metal nanoparticles (NPs) that serve as UV energy absorbers. Separate studies utilizing thin films impregnated with α-cyano-4-hydroxycinnamic acid (CHCA) and 2,5-dihydroxybenzoic acid (DHB) were capable of detecting a number of small molecules and proteins, respectively.[132,133] Several oligonucleotides were successfully analyzed by doping 3,4-diaminobenzoic acid (DABA) or 3,5-DABA into sol-gel solutions during the preparation of thin films - a method that also proved to be effective in reducing interference signals associated with alkali metal salts without desalting steps prior to analysis.[134] Incorporation of TiO_2 into the sol-gel allowed for the detection of surfactants, peptides and tryptic digest products; however, the addition of a proton source in the form of citrate buffer was necessary for useful MS data.[135]

There are distinct advantages of the sol-gel method for the synthesis of metal NPs compared to traditional chemical reduction methods. Namely, organo-metallic precursors such as metal salts are often miscible with the starting solution, and controlled homogenous doping is easily achieved. Moreover, since high annealing temperatures are oftentimes employed, low mass organic residuals that may potentially interfere in MS analysis are incinerated during the process, thereby eliminating additional clean up steps.[53,54] Here, we describe the preparation and implementation of a

porous AgNP-embedded thin film platform prepared using standard sol-gel chemistry to form an optically active LDI-MS biosensor platform. The AgNP/thin film serves as an alternative matrix-free MS platform for the sensitive detection of a number of low abundance sterols from lipid vesicles as well as several analytes in various chemical classes. The combination of optically active NP with the high concentration of pores on the film surface provides several advantages from an analytical standpoint including: (i) increased sample loading offered by the larger surface area of the system, (ii) minimized sample preparation, (iii) high tolerance to salts by elimination of chemical stabilizers, and (iv) an extended shelf life (>1 year).

Materials and Methods

All peptides (Angiotensin I, Angiotensin II, Angiotensin III, [Val4] Angiotensin III, Bradykinin, Substance P, etc.) were purchased from American Peptide Co., Inc. (Sunnyvale, CA). 1-2,-dioleoyl-sn-glycero-3-phosphocholine (DOPC), 1-palmitoyl-2-oleoyl-sn-glycero-3-phosphocholine (POPC), 1,2-dipalmitoyl-sn-glycero-3-phosphocholine (DPPC), and 1,2-dimyristoyl-sn-glycero-3-phosphocholine (DMPC) were acquired from Avanti Polar Lipids (Alabaster, AL). Triglyceride standard mixture, tetraethyl orthosilicate (TEOS), 2-ethoxyethanol and silver nitrate were purchased from Sigma-Aldrich, Inc. (St. Louis, MO). All aqueous solutions were prepared using 18.2 $M\Omega/cm^2$ water (Barnstead EasyPure II, Thermo Scientific, Dubuque, IA). Boro-aluminosilicate glass wafers, (25.4 x 25.4 mm; 0.5 mm thick) were purchased from Precision Glass & Optics. (Santa Ana, CA.) Glass wafers were cleaned by immersion in

a piranha solution (75% concentrated sulfuric acid, 25% concentrated hydrogen peroxide. Note: piranha solution is a vigorous oxidant and should be used with extreme caution) at 100°C for 30 minutes. Next, the wafers were rinsed thoroughly with water and baked at 150°C for 2 hours prior to use.

Porous AgNP impregnated thin films were prepared by the sol-gel method. First, 15.9 mL of TEOS, 15.3 mL of 2-ethoxyethanol and 4.8 mL of distilled water were mixed at room temperature with stirring. Next, 0.5 mL of 0.5M nitric acid was added to the mixture to make the pH of the solution acidic. This solution was stirred at room temperature for 4 hours, then 1.46 g of silver nitrate was added and the mixture was allowed to stir for an additional 2 hours. After stirring, the clean glass wafers were coated with the silver-containing sol-gel solution by a spin coating process. Individual glass slides were placed on the spin coating platform, and the surfaces were subjected to 4 mL of silver-containing sol-gel solution while spinning at 1200 RPM, for 30 seconds. The freshly coated wafers were then thermally treated in a furnace, in air. The furnace was ramped from room temperature to 700°C over 7 hours, then held at 700°C for 3hours, and then followed by a ramp down to room temperature over 7 hours. The thermally treated films were stored under atmospheric conditions and used without further treatment.

Mass spectrometry data were acquired with a Voyager DE-STR MALDI-TOF-MS (Applied Biosystems, Foster City, CA). UV-LDI-MS (337 nm) was obtained using a nitrogen laser (model VSL-337ND-S, Thermo Laser Science, Franklin, MA).

UV-vis absorption spectra of the thin films were acquired with an Agilent 8453 spectrophotometer. SEM images were acquired with a FEI Quanta 600 FE-SEM and pore size distributions were determined directly from the SEM images using ImageJ particle size analysis software. X-ray Photoelectron Spectroscopy (XPS) measurements were carried out using Kratos Axis Ultra Imaging X-ray photoelectron spectrometer. A monochromated Al Kα source of hν = 1486.6 eV was used to probe the thin films. Binding energies were corrected by C 1s as a reference energy (C 1s = 248.8 eV).[136] Narrow scans of the Ag 3d regions were collected at analyzer pass energy of 40 eV after 5 scan repetitions with a measuring step of 0.1 eV and a dwell time of 450 ms.

Thin films were taped directly to the surface of a standard stainless steel MALDI plate with copper tape. Samples (1.0 μL) analyzed were spotted directly to the surface of the AgNP impregnated films. Data acquisition was performed on a Voyager DE-STR equipped with a nitrogen laser (337 nm) in reflected mode. Laser intensities were adjusted to optimize the signal-to-noise ratio and desorbed ions were extracted into the flight tube with 20 kV after a 200 ns delay. Laser energies used for signal production ranged from ~3.5 to 6.0 μJ/pulse and laser energy measurements were acquired using an Ophir Nova Power/Energy meter coupled to a PE-10 Ophir Pyroelectric head (Ophir Laser Measurement Group, North Logan, UT). Values were recorded every 200 shots from a total of 1000 laser shots and measurements were taken in increments of 50 arbitrary units via the instrument control settings.

Results and Discussion

The utility of AgNP impregnated thin films as platform for mass spectrometry analysis is demonstrated for a number of analytes which were individually spotted directly onto the surface and vacuum dried. LDI-MS analysis was performed by irradiation of each sample spot with 337 nm photons. It should be emphasized that LDI was carried out without the addition of organic matrices. We hypothesize that the overlap of the SPR band of the AgNP is capable of absorbing the incoming laser radiation which results in i) a rapid rise in temperature of the nanoparticles,[36] which facilitates thermal desorption of the analyte, and ii) production of silver ions[87] that ionize the samples spotted at the surface. LDI yields primarily silver ion clusters and the analytes are typically observed as Ag^+ adducts that have a characteristic isotopic pattern consisting of two dominant peaks with an approximate 1:1 intensity ratio separated by 2 *m/z* units. Data in **Figure 28** demonstrate capability for the thin films to produce signals when 2.5 picomoles of Angiotensin II, (DRVYIHPF) are spotted on the surface and analyzed. Here, the only signal observed corresponds to a silver adduct of the peptide, $[\text{Angiotensin II+Ag}]^+$ (*m/z* = 1152.5). The inset of **Figure 28** shows the unique isotope pattern of the silver adducted analyte. Moreover, the spectrum shows minimal background noise and high signal-to-noise ratio (s/n ~250). Similar results were observed for a number of analytes, and the results are summarized in **Table 1**.

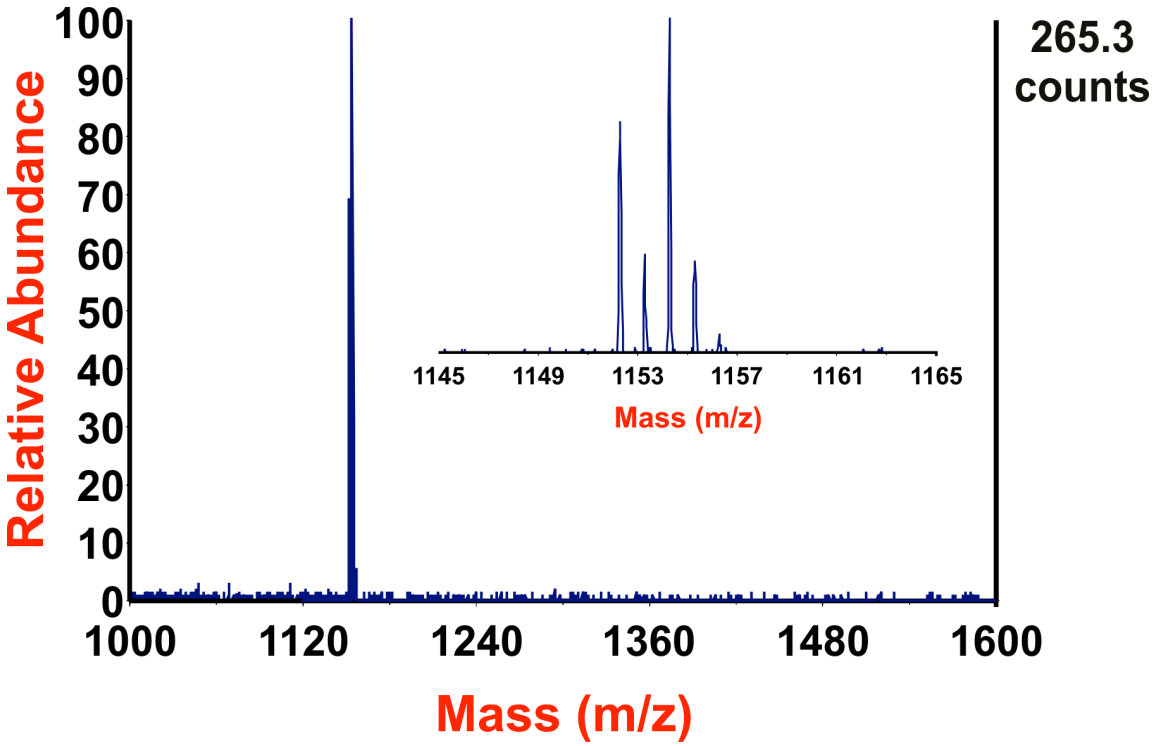

Figure 28. Mass spectrum of 2.5 pmol Angiotensin II (*m/z* = 1152.5) spotted on AgNP thin film surface and analyzed by LDI-MS. Inset shows a zoom-in view of the resulting peak.

	Sequence	[M+Ag]	pmol
Angiotensin II	DRVYIHPF	1152.4	2.5
Angiotensin III	RVYIHPF	1037.4	2.5
Bradykinin	RPPGFSPFR	1166.5	2.5
Bradykinin 1-8	RPPGFSPF	1010.4	2.5
Bradykinin 2-9	PPFFSPFR	1010.4	2.5
[Arg8] Vasopressin	CYRQNCPRG-NH_2	1190.3	2.5
Angiotensin I	DRVYIHPFHL	1402.6	5
[Val4] Angiotensin III	RVYVHPF	1023.4	5
Bradykinin 1-7	RPPGFSP	863.3	5
Flag	DYKDDDK	1119.3	5
Substance P	RPKPQQFFGLM-NH_2	1453.6	10
P60	Ac-IYGEF-NH_2	777.2	50
P60 Phosphorylated	Ac-IpYGEF-NH_2	855.2	100
Valinomycin	Cyclo (L-Val-D-Hyiva-D-Val-L-Lac-)3	1217.5	100
Bradykinin 1-5	RPPGF	679.2	100
Indolicidin	ILPWKWPWWPWRR-NH_2	2012.0	100

Table 1. Analytes observed by spotting on the surface of the films and their respective sequence, mass to charge ratio (*m/z*) and limits of detection.

The versatility of AgNP thin films as a mass spectrometry platform was evaluated by analyzing a mixture of triglycerides (TAGs; C8-C16), and phosphatidylcholines (DMPC, DPPC, and POPC). The analytes in the mixture contain saturated hydrocarbon chain moieties, except for POPC, which has a single site of unsaturation in one of the hydrocarbon chains. As previously mentioned, the thin film was left untreated after initial preparation and the mixture was spotted directly onto the surface, dried and analyzed. The resulting mass spectrum **(Figure 29)** contains $[M+Ag]^+$

signals for each of the TAGs and phospholipids in the mixture. Interestingly, POPC, the only olefin present in the mixture, produced the lowest ion abundance despite being spotted at equal concentration (~6 picomoles) as the other analytes. This observation is consistent with our previous investigation, in which we attributed the lower ionization efficiency of POPC to a weaker interaction between the silver ions and the double bond owing to the steric hindrance imposed on the silver ion by the freely rotating long hydrocarbon chains.[32,137] Table 2 includes the amount of picomoles of each analyte spotted onto the surface of the biosensor and the corresponding counts produced for each analyte. Similar results were obtained for small unilamellar vesicles composed of different sterols and phosphatidylcholines with either one or two unsaturated tails. In these experiments, the vesicles prepared were composed of ~99.5 mol% POPC and ~0.5 mol% of stigmasterol, lanosterol, β-sitosterin, or cholecalciferol. For each of the preparations containing the olefins, preferential ionization of the sterols is observed, and the dominant peak in each of the resulting spectra corresponds to the Ag^+ adduct of the sterol. **Figure 30** contains a typical spectrum for the analysis of the sterol/unsaturated lipid vesicle mixture. For this analysis, the vesicles were diluted such that ~2 picomoles of stigmasterol and ~330 picomoles of POPC are spotted onto the surface. Despite the lower concentration of sterols compared to the phospholipids, the dominant signal corresponds to each of the individual sterols for the respective analyses. It should be noted that the sterols were also preferentially ionized from preparations using DOPC lipid vesicles **(Figure 31)**.

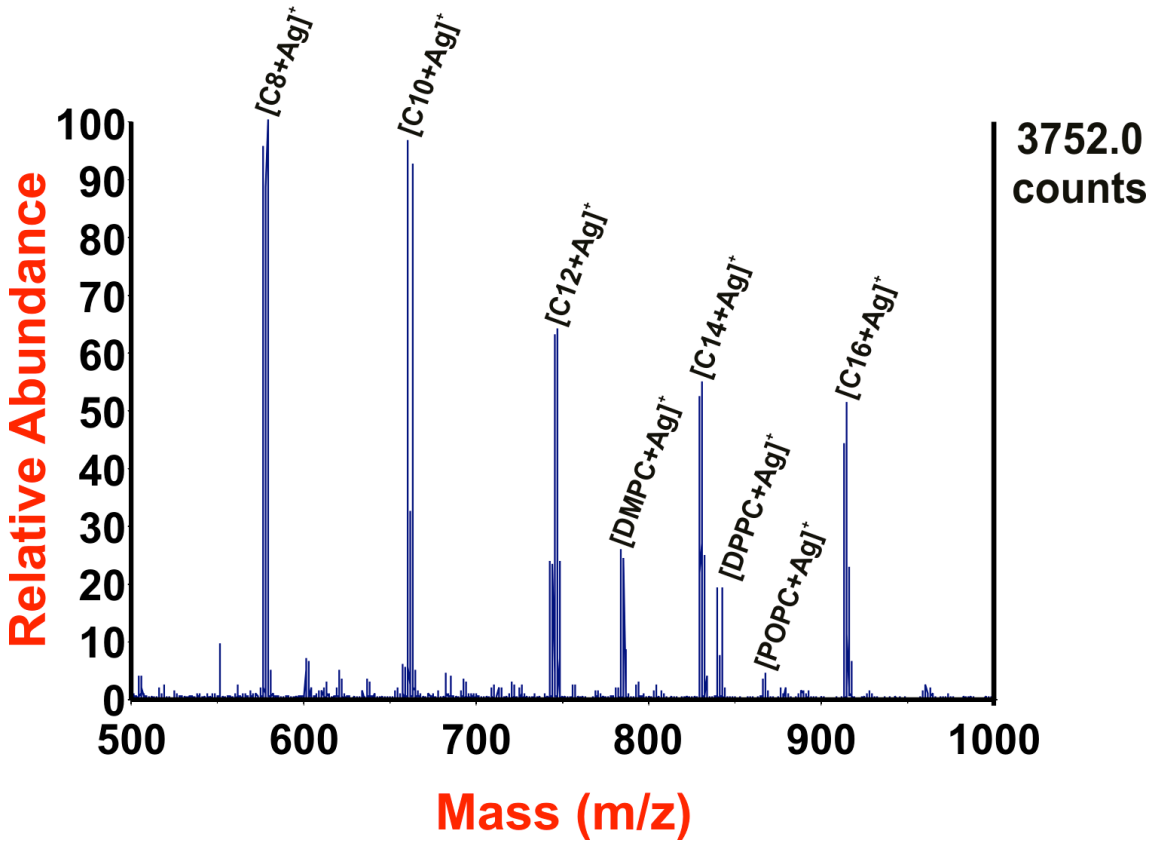

Figure 29. Mass spectrum of a solution containing a mixture of triglycerides and three phosphatidylcholines (DMPC, DPPC, and POPC) analyzed by LDI-MS.

	Chain Length	$[M+Ag]^+$	Counts	pmol spotted
TAG	8:0	577.3	3752.0	10.6
TAG	10:0	661.4	3623.9	9.01
TAG	12:0	745.5	2394.7	7.82
TAG	14:0	829.5	2058.1	6.91
TAG	16:0	913.6	1920.8	6.19
DMPC	PC(14:0/14:0)	784.4	972.9	7.37
DPPC	PC(16:0/16:0)	840.5	723.4	6.81
POPC	PC(16:0/18:1)	866.5	179.2	6.58

Table 2. The table lists the amount in picomoles of each triglyceride and phosphatidylcholine spotted on the surface and the corresponding counts produced for each analyte.

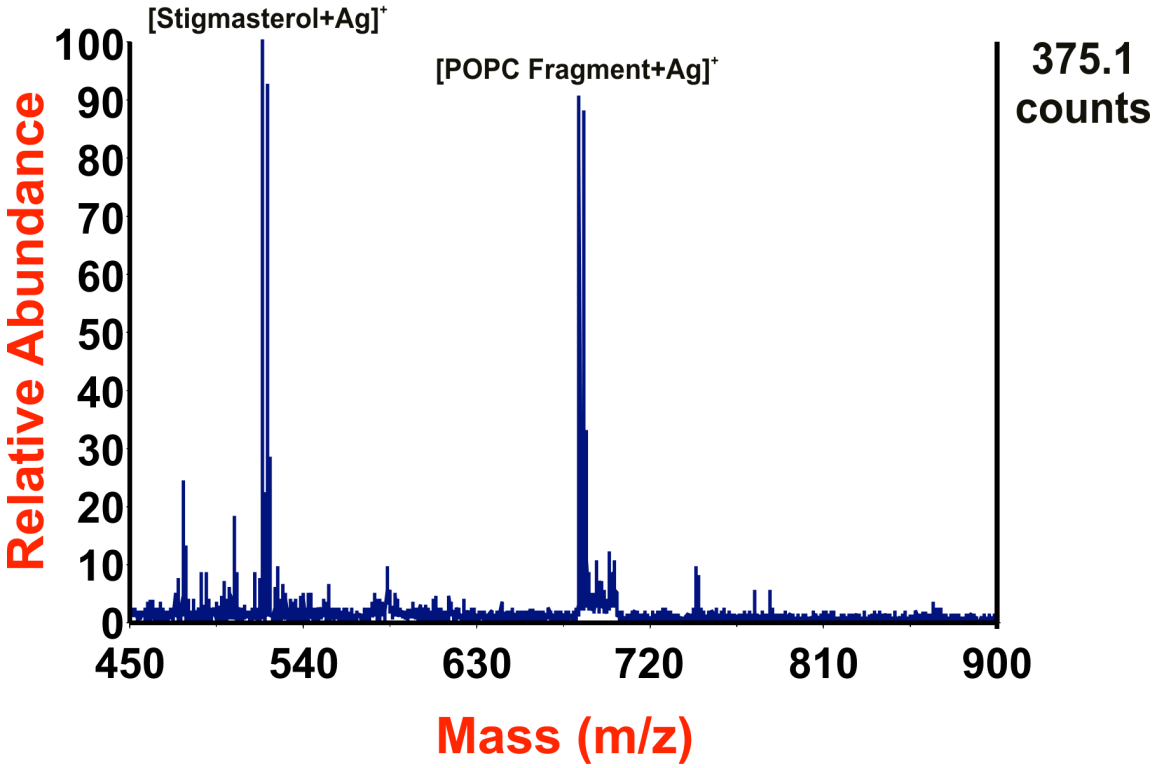

Figure 30. Mass spectrum of vesicles composed of 99.5 mol % POPC and 0.5 mol % stigmasterol. The vesicles were diluted so that ~2 pmol of stigmasterol and ~330 pmol of POPC were spotted onto the surface. The POPC fragment corresponds to the loss of the phosphatidylcholine headgroup.

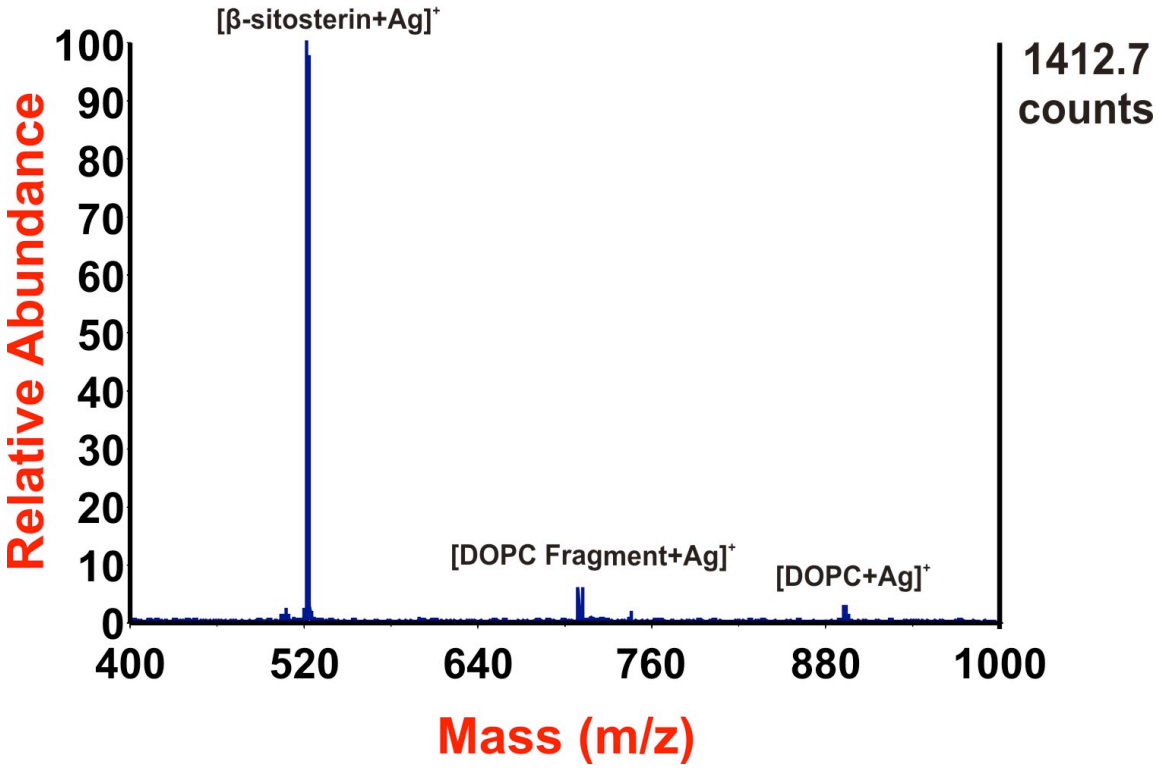

Figure 31. Mass spectrum of vesicles composed of ~83 mol % DOPC and ~17 mol % β-sitosterin. The vesicles were diluted so that ~ 9 pmol of β-sitosterin and ~46 pmol of DOPC were spotted onto the surface. The DOPC fragment corresponds to the loss of the phosphatidylcholine headgroup.

Minimizing sample handling that might lead to sample loss is essential for successful detection of target molecules in the analysis of complex mixtures. This is especially true in the case of biological fluids that require clean up steps to reduce the high salt concentrations that frequently complicate mass spectrometry analysis owing to formation of salt adducts or production of chemical background noise. **Figure 32** contains mass spectra produced when three analytes were diluted to their final concentrations in 1.0 mM sodium chloride and analyzed using the AgNP thin films. Although the analytes are present at concentrations of ~10 pmol in high salt conditions,

the dominant signal in each of the individual spectra corresponds to $[M+Ag]^+$ rather than $[M+Na]^+$ for the respective analytes with little to no background noise or interference peaks. The concentrations for each of the analytes and the corresponding counts at those concentrations are summarized in the figure. Similar results were observed for a number of other biological buffers including 1.0 mM urea **(Figure 33)**, 1.0 mM ammonium acetate **(Figure 34)**, and tris-buffered saline (1.0 mM tris/3.0 mM NaCl) **(Figure 35)**. Additionally, these results were acquired from the surface of a platform which had been prepared 16 months prior to the analysis (platform prepared December 2011; data taken April 2013).

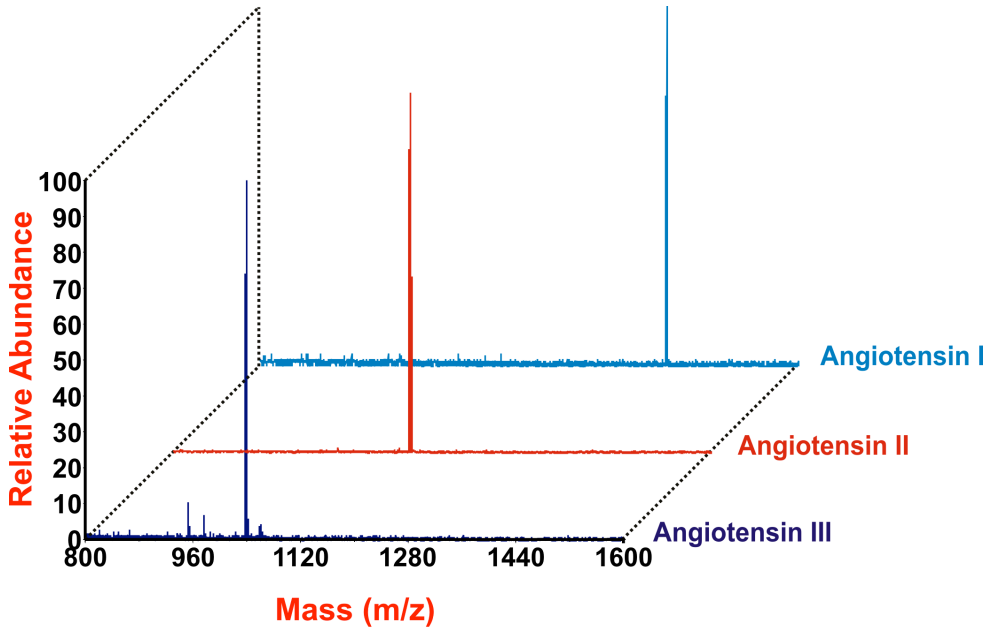

	Sequence	$[M+Ag]^+$	Counts	pmol spotted
Angiotensin I	DRVYIHPFHL	1402.6	236.2	7.71
Angiotensin II	DRVYIHPF	1152.4	1069.5	9.55
Angiotensin III	RVYIHPF	1037.4	381.1	10.7

Figure 32. Mass spectra of Angiotensin I, II, and III when diluted in 1.0 mM NaCl and analyzed by LDI-MS.

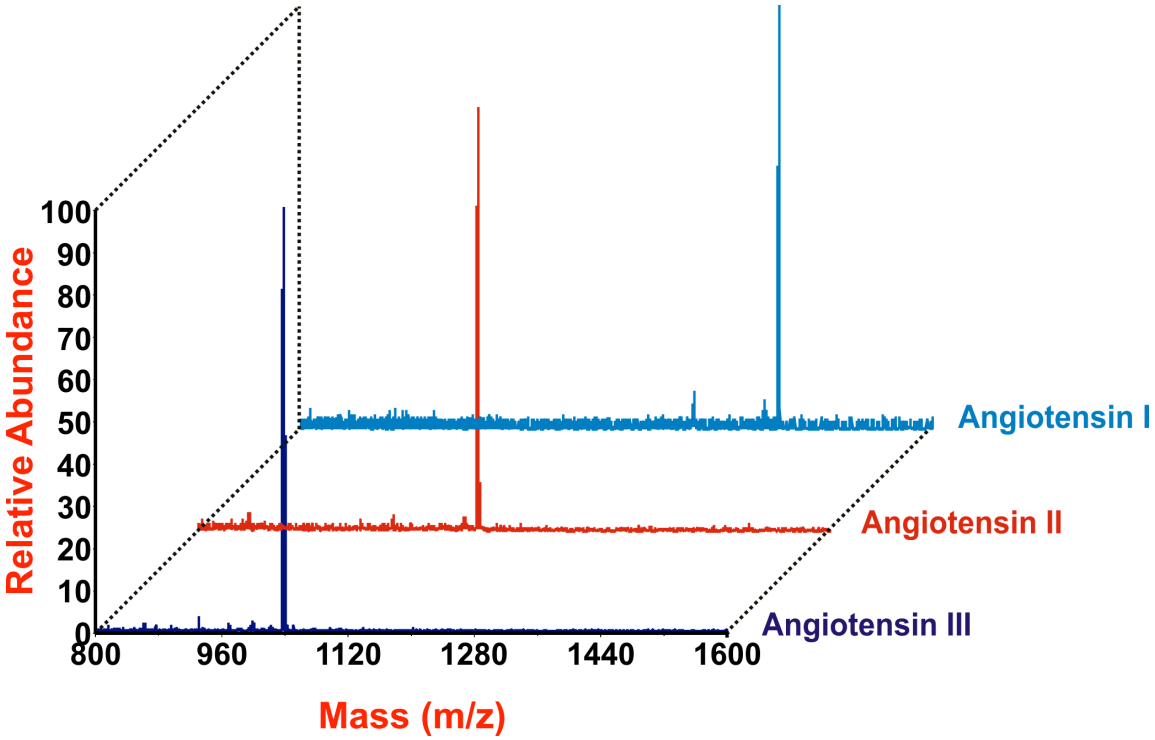

	Sequence	$[M+Ag]^+$	Counts	pmol spotted
Angiotensin I	DRVYIHPFHL	1402.6	187.6	7.71
Angiotensin II	DRVYIHPF	1152.4	470.1	9.55
Angiotensin III	RVYIHPF	1037.4	559.1	10.7

Figure 33. Mass spectra of Angiotensin I, II, and III when diluted in 1.0 mM urea and analyzed by LDI-MS, 16 months after initial preparation of the thin film.

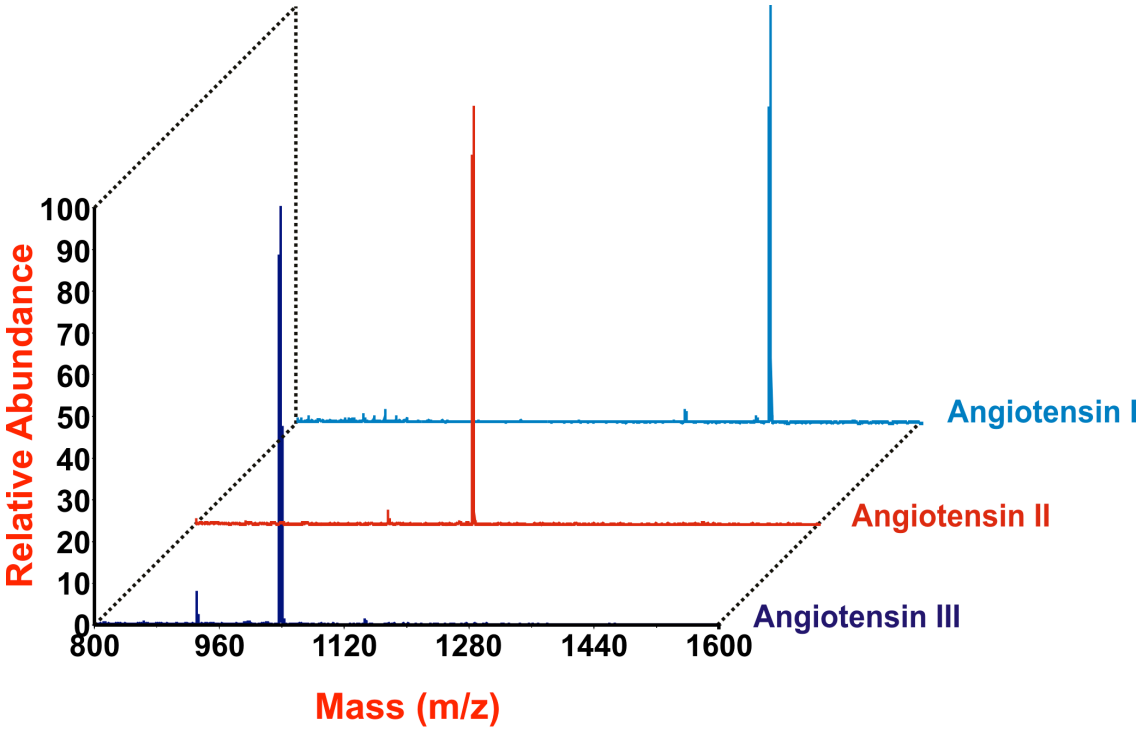

	Sequence	$[M+Ag]^+$	Counts	pmol spotted
Angiotensin I	DRVYIHPFHL	1402.6	1771.4	7.71
Angiotensin II	DRVYIHPF	1152.4	1101.0	9.55
Angiotensin III	RVYIHPF	1037.4	2423.1	10.7

Figure 34. Mass spectra of Angiotensin I, II, and III when diluted in 1.0 mM ammonium acetate and analyzed by LDI-MS, 16 months after initial preparation of the thin film.

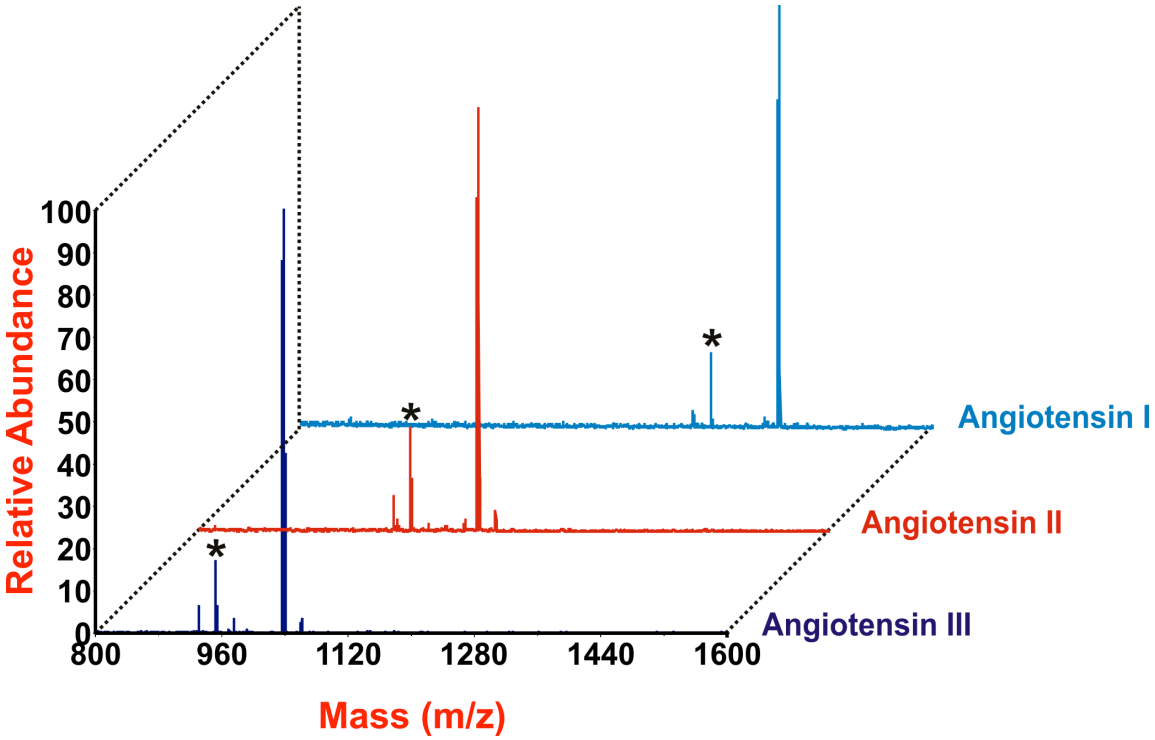

	Sequence	$[M+Ag]^+$	Counts	pmol spotted
Angiotensin I	DRVYIHPFHL	1402.6	733.2	7.71
Angiotensin II	DRVYIHPF	1152.4	1766.8	9.55
Angiotensin III	RVYIHPF	1037.4	2125.2	10.7

Figure 35. Mass spectra of Angiotensin I, II, and III when diluted in 1.0 mM Tris; 3.0 mM NaCl and analyzed by LDI-MS, 16 months after initial preparation of the thin film. The peaks in each of the individual traces labeled with an asterisk (*) corresponds to sodium adducts ($[M+Na]^+$) of the peptide.

During the course of developing the technology, AgNP embedded sol-gels were stored at atmospheric conditions for periods >1 year. Lengthy storage periods did not compromise the functionality of the platform. For example, the feasibility of preparing the thin films for future use as a durable analysis platform is demonstrated by the low mass region of a mass spectrum (data taken December 2011) of an unspotted thin film prepared in September of 2010 **(Figure 36)**. The film is still capable of producing an

abundance of silver ions, which can be used to ionize analytes spotted on the surface a year after initial preparation, despite remaining under atmospheric conditions. In fact, when several different analytes were spotted on the surface of an aged film, abundant signal for 5.0 pmol of Angiotensin I **(Figure 37)**, 2.5 pmol of Angiotensin II **(Figure 38)**, and 2.5 pmol of Angiotensin III **(Figure 39)** spotted onto the surface could still be produced. It should be noted that the low mass region does contain additional unidentified interference peaks, however, the higher mass region where analyte signal is produced remains relatively unchanged and analyte identification is easily achieved.

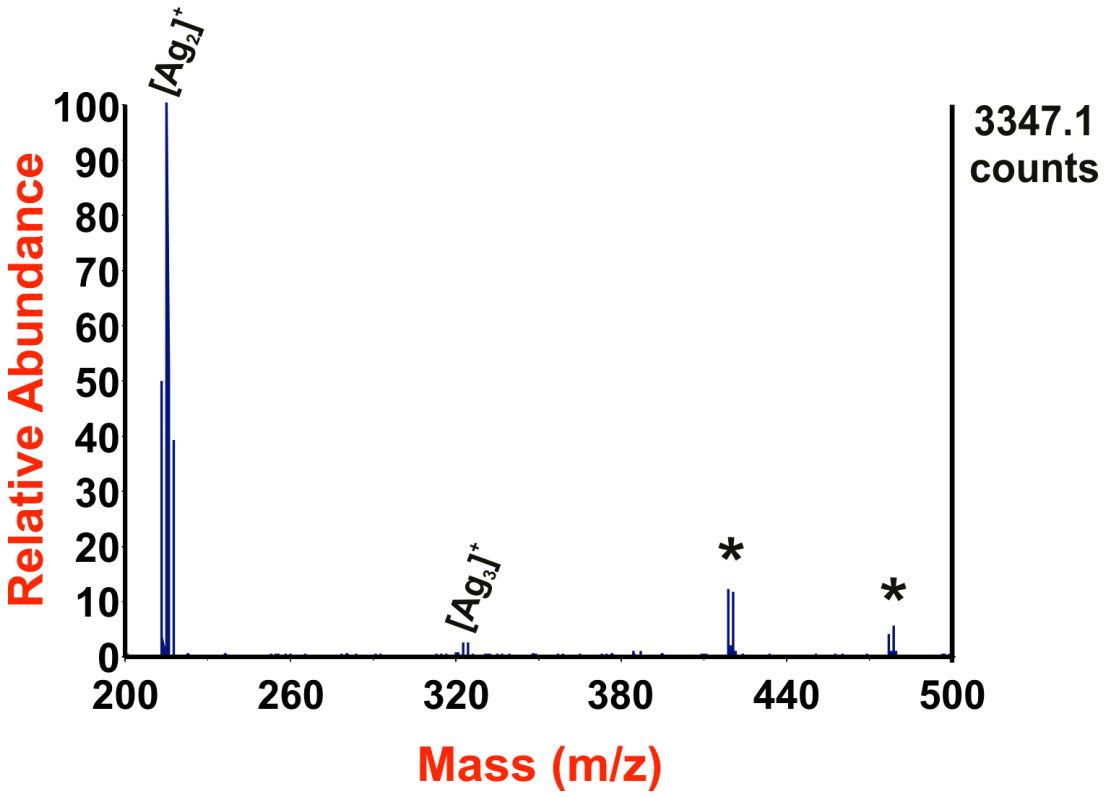

Figure 36. Spectrum of the low mass region of an AgNP impregnated thin film taken 15 months after initial preparation. Minimal interference peaks result (asterisks), despite remaining under atmospheric conditions and no additional surface treatment or washing steps after initial preparation.

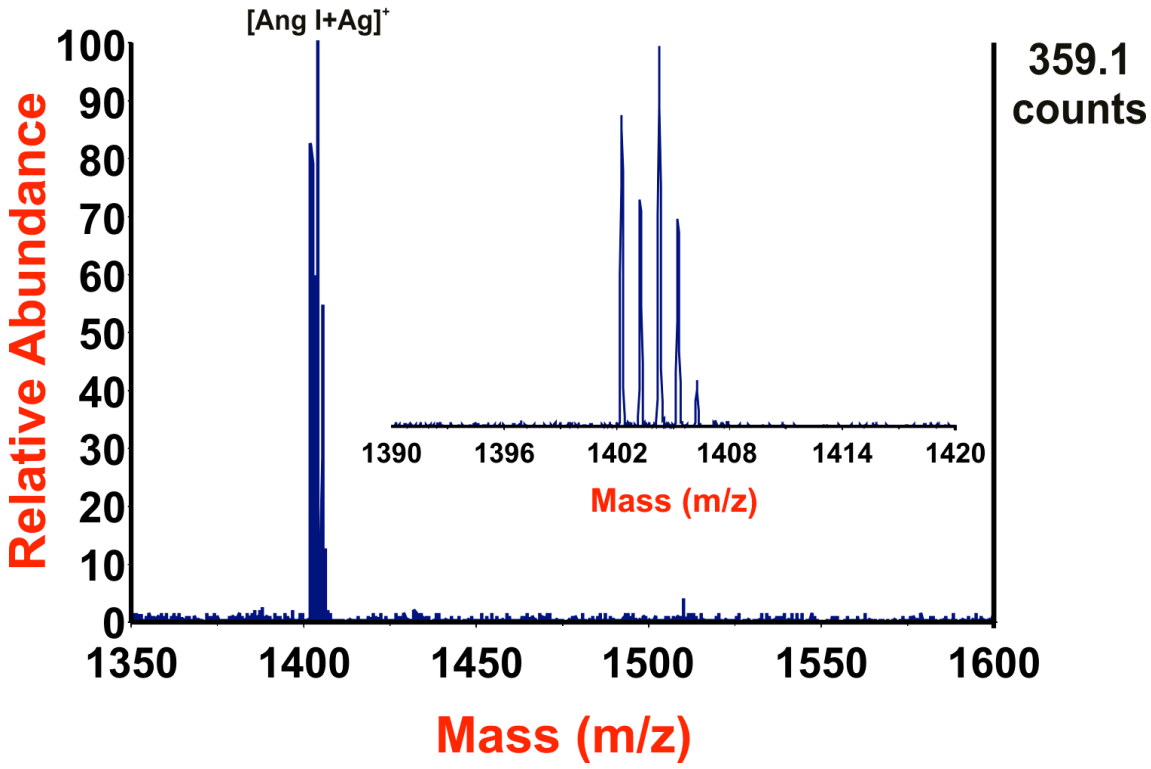

Figure 37. Spectrum of analyte region of 5.0 pmol Angiotensin I spotted onto a silver nanoparticle embedded thin film. Analysis was performed 16 months after initial preparation of the thin film. Inset is a zoom-in view of the $[M+Ag]^+$ peak.

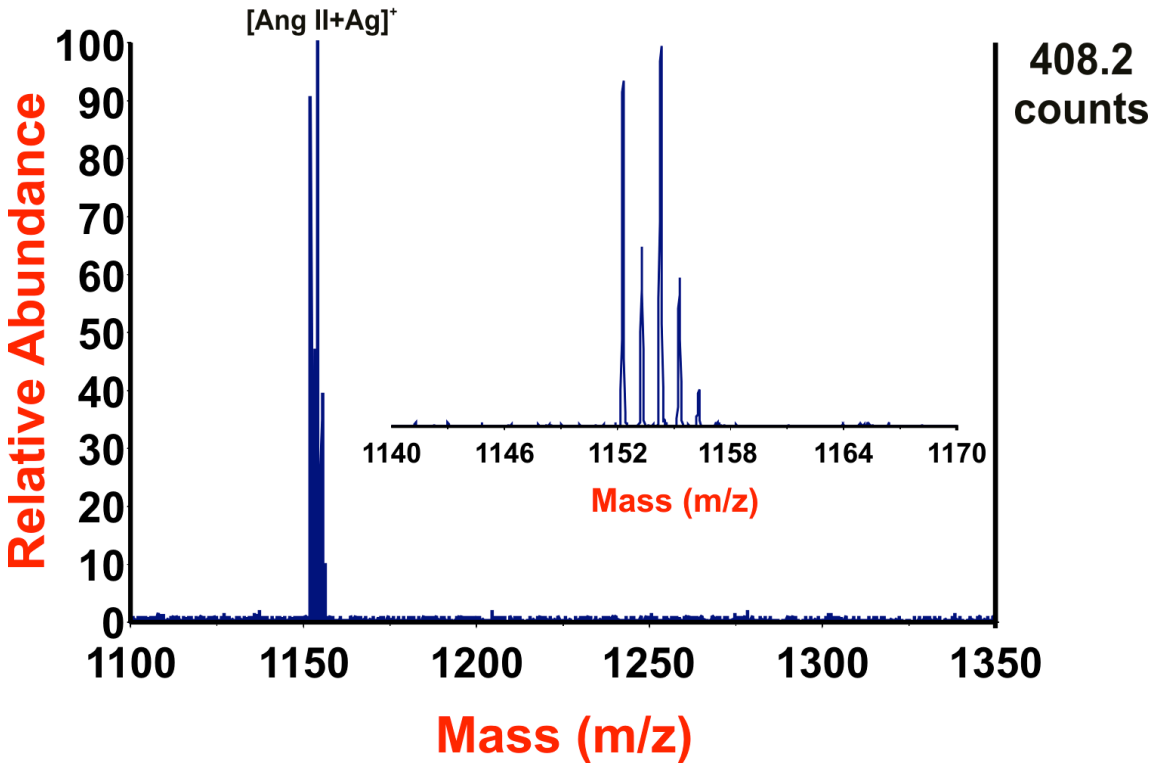

Figure 38. Spectrum of analyte region of ~2.5 pmol Angiotensin II spotted onto a silver nanoparticle embedded thin film. Analysis was performed 16 months after initial preparation of the thin film. Inset is a zoom-in view of the $[M+Ag]^+$ peak.

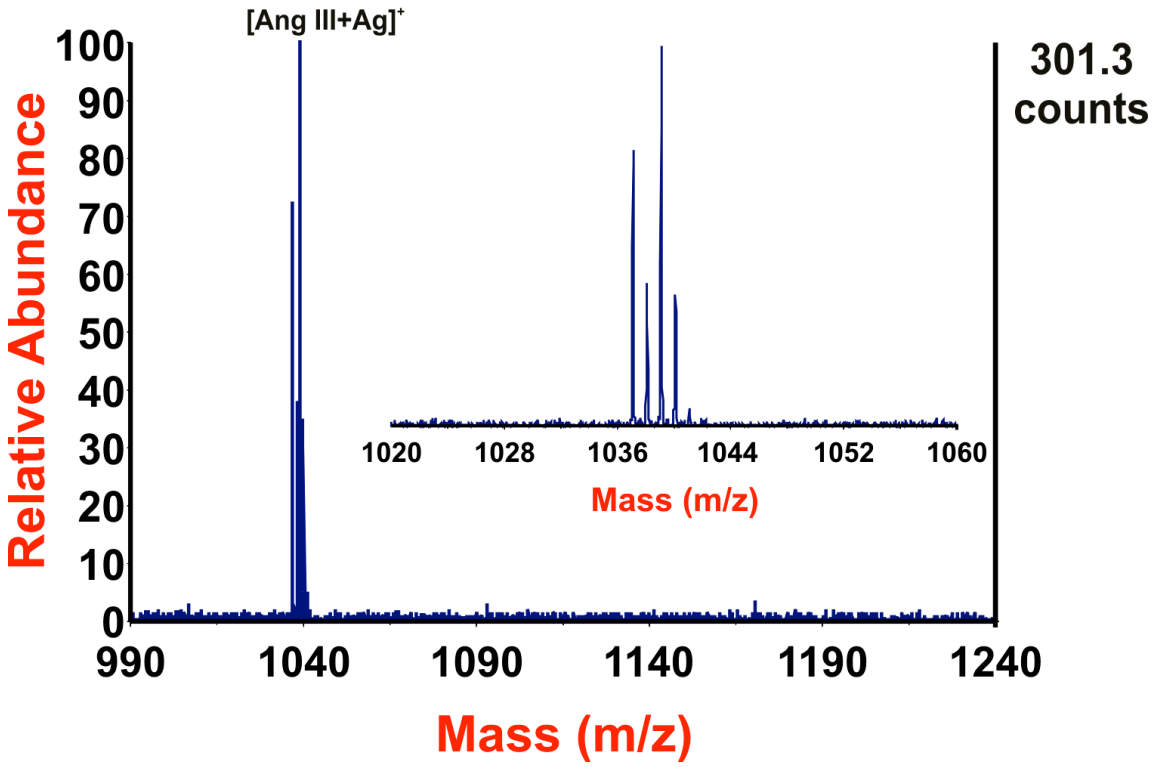

Figure 39. Spectrum of analyte region of ~2.5 pmol Angiotensin III spotted onto a silver nanoparticle embedded thin film. Analysis was performed 16 months after initial preparation of the thin film. Inset is a zoom-in view of the $[M+Ag]^+$ peak.

Despite these results demonstrating the thin films as a suitable method for mass spectrometry based biosensing, experiments aimed at tailoring the surface chemistry of the platform to improve selectivity have also been investigated. Selectivity becomes especially important when analyzing complex mixtures, as unwanted analytes may complicate identification of a target analyte during analysis if an enrichment method is unable to selectively capture, or "pull down" a specific type of compound. Previously, we demonstrated the selectivity of gold nanorods by functionalizing their surface with a lipid coating for the capture of lipophilic and membrane active components from fetal

bovine serum. Here, we aimed to target hydrophobic analytes by treating the surface of the thin films with, Bis(tridecafluoro-1,1,2,2-tetrahydrooctyl)tetramethyldisiloxane, Bis-F26, a fluorinated siloxane compound previously demonstrated by Woo, *et al.* to aid in the desorption of analytes from the surface of porous silicon wafers. If left untreated, the porous silver nanoparticle embedded thin films result in a hydrophilic surface, owing to the presence of silanol groups at the surface of the film; hence functionalization is necessary to make the surface considerably more hydrophobic in nature. A typical surface treatment using Bis-F26 of the thin films follows a modified version of a nanostructure-initiator mass spectrometry (NIMS) protocol [15]. In this modified protocol, the thin films are first cleaned with a piranha solution for 30 minutes, and then rinsed with water, and dried in an oven at 150°C. After drying, 100 μL of Bis-F26 was applied to the surface of the film and allowed to soak for 30 minutes. Excess Bis-F26 was removed from the surface of the film with a stream of nitrogen and then put in the oven at 150°C to dry for 15 minutes. If the thin film was not completely dried, this process was repeated until the thin film was completely dry. This platform was then used for an on-plate enrichment of hydrophobic analytes from fetal bovine serum. In a typical enrichment experiment, a target analyte was diluted to its final concentration in 3.0 mg/ml fetal bovine serum, and a 5.0 μL aliquot was spotted to the surface of the film, and allowed to sit at room temperature for 30 minutes. Afterwards, the sample spot area was rinsed several times with water to remove any species that were not interacting with the surface. The thin film was then taped directly to the surface of a standard stainless steel MALDI plate with copper tape and MALDI-MS was performed by spotting 1.0 μL

of 5.0 mg/mL CHCA over the sample area. Data acquisition was performed on an Applied Biosystems 4800 Plus MALDI TOF/TOF equipped with a frequency tripled Nd:Yag laser (355 nm). Laser intensities were adjusted to optimize the signal-to-noise ratio and desorbed ions were extracted into the flight tube with 20 kV after a 200 ns delay. To compare the efficacy of this platform to our previously developed method utilizing lipid coated gold nanorods, an identical experiment was performed in which the target analyte was the lipopeptide, Myristoyl-Lys-Arg-Thr-Leu-Arg (Myr-KRTLR). Utilizing the gold nanorod platform, the lowest limits of detection for lipopeptide after enrichment resulted from a 500 μL aliquot of an 11 nM solution in fetal bovine serum, which is equal to a total of 5.0 nanograms (~5.5 picomoles) of lipopeptide available for enrichment from the mixture. **Figure 40** demonstrates the capability of the on-plate enrichment method using the treated silver thin films to enrich an identical amount (5.0 nanograms) of lipopeptide from a 3.0 mg/mL fetal bovine serum solution. In **Figure 40**, there is abundant signal corresponding to the target analyte with little to no background signal from any interfering species. A similar experiment was performed in which a total of 500 picograms of lipopeptide in 3.0 mg/ml in fetal bovine serum were spotted to the surface of a treated thin film for enrichment. **Figure 41** demonstrates the resulting MALDI mass spectrum from 500 picograms of lipopeptide using the on-plate enrichment method. Similarly, the primary signal corresponds to the target analyte with little to no background signal from any interfering species. MALDI analysis of the same amount of lipopeptide in 3.0 mg/ml fetal bovine serum failed to produce any discernable signal for the target analyte **(Figure 42)**. Additionally, the use of an untreated thin film

failed to produce the same results as those films treated with Bis-F26, indicating that the platform alone is not sufficient enough to enrich the analyte (**Figure 43**).

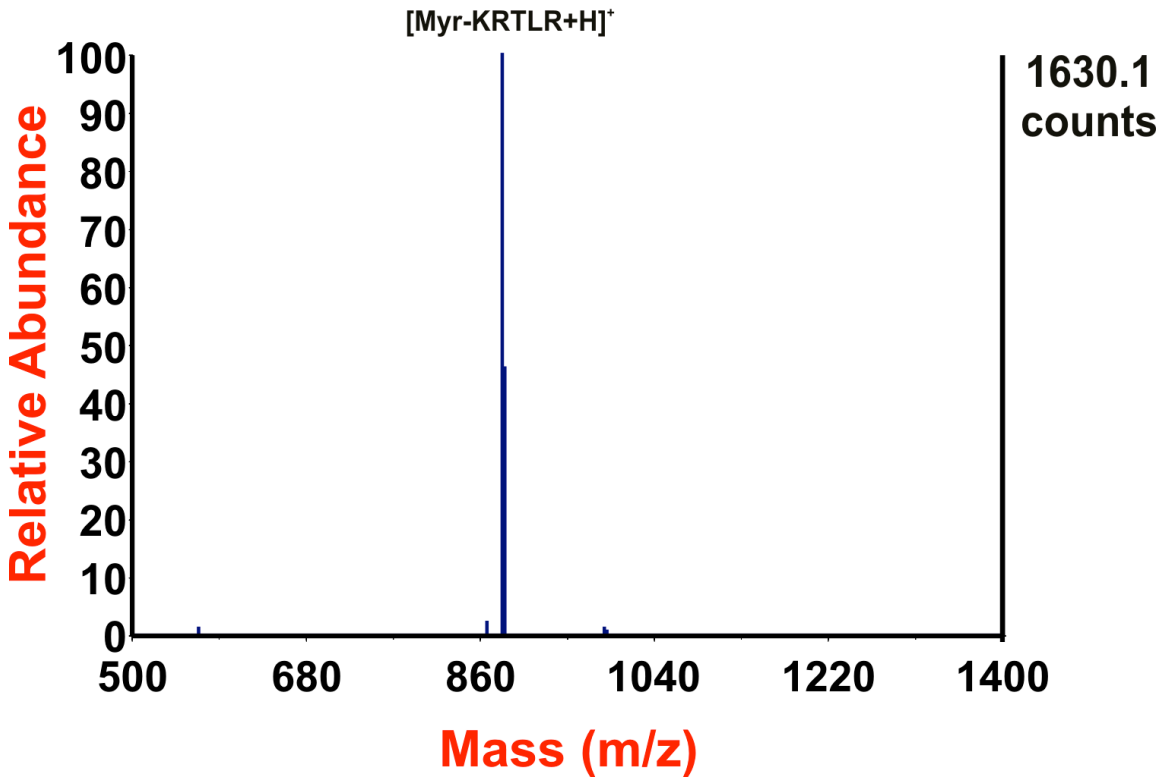

Figure 40. MALDI mass spectrum of 5.0 nanograms of lipopeptide frfom a 3.0 mg/ml fetal bovine serum solution after on-plate enrichment using Bis-F26 treated thin film.

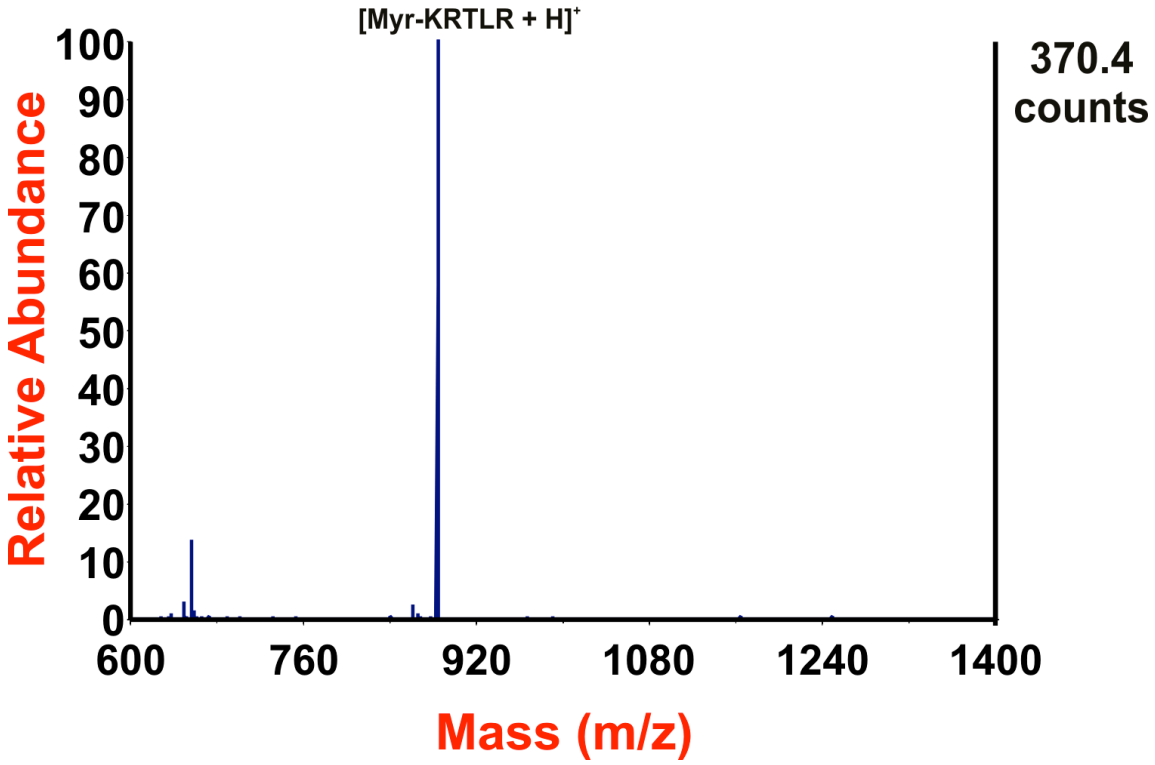

Figure 41. MALDI mass spectrum of 500 picograms of lipopeptide from a 3.0 mg/ml fetal bovine serum solution after on-plate enrichment using Bis-F26 treated thin film.

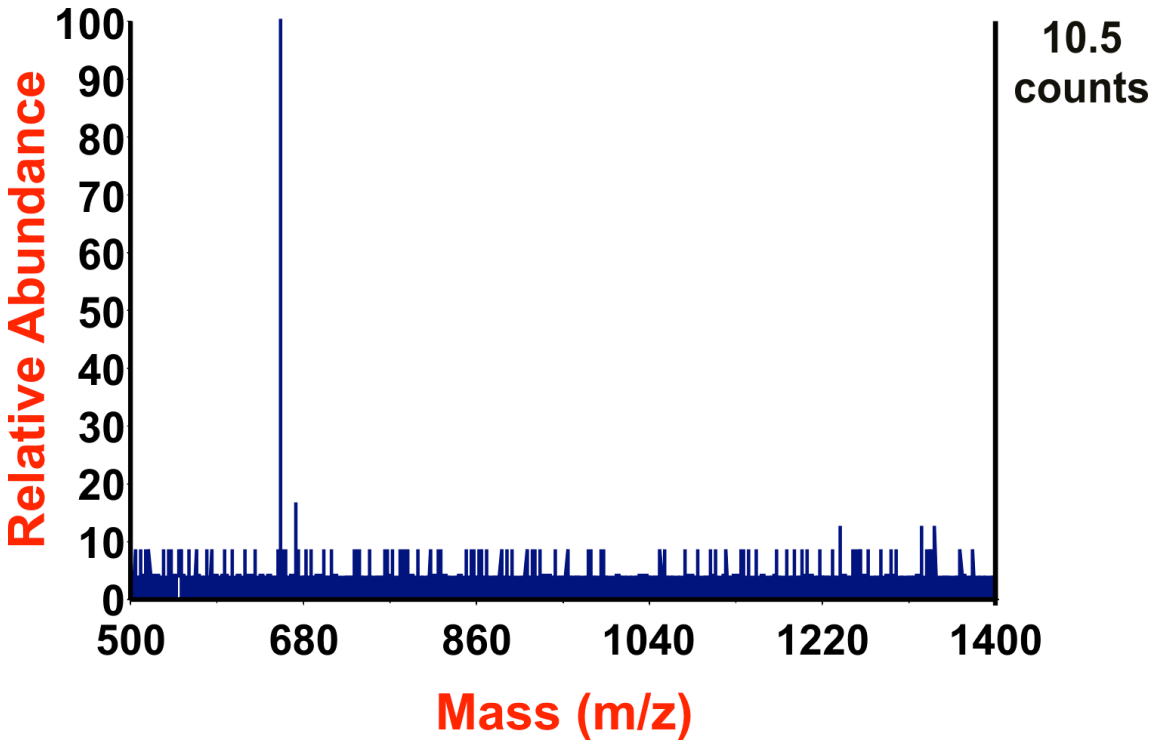

Figure 42. MALDI mass spectrum of the mixture containing 5.0 nanograms of lipopeptide in 3.0 mg/ml fetal bovine serum without on-plate enrichment. The only discernable signal is an unidentified background peak and the target analyte is not present.

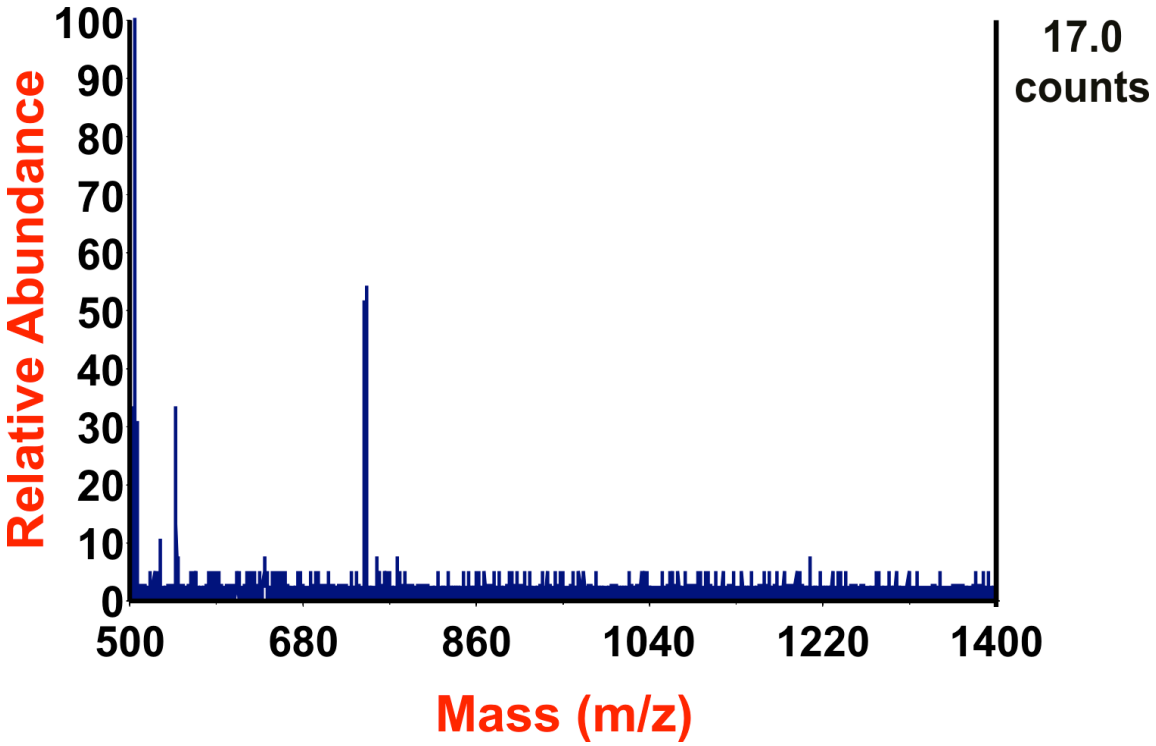

Figure 43. MALDI mass spectrum of a control experiment of attempted on-plate enrichment of 500 picograms of lipopeptide from 3.0 mg/ml fetal bovine serum performed on an untreated film. The presence of the porous film is not sufficient enough to pull the target analyte out of the complex mixture.

Several additional analytes containing hydrophobic amino acid residues were also successfully enriched using Bis-F26 treated thin films. Indolicidin, (ILPWKWPWWPWRR) a cationic antimicrobial peptide and Neuropeptide Y Fragment (3-36) (SKPDNPGEDAPAEDMARYYSALRHYINLITRQRY) are two such examples. **Figures 44** and **45** demonstrate the successful enrichment of 5.0 nanograms of Indolicidin and Neuropeptide Y Fragment (3-36) in 3.0 mg/ml fetal bovine serum, respectively. In each of the individual spectra, the dominant signal corresponds to $[M+H]^+$ for the target analyte and little to no background noise is observed.

These results demonstrate the flexibility offered by surface treatment as a method to incorporate a level of specificity for on-plate capture of low abundance analytes from complex mixtures using the sol-gel derived thin films when combined with traditional MALDI-MS. Although the results presented here are relatively preliminary, they demonstrate an improvement on the detection limit of low abundance analytes in a complex mixture, such as fetal bovine serum in comparison to our previously established method using lipid coated gold nanorods.

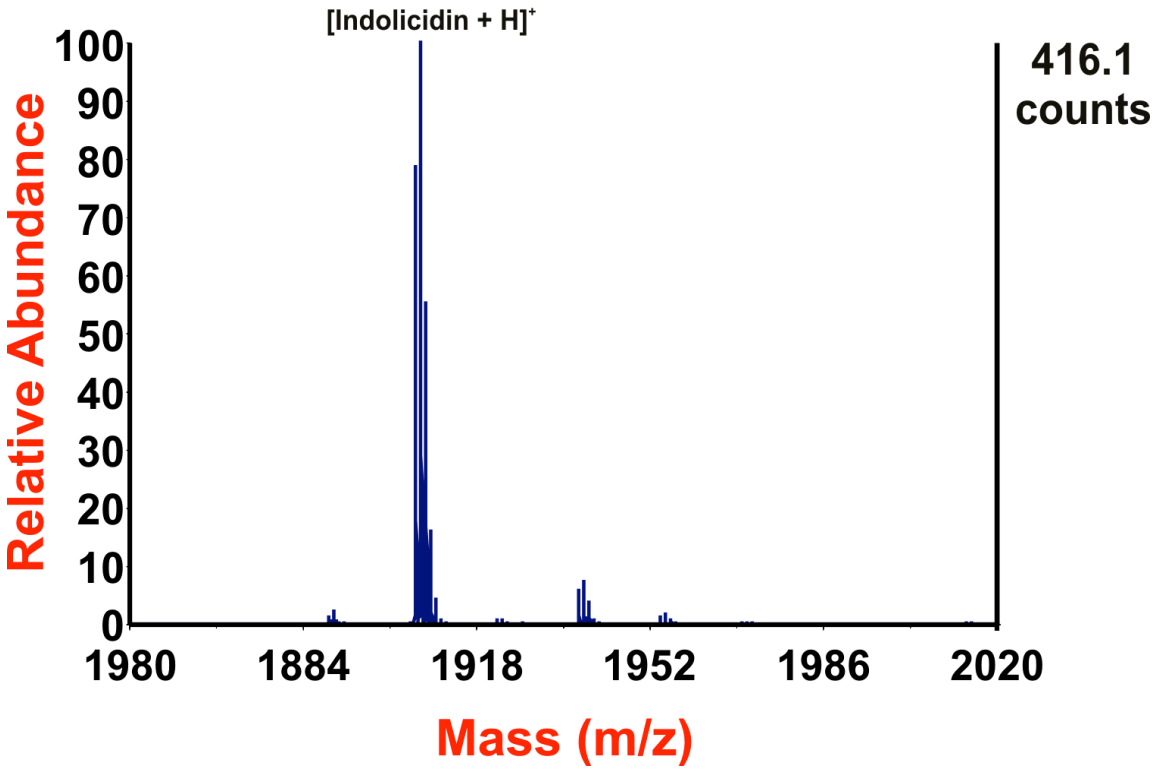

Figure 44. MALDI mass spectrum of 5.0 nanograms of Indolicidin from a 3.0 mg/ml fetal bovine serum solution after on-plate enrichment using a Bis-F26 treated thin film.

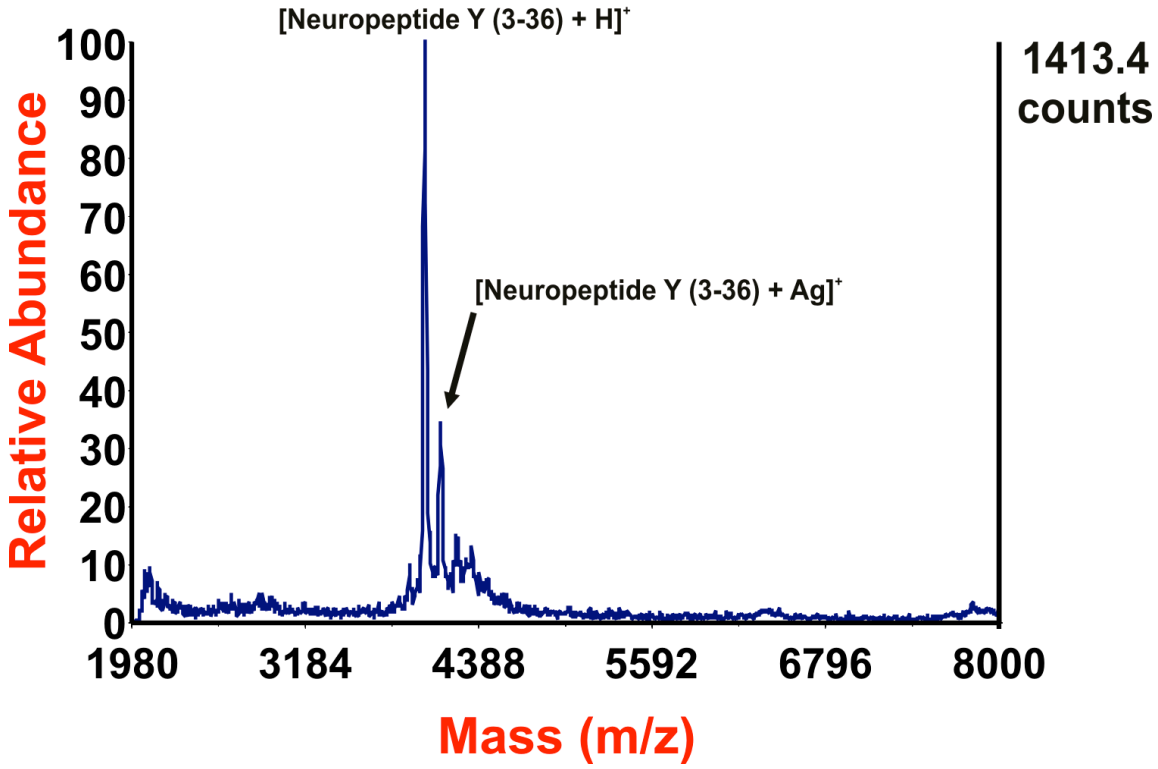

Figure 45. MALDI mass spectrum of 5.0 nanograms of Neuropeptide Y Fragment (3-36) from a 3.0 mg/ml fetal bovine serum solution after on-plate enrichment using a Bis-F26 treated thin film.

After thermal treatment at 700°C, the resulting AgNP thin film has a distinct yellow color **(Figure 46)** which remains unchanged for a period of several months despite being stored under atmospheric conditions. The optical absorption spectrum of the silver doped thin film displays a strong absorption band centered at ~390 nm that is attributed to the surface plasmon resonance (SPR) of the AgNP in the film.[34] Optical absorption of several regions of the films showed minimum variability in the optical properties across the platform **(Figure 47)**. As evident from an overlay of the optical spectra of fresh and aged films shown in **Figure 48**, long storage periods under ambient

conditions did not appear to significantly alter the optical properties of the film. The surface morphology of the thin films was examined by scanning electron microscopy (SEM), revealed the porous nature of the film (1400x magnification) (**Figure 49**) and the presence of AgNP at the surface (20,000x magnification) (**Figure 50**). A The average pore size distribution was determined to be ~650 nm in diameter which remained consistent across individual thin film preparations **(Figure 51)**.

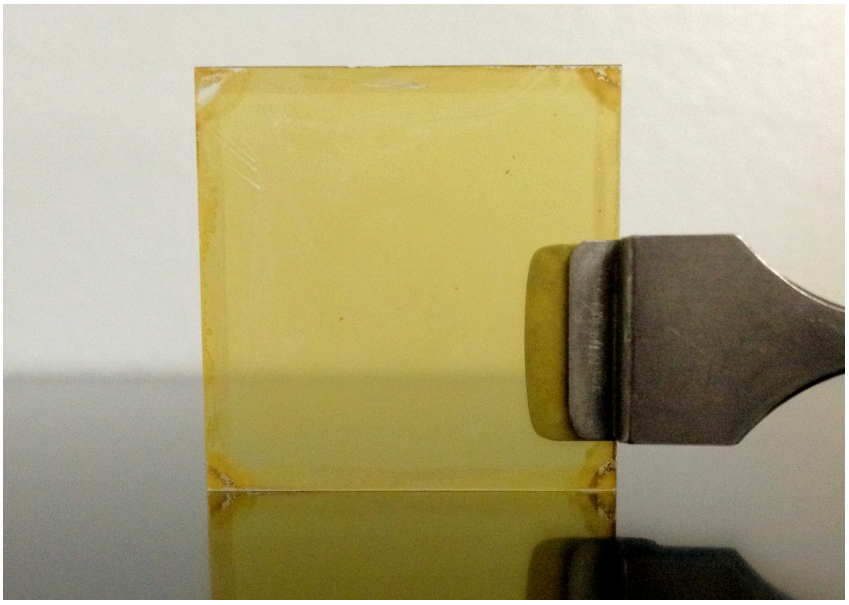

Figure 46. Resulting thin film after spin coating and thermal treatment.

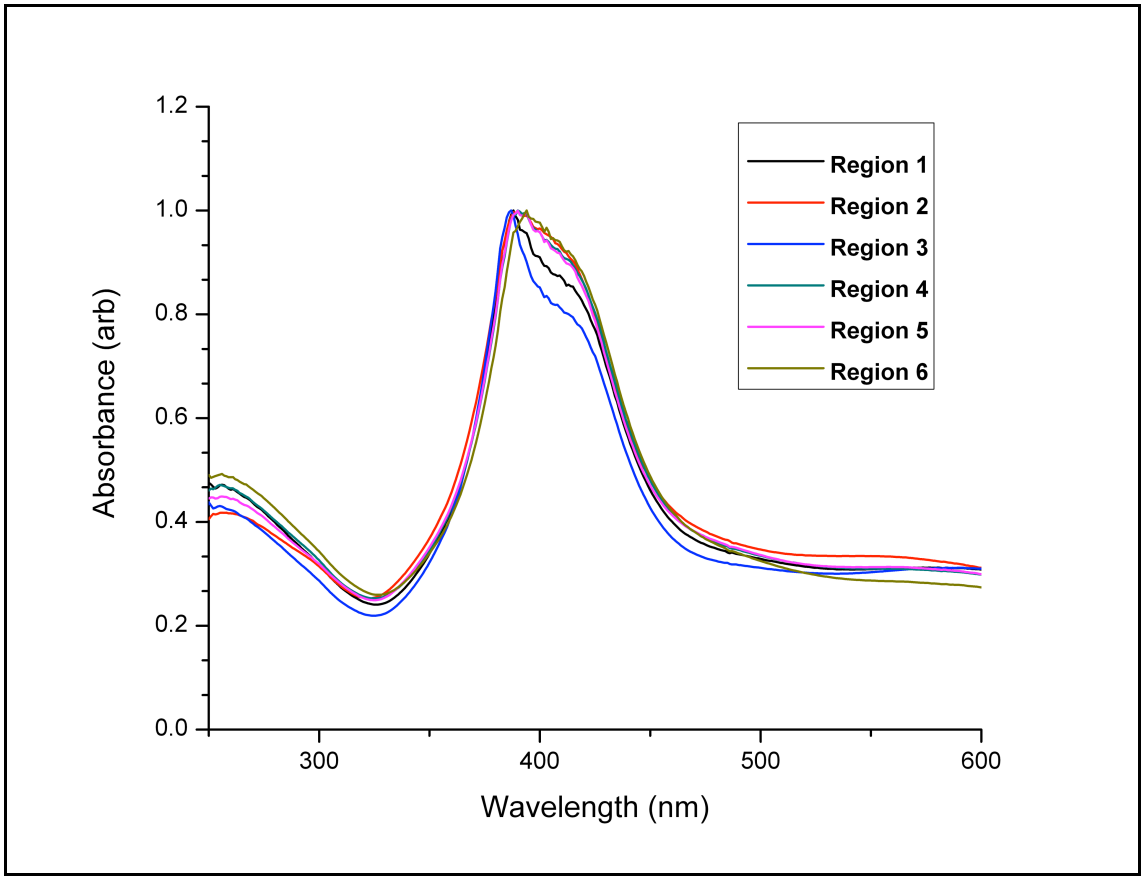

Figure 47. UV-vis of several different regions of a typical thin film prepared by thermally treating at 700°C. The strong surface plasmon band at around 400 nm remains constant across different regions of the film.

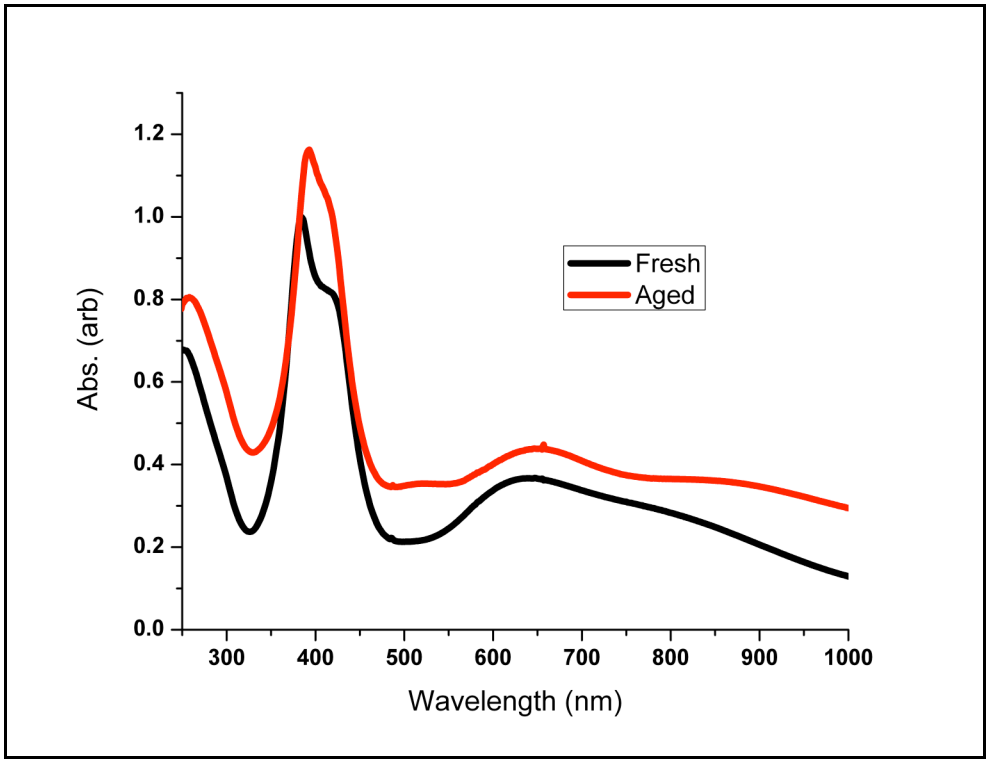

Figure 48. Optical absorption spectra of a (black) fresh and an (red) aged (>1 year) AgNP thin film. Note: the spectrum of the aged film is offset by 0.2 Abs for clarity.

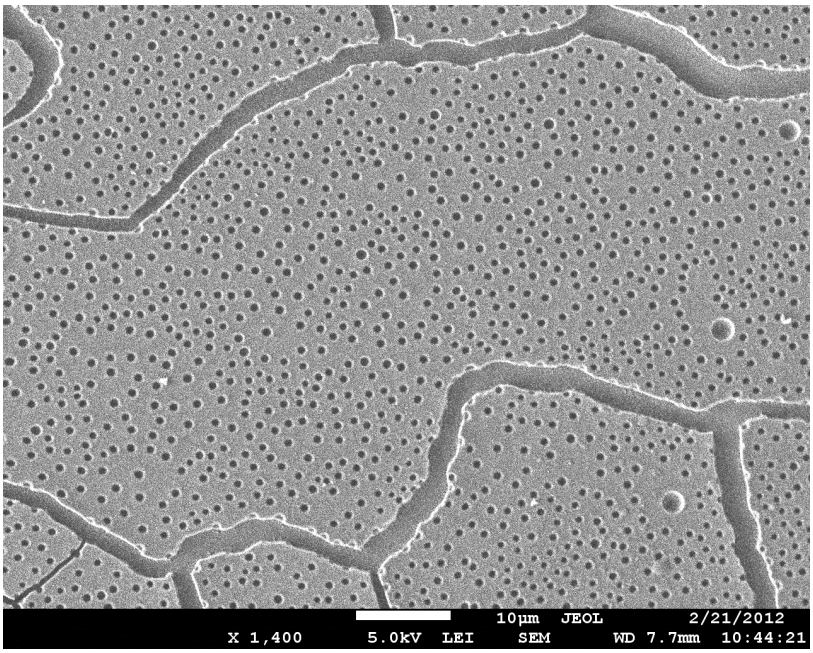

Figure 49. SEM image of thin film surface at 1400x magnification revealing the porous nature of the surface of the thin film.

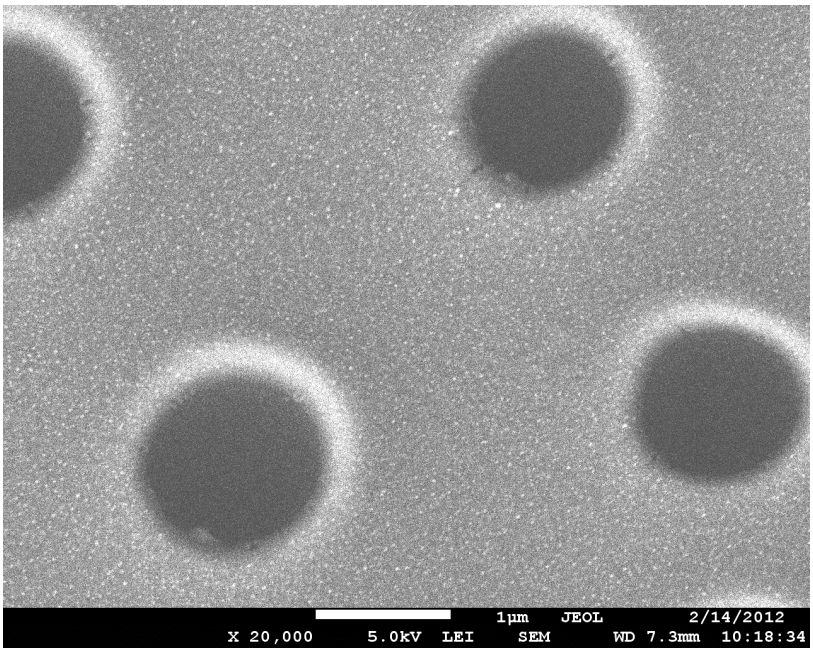

Figure 50. SEM image of thin film surface at 20,000x magnification. The bright spots in the image are AgNPs.

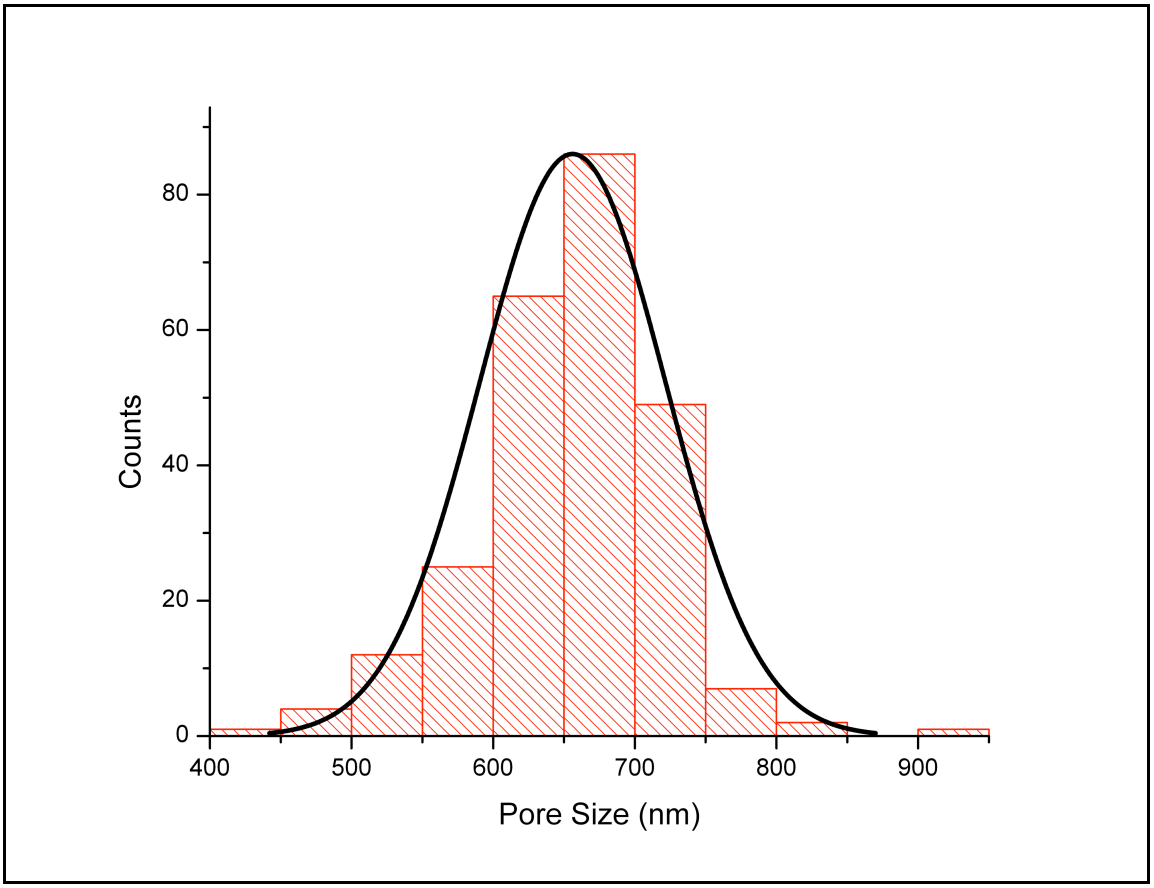

Figure 51. Histogram of the pore sizes for a typical preparation of the AgNP embedded thin film. Average pore size was found to be 656±65.8nm across several individual preparations.

Although the mechanism governing the formation of the AgNPs is not yet entirely understood, there have been several investigations focused on the production and characterization of Ag-doped films utilizing the sol-gel method.[52,55,56,138] In these studies it was discovered that reduction of the Ag^{+} is only achieved at temperatures above 500°C and that lower annealing temperatures do not yield nanoparticles. Epifani et al. suggested that reduction of the Ag^{+} to Ag^{0} is inhibited by the formation of silver complexes and reduction can only be achieved by thermal decomposition of the

complexes. This conclusion was supported by the fact that heating at lower temperatures (300°C) produced no detectable optical absorption corresponding to the SPR band for AgNPs; a similar result was obtained when lower heating temperatures were used in our method of preparation **(Figure 52)**. Previously, Weaver and Hoflund studied the thermal decomposition of Ag_2O by X-ray photoelectron spectroscopy (XPS) and discovered annealing at a temperature of 490°C for 60 minutes was sufficient to reduce the bulk of the Ag_2O sample to Ag metal.[139] In our experiments, the formation of AgNP is further supported by XPS measurements of the films. Ag metal, AgO and Ag_2O powder have been studied extensively by XPS and it has been established that an increase in the oxidation state of silver results in a negative shift of the binding energy of Ag 3d peaks.[139-142] **Figure 53** shows the Ag 3d core-level spectrum of the Ag thin film which exhibits an expected Ag 3d doublet. The peak at a binding energy of 368.2 eV is consistent with the previous assignment of the binding energy for the Ag $3d_{5/2}$ peak from Ag^0at 368.1± 0.1eV.[143] It should be noted that the best signal for the XPS experiments was obtained when the surface of the film was scratched just prior to analysis, leading us to hypothesize that AgNPs are not only at the surface of the film but embedded within the SiO_2 matrix as well.

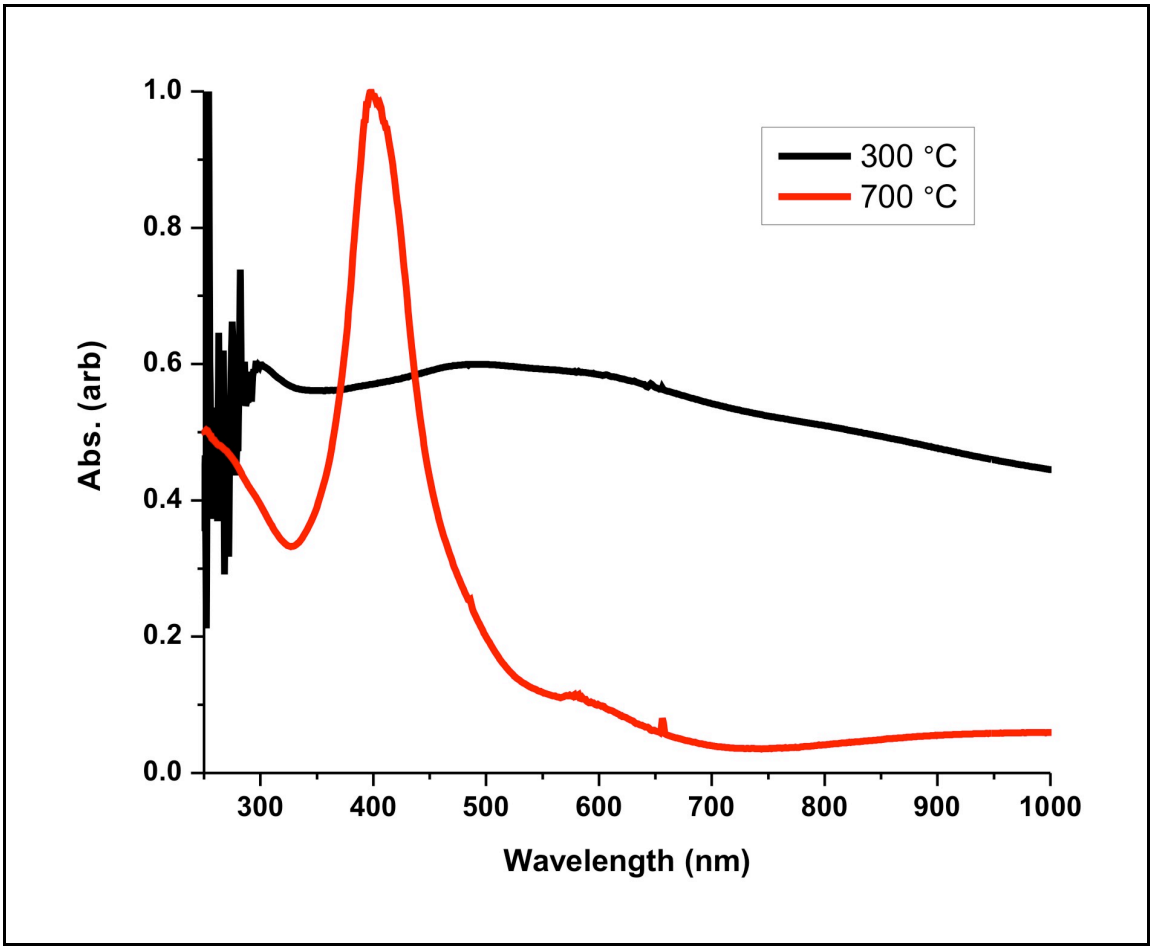

Figure 52. UV-vis of thin film prepared by thermally treating at 300°C (black) and 700°C (red). The absence of the strong surface plasmon band at around 400 nm for the slides treated at 300°C suggests the lack of metallic silver nanoparticles.

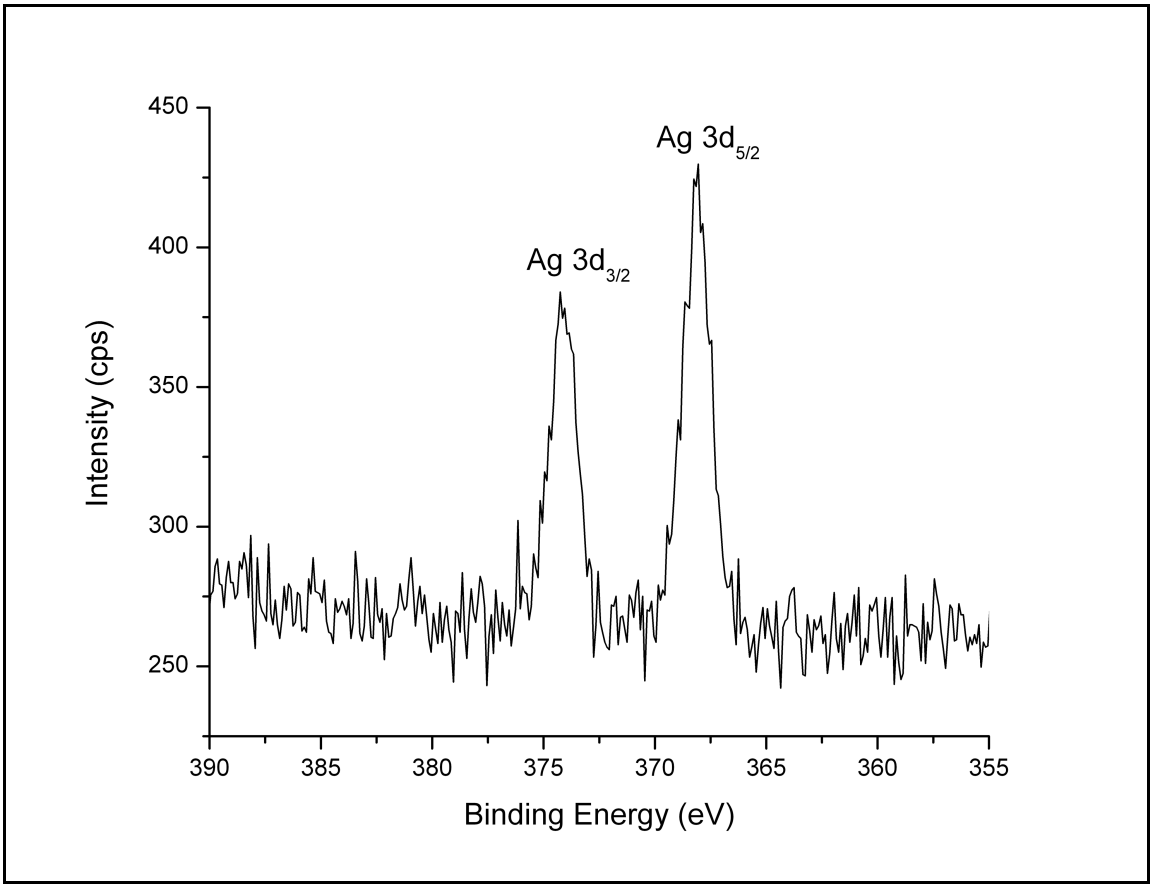

Figure 53. The Ag 3d binding energy XPS spectrum of an AgNP embedded thin film. The resulting peaks indicate that silver exists in the elemental form.

In our method, the thin films were heated to a final temperature of 700°C to ensure the formation of AgNP and the decomposition of residual organics that can complicate the spectra during mass spectrometric analysis. The fact that there are few low mass interference peaks when the surface is interrogated by LDI-MS manifests the decomposition of organics. Additionally, the higher temperature also allows for the

freshly prepared AgNP films to be used without any additional handling steps such as washing or surface treatment after initial preparation.

Conclusions

A porous AgNP impregnated thin film prepared by a sol-gel method is demonstrated as a flexible platform for LDI-MS of analytes of various chemical classes. The AgNP impregnated thin film absorbs incoming photons, resulting in desorption and ionization of analytes, which are observed as Ag^+ adducts. This investigation focuses on the analysis of several non-olefin analytes, specifically peptides and several phospholipids/triglycerides with fully saturated hydrocarbon tails. Possibly of greater interest is the preferential ionization of sterols from vesicles composed primarily of olefinic phosphosphatidylcholines, which offers the possibility of a simplified approach for sterol analysis from mixtures. Moreover, the platform displayed an excellent shelf life and retained optical properties for over a year without compromising LDI-MS function - an appealing quality from a diagnostic standpoint where minimal sample preparation is often required for rapid analysis.

CHAPTER IV

SUMMARY AND CONCLUSIONS

The use of nanomaterials for sensing applications has developed significantly over the past several years owing to the unique optical properties, and the ease of preparation. In this dissertation, we describe the utilization of the longitudinal surface plasmon resonance exhibited by gold nanorods (AuNRs) coupled with surface functionalization to promote laser desorption ionization and mass spectrometric detection of peptides utilizing near-IR wavelength laser pulses. In this investigation, it was also discovered that the hydrophobic nature of the surfactant used for the preparation of the AuNRs could be utilized to enrich low abundance hydrophobic analytes from aqueous solutions. These analytes were concentrated by the AuNRs and subsequently detected using the near-IR laser desorption ionization method previously discussed.

Similarly, an alternative method to stabilize and protect the AuNRs using phospholipids was developed and optimized to enrich not only hydrophobic, but membrane active components from aqueous and complex mixtures. By exploiting the unique optical properties of AuNRs, the successful analyte capture of a membrane active analyte from an aqueous solution by the phospholipid coated AuNRs was also demonstrated. Following the optical detection method, MALDI-MS was further used confirm the presence of the target analytes, whereas before enrichment, they were either previously undetectable or barely discernable against background noise in the spectra.

To further emphasize the utility of the phospholipid coated AuNRs as a versatile platform to enrich and pull down target analytes, it was demonstrated that they were capable of enriching an analyte in low abundance from a complex mixture, fetal bovine serum. Additionally, the AuNRs were capable of withstanding several centrifugation cycles, which was necessary for the removal of excess, unwanted or unbound species which could possibly interfere and complicate the analysis. Most importantly among these experiments, was the clear presence of the target analyte in each of the resulting spectra along with baseline resolution and excellent signal to noise, with few interference peaks.

The development and characterization of a silver nanoparticle based biosensor is also described. Using a silica based sol-gel method, a porous thin film with silver nanoparticles embedded within the structure was able to be produced. This thin film proved to be successful as a matrix-free platform for laser desorption ionization of a number of peptides, triglycerides, and lipids. Additionally, the platform displayed an excellent shelf-life, retaining its ability to produce signal for analytes spotted to the surface despite being left under atmospheric conditions for over one year. Preferential ionization of low abundance sterols from vesicles composed primarily of olefinic phospholipids was also observed, offering the possibility of a simplified approach for sterol analysis from complex mixtures.

Overall, the data presented in this dissertation has provided examples of the efficacy of nanomaterials of different shapes and composition to be utilized as mass spectrometry based biosensors. Several avenues exist for future work involving

phospholipid coated AuNRs. One such example, which was briefly investigated, however, not entirely optimized was the possibility of incorporating different lipids with functional headgroups for capture and pull down of specific side chains on peptides or proteins. Following a similar exchange protocol as outlined in Chapter III, one should be able to prepare phospholipid coated AuNRs and exchange the surface coating by incubating the AuNRs with vesicles composed primarily of the functional lipid headgroup of interest. In fact, preliminary experiments performed using this approach suggests that lipid exchange at the surface of the AuNRs is indeed possible by this method. Following derivatization, the functional AuNRs can be incubated with a mixture or solution under optimum reaction conditions containing a target analyte to produce a complex which can be pulled out of the solution and analyzed. Additionally, by producing and combining different types of functional AuNRs, a multiplex approach for enrichment and pull down of various kinds of analytes from a mixture is also possible.

The flexibility of the sol-gel method for production of thin films with different structural properties also presents an opportunity for future investigations. As noted in the discussion focusing on sol-gel chemistry in Chapter I, by simply changing the ratios of starting materials or the type of catalyst used, one can greatly influence the outcome of the final three dimensional structure of the silica network. Additionally, since most metal precursor salts are miscible with the starting solution, alternative metals can be doped into the solution to develop films containing different metal nanoparticles. Preliminary findings to produce similar silver nanoparticle embedded thin films have found that the production of film with smaller pore size (~100 nm diameter) is possible

by simply doping a surfactant, Tween-20, into the reaction mixture after an allotted time while maintaining other reaction conditions. The use of a thin film with smaller pore size is intriguing from a sample loading perspective, since for a given area, a higher density of pores would result in an increase in surface area and sample loading. A comparative study investigating the influence on the amount of signal produced for a given amount of analyte for smaller pore size versus larger pore size thin films could be undertaken. Alternatively, the treatment of the thin films with hydrophobic coatings for an on-plate enrichment method was briefly mentioned in Chapter IV. Using these surface coatings, and coupling with MALDI-MS, a method for selective enrichment of hydrophobic analytes from complex mixtures was demonstrated. Other surface modifications could feature a silane chemistry approach, which would give the possibility of decorating the surface of the thin films with functional groups that target side chains of peptides and proteins for added selectivity.

REFERENCES

(1) Karas, M.; Hillenkamp, F. *Anal. Chem.* **1988**, *60*, 2299.

(2) Karas, M.; Bahr, U. *Trac-Trends Anal. Chem.* **1990**, *9*, 321.

(3) Strupat, K.; Karas, M.; Hillenkamp, F. *Int. J. Mass Spectrom. Ion Process.* **1991**, *111*, 89.

(4) Cohen, L. H.; Gusev, A. I. *Anal. Bioanal. Chem.* **2002**, *373*, 571.

(5) Karas, M.; Bachmann, D.; Hillenkamp, F. *Anal Chem* **1985**, *57*, 2935.

(6) Karas, M.; Bahr, U.; Ingendoh, A.; Hillenkamp, F. *Angewandte Chemie-International Edition in English* **1989**, *28*, 760.

(7) Peterson, D. S. *Mass Spectrom. Rev.* **2007**, *26*, 19.

(8) Szajli, E.; Feher, T.; Medzihradszky, K. F. *Molecular & Cellular Proteomics* **2008**, *7*, 2410.

(9) Tanaka, K.; Waki, H.; Ido, Y.; Akita, S.; Yoshida, Y.; Yoshida, T. *Rapid Communications in Mass Spectrometry* **1988**, *2*, 151.

(10) Sunner, J.; Dratz, E.; Chen, Y. C. *Anal Chem* **1995**, *67*, 4335.

(11) Shen, Z. X.; Thomas, J. J.; Averbuj, C.; Broo, K. M.; Engelhard, M.; Crowell, J. E.; Finn, M. G.; Siuzdak, G. *Anal. Chem.* **2001**, *73*, 612.

(12) Lewis, W. G.; Shen, Z. X.; Finn, M. G.; Siuzdak, G. *Int. J. Mass Spectrom.* **2003**, *226*, 107.

(13) Thomas, J. J.; Shen, Z. X.; Crowell, J. E.; Finn, M. G.; Siuzdak, G. *Proc. Natl. Acad. Sci. U. S. A.* **2001**, *98*, 4932.

(14) Northen, T. R.; Yanes, O.; Northen, M. T.; Marrinucci, D.; Uritboonthai, W.; Apon, J.; Golledge, S. L.; Nordstrom, A.; Siuzdak, G. *Nature* **2007**, *449*, 1033.

(15) Woo, H. K.; Northen, T. R.; Yanes, O.; Siuzdak, G. *Nat Protoc* **2008**, *3*, 1341.

(16) Castellana, E. T.; Gamez, R. C.; Gomez, M. E.; Russell, D. H. *Langmuir* **2010**, *26*, 6066.

(17) Castellana, E. T.; Gamez, R. C.; Russell, D. H. *Journal of the American Chemical Society* **2011**, *133*, 4182.

(18) Castellana, E. T.; Russell, D. H. *Nano Lett* **2007**, *7*, 3023.

(19) He, P. L.; Shen, L.; Liu, R. Y.; Luo, Z. P.; Li, Z. *Anal Chem* **2011**, *83*, 6988.

(20) Mayer, K. M.; Lee, S.; Liao, H.; Rostro, B. C.; Fuentes, A.; Scully, P. T.; Nehl, C. L.; Hafner, J. H. *Acs Nano* **2008**, *2*, 687.

(21) Huang, H. W.; Tang, C. R.; Zeng, Y. L.; Yu, X. Y.; Liao, B.; Xia, X. D.; Yi, P. G.; Chu, P. K. *Colloids and Surfaces B-Biointerfaces* **2009**, *71*, 96.

(22) Eustis, S.; El-Sayed, M. A. *Chem. Soc. Rev.* **2006**, *35*, 209.

(23) Oyelere, A. K.; Chen, P. C.; Huang, X. H.; El-Sayed, I. H.; El-Sayed, M. A. *Bioconjugate Chem.* **2007**, *18*, 1490.

(24) Chen, J. Y.; Wang, D. L.; Xi, J. F.; Au, L.; Siekkinen, A.; Warsen, A.; Li, Z. Y.; Zhang, H.; Xia, Y. N.; Li, X. D. *Nano Lett* **2007**, *7*, 1318.

(25) Hirsch, L. R.; Stafford, R. J.; Bankson, J. A.; Sershen, S. R.; Rivera, B.; Price, R. E.; Hazle, J. D.; Halas, N. J.; West, J. L. *Proc. Natl. Acad. Sci. U. S. A.* **2003**, *100*, 13549.

(26) Huang, X. H.; El-Sayed, I. H.; Qian, W.; El-Sayed, M. A. *Journal of the American Chemical Society* **2006**, *128*, 2115.

(27) Pissuwan, D.; Valenzuela, S. M.; Killingsworth, M. C.; Xu, X. D.; Cortie, M. B. *J. Nanopart. Res.* **2007**, *9*, 1109.

(28) El-Sayed, M. A. *Accounts Chem Res* **2001**, *34*, 257.

(29) Tong, L.; Zhao, Y.; Huff, T. B.; Hansen, M. N.; Wei, A.; Cheng, J. X. *Adv Mater* **2007**, *19*, 3136.

(30) Stumpo, K. A.; Russell, D. H. *Journal of Physical Chemistry C* **2009**, *113*, 1641.

(31) McLean, J. A.; Stumpo, K. A.; Russell, D. H. *Journal of the American Chemical Society* **2005**, *127*, 5304.

(32) Sherrod, S. D.; Diaz, A. J.; Russell, W. K.; Cremer, P. S.; Russell, D. H. *Anal. Chem.* **2008**, *80*, 6796.

(33) Mie, G. *Ann Phys-Berlin* **1908**, *25*, 377.

(34) Kreibig, U.; Vollmer, M. *Optical Properties of Metal Clusters*; Springer-Verlag: Heidelberg, Germany, 1995.

(35) Gans, R. *Ann Phys-Berlin* **1915**, *47*, 270.

(36) Link, S.; El-Sayed, M. A. *J. Phys. Chem. B* **1999**, *103*, 8410.

(37) Huang, X. H.; Neretina, S.; El-Sayed, M. A. *Adv Mater* **2009**, *21*, 4880.

(38) Link, S.; Mohamed, M. B.; El-Sayed, M. A. *J. Phys. Chem. B* **1999**, *103*, 3073.

(39) Stephens, W. E. *Phys Rev* **1946**, *69*, 691.

(40) Cameron, A. E.; Eggers, D. F. *Rev Sci Instrum* **1948**, *19*, 605.

(41) Wiley, W. C.; Mclaren, I. H. *Rev Sci Instrum* **1955**, *26*, 1150.

(42) Cotter, R. J. *Time-of-flight mass spectrometry : instrumentation and applications in biological research*; American Chemical Society: Washington, DC, 1997.

(43) Juhasz, P.; Roskey, M. T.; Smirnov, I. P.; Haff, L. A.; Vestal, M. L.; Martin, S. A. *Anal Chem* **1996**, *68*, 941.

(44) Vestal, M. L.; Juhasz, P.; Martin, S. A. *Rapid Communications in Mass Spectrometry* **1995**, *9*, 1044.

(45) Brown, R. S.; Lennon, J. J. *Anal Chem* **1995**, *67*, 1998.

(46) Colby, S. M.; Reilly, J. P. *Anal Chem* **1996**, *68*, 1419.

(47) Mamyrin, B. A.; Karataev, V. I.; Shmikk, D. V.; Zagulin, V. A. *Zh Eksp Teor Fiz+* **1973**, *64*, 82.

(48) Mamyrin, B. A. *Int. J. Mass Spectrom. Ion Process.* **1994**, *131*, 1.

(49) Brinker, C. J.; Scherer, G. W. *Sol-gel science : the physics and chemistry of sol-gel processing*; Academic Press: Boston, 1990.

(50) Pierre, A. C. *Introduction to sol-gel processing*; Kluwer Academic Publishers: Boston, 1998.

(51) Bansal, N. P. *J. Am. Ceram. Soc.* **1990**, *73*, 2647.

(52) Epifani, M.; Giannini, C.; Tapfer, L.; Vasanelli, L. *J. Am. Ceram. Soc.* **2000**, *83*, 2385.

(53) Gurav, J. L.; Jung, I. K.; Park, H. H.; Kang, E. S.; Nadargi, D. Y. *J. Nanomater.* **2010**, *2010*, 1.

(54) Pierre, A. C.; Pajonk, G. M. *Chem. Rev.* **2002**, *102*, 4243.

(55) De, G.; Licciulli, A.; Massaro, C.; Tapfer, L.; Catalano, M.; Battaglin, G.; Meneghini, C.; Mazzoldi, P. *J. Non-Cryst. Solids* **1996**, *194*, 225.

(56) Jeon, H. J.; Yi, S. C.; Oh, S. G. *Biomaterials* **2003**, *24*, 4921.

(57) Oldenburg, S. J.; Westcott, S. L.; Averitt, R. D.; Halas, N. J. *Journal of Chemical Physics* **1999**, *111*, 4729.

(58) McFarland, A. D.; Van Duyne, R. P. *Nano Lett* **2003**, *3*, 1057.

(59) Nikoobakht, B.; El-Sayed, M. A. *Journal of Physical Chemistry A* **2003**, *107*, 3372.

(60) Tao, A.; Kim, F.; Hess, C.; Goldberger, J.; He, R. R.; Sun, Y. G.; Xia, Y. N.; Yang, P. D. *Nano Lett* **2003**, *3*, 1229.

(61) Yun, S.; Oh, M. K.; Kim, S. K.; Park, S. *Journal of Physical Chemistry C* **2009**, *113*, 13551.

(62) Chen, J.; Wang, D.; Xi, J.; Au, L.; Siekkinen, A.; Warsen, A.; Li, Z.-Y.; Zhang, H.; Xia, Y.; Li, X. *Nano Lett* **2007**, *7*, 1318.

(63) von Maltzahn, G.; Park, J. H.; Agrawal, A.; Bandaru, N. K.; Das, S. K.; Sailor, M. J.; Bhatia, S. N. *Cancer Res.* **2009**, *69*, 3892.

(64) Wei, J.; Buriak, J. M.; Siuzdak, G. *Nature* **1999**, *399*, 243.

(65) Finkel, N. H.; Prevo, B. G.; Velev, O. D.; He, L. *Anal Chem* **2005**, *77*, 1088.

(66) Go, E. P.; Apon, J. V.; Luo, G.; Saghatelian, A.; Daniels, R. H.; Sahi, V.; Dubrow, R.; Cravatt, B. F.; Vertes, A.; Siuzdak, G. *Anal Chem* **2005**, *77*, 1641.

(67) Mengistu, T. Z.; DeSouza, L.; Morin, S. *Chemical Communications* **2005**, 5659.

(68) Okuno, S.; Arakawa, R.; Okamoto, K.; Matsui, Y.; Seki, S.; Kozawa, T.; Tagawa, S.; Wada, Y. *Anal Chem* **2005**, *77*, 5364.

(69) Chen, Y.; Vertes, A. *Anal Chem* **2006**, *78*, 5835.

(70) Chen, L. C.; Ueda, T.; Sagisaka, M.; Hori, H.; Hiraoka, K. *Journal of Physical Chemistry C* **2007**, *111*, 2409.

(71) Northen, T. R.; Yanes, O.; Northen, M. T.; Marrinucci, D.; Uritboonthai, W.; Apon, J.; Golledge, S. L.; Nordstrom, A.; Siuzdak, G. *Nature* **2007**, *449*, 1033.

(72) Wen, X. J.; Dagan, S.; Wysocki, V. H. *Anal Chem* **2007**, *79*, 434.

(73) Northen, T. R.; Lee, J. C.; Hoang, L.; Raymond, J.; Hwang, D. R.; Yannone, S. M.; Wong, C. H.; Siuzdak, G. *Proc. Natl. Acad. Sci. U. S. A.* **2008**, *105*, 3678.

(74) Qiu, F.; Jiang, D. W.; Ding, Y. B.; Zhu, J.; Huang, L. L. *Angew. Chem.-Int. Edit.* **2008**, *47*, 5009.

(75) Zhu, Z. J.; Ghosh, P. S.; Miranda, O. R.; Vachet, R. W.; Rotello, V. M. *Journal of the American Chemical Society* **2008**, *130*, 14139.

(76) Yu, C. X.; Irudayaraj, J. *Anal Chem* **2007**, *79*, 572.

(77) Alkilany, A. M.; Frey, R. L.; Ferry, J. L.; Murphy, C. J. *Langmuir* **2008**, *24*, 10235.

(78) Murphy, C. J.; Gole, A. M.; Hunyadi, S. E.; Stone, J. W.; Sisco, P. N.; Alkilany, A.; Kinard, B. E.; Hankins, P. *Chemical Communications* **2008**, 544.

(79) Link, S.; Burda, C.; Mohamed, M. B.; Nikoobakht, B.; El-Sayed, M. A. *Journal of Physical Chemistry A* **1999**, *103*, 1165.

(80) Huff, T. B.; Tong, L.; Zhao, Y.; Hansen, M. N.; Cheng, J. X.; Wei, A. *Nanomedicine* **2007**, *2*, 125.

(81) Dickerson, E. B.; Dreaden, E. C.; Huang, X. H.; El-Sayed, I. H.; Chu, H. H.; Pushpanketh, S.; McDonald, J. F.; El-Sayed, M. A. *Cancer Letters* **2008**, *269*, 57.

(82) Huang, Y. F.; Sefah, K.; Bamrungsap, S.; Chang, H. T.; Tan, W. *Langmuir* **2008**, *24*, 11860.

(83) Li, J. L.; Day, D.; Gu, M. *Adv Mater* **2008**, *20*, 3866.

(84) Wijaya, A.; Schaffer, S. B.; Pallares, I. G.; Hamad-Schifferli, K. *Acs Nano* **2008**, *3*, 80.

(85) Kim, C. B.; Yi, D. K.; Kim, P. S. S.; Lee, W.; Kim, M. J. *Journal of Nanoscience and Nanotechnology* **2009**, *9*, 2841.

(86) Lee, S. E.; Liu, G. L.; Kim, F.; Lee, L. P. *Nano Lett* **2009**, *9*, 562.

(87) Kamat, P. V.; Flumiani, M.; Hartland, G. V. *J. Phys. Chem. B* **1998**, *102*, 3123.

(88) Kurita, H.; Takami, A.; Koda, S. *Appl. Phys. Lett.* **1998**, *72*, 789.

(89) Hoheisel, W.; Jungmann, K.; Vollmer, M.; Weidenauer, R.; Trager, F. *Physical Review Letters* **1988**, *60*, 1649.

(90) Lee, I.; Callcott, T. A.; Arakawa, E. T. *Physical Review B* **1993**, *47*, 6661.

(91) Shea, M. J.; Compton, R. N. *Physical Review B* **1993**, *47*, 9967.

(92) Brewer, J.; Rubahn, H. G. *Chemical Physics* **2004**, *303*, 1.

(93) Lee, I.; Callcott, T. A.; Arakawa, E. T. *Anal Chem* **1992**, *64*, 476.

(94) Owega, S.; Lai, E. P. C.; Bawagan, A. D. O. *Anal Chem* **1998**, *70*, 2360.

(95) Owega, S.; Lai, E. P. C.; Mullett, W. M. *Journal of Photochemistry and Photobiology a-Chemistry* **1998**, *119*, 123.

(96) Spencer, M. T.; Furutani, H.; Oldenburg, S. J.; Darlington, T. K.; Prather, K. A. *Journal of Physical Chemistry C* **2008**, *112*, 4083.

(97) Chen, L. C.; Yonehama, J.; Ueda, T.; Hori, H.; Hiraoka, K. *Journal of Mass Spectrometry* **2007**, *42*, 346.

(98) Chen, L. C.; Mori, K.; Hori, H.; Hiraoka, K. *Int. J. Mass Spectrom.* **2009**, *279*, 41.

(99) Nikoobakht, B.; El-Sayed, M. A. *Chemistry of Materials* **2003**, *15*, 1957.

(100) Xiang, Y. J.; Wu, X. C.; Liu, D. F.; Feng, L. L.; Zhang, K.; Chu, W. G.; Zhou, W. Y.; Xie, S. S. *Journal of Physical Chemistry C* **2008**, *112*, 3203.

(101) Chang, S.-S.; Shih, C.-W.; Chen, C.-D.; Lai, W.-C.; Wang, C. R. C. *Langmuir* **1998**, *15*, 701.

(102) Link, S.; Burda, C.; Nikoobakht, B.; El-Sayed, M. A. *The Journal of Physical Chemistry B* **2000**, *104*, 6152.

(103) Horiguchi, Y.; Honda, K.; Kato, Y.; Nakashima, N.; Niidome, Y. *Langmuir* **2008**, *24*, 12026.

(104) Jain, P. K.; Huang, X. H.; El-Sayed, I. H.; El-Sayed, M. A. *Accounts Chem Res* **2008**, *41*, 1578.

(105) Murphy, C. J.; San, T. K.; Gole, A. M.; Orendorff, C. J.; Gao, J. X.; Gou, L.; Hunyadi, S. E.; Li, T. *J. Phys. Chem. B* **2005**, *109*, 13857.

(106) Faccenda, A.; Bonham, C. A.; Vacratsis, P. O.; Zhang, X.; Mutus, B. *Journal of the American Chemical Society* **2010**, *132*, 11392.

(107) West, J. L.; Halas, N. J. *Annu Rev Biomed Eng* **2003**, *5*, 285.

(108) Allen, T. M.; Cullis, P. R. *Science* **2004**, *303*, 1818.

(109) Garcia-Reyes, J. F.; Gilbert-Lopez, B.; Molina-Diaz, A.; Fernandez-Alba, A. R. *Anal Chem* **2008**, *80*, 8966.

(110) Quehenberger, O.; Armando, A. M.; Brown, A. H.; Milne, S. B.; Myers, D. S.; Merrill, A. H.; Bandyopadhyay, S.; Jones, K. N.; Kelly, S.; Shaner, R. L.; Sullards, C. M.; Wang, E.; Murphy, R. C.; Barkley, R. M.; Leiker, T. J.; Raetz, C. R.; Guan, Z.; Laird, G. M.; Six, D. A.; Russell, D. W.; McDonald, J. G.; Subramaniam, S.; Fahy, E.; Dennis, E. A. *J Lipid Res* **2010**, *51*, 3299.

(111) Wenk, M. R. *Nat Rev Drug Discov* **2005**, *4*, 594.

(112) Fernandis, A. Z.; Wenk, M. R. *Journal of Chromatography B-Analytical Technologies in the Biomedical and Life Sciences* **2009**, *877*, 2830.

(113) Conrads, T. P.; Hood, B. L.; Veenstra, T. D. *Biotechniques* **2006**, *40*, 799.

(114) Marinakos, S. M.; Chen, S. H.; Chilkoti, A. *Anal Chem* **2007**, *79*, 5278.

(115) Huang, H.; He, C. C.; Zeng, Y. L.; Xia, X. D.; Yu, X. Y.; Yi, P. G.; Chen, Z. *Biosensors & Bioelectronics* **2009**, *24*, 2255.

(116) Durr, N. J.; Larson, T.; Smith, D. K.; Korgel, B. A.; Sokolov, K.; Ben-Yakar, A. *Nano Lett* **2007**, *7*, 941.

(117) Kuo, T. R.; Hovhannisyan, V. A.; Chao, Y. C.; Chao, S. L.; Chiang, S. J.; Lin, S. J.; Dong, C. Y.; Chen, C. C. *Journal of the American Chemical Society* **2010**, *132*, 14163.

(118) Lee, S. E.; Sasaki, D. Y.; Perroud, T. D.; Yoo, D.; Patel, K. D.; Lee, L. P. *Journal of the American Chemical Society* **2009**, *131*, 14066.

(119) Salem, A. K.; Searson, P. C.; Leong, K. W. *Nat Mater* **2003**, *2*, 668.

(120) Takahashi, H.; Niidome, Y.; Yamada, S. *Chemical Communications* **2005**, 2247.

(121) Orendorff, C. J.; Alam, T. M.; Sasaki, D. Y.; Bunker, B. C.; Voigt, J. A. *Acs Nano* **2009**, *3*, 971.

(122) Nakashima, H.; Furukawa, K.; Kashimura, Y.; Torimitsu, K. *Langmuir* **2008**, *24*, 5654.

(123) Takahashi, H.; Niidome, Y.; Niidome, T.; Kaneko, K.; Kawasaki, H.; Yamada, S. *Langmuir* **2006**, *22*, 2.

(124) Pierce, K. L.; Premont, R. T.; Lefkowitz, R. J. *Nat Rev Mol Cell Bio* **2002**, *3*, 639.

(125) Kenakin, T. P. *Pharmacol Rev* **1984**, *36*, 165.

(126) Sato, H.; Felix, J. B. *Bba-Biomembranes* **2006**, *1758*, 1245.

(127) Bolard, J.; Legrand, P.; Heitz, F.; Cybulska, B. *Biochemistry-Us* **1991**, *30*, 5707.

(128) Cohen, B. E. *Biochim Biophys Acta* **1992**, *1108*, 49.

(129) Wei, F.; Patel, P.; Liao, W.; Chaudhry, K.; Zhang, L.; Arellano-Garcia, M.; Hu, S.; Elashoff, D.; Zhou, H.; Shukla, S.; Shah, F.; Ho, C. M.; Wong, D. T. *Clinical Cancer Research* **2009**, *15*, 4446.

(130) Levin, C. S.; Kundu, J.; Janesko, B. G.; Scuseria, G. E.; Raphael, R. M.; Halas, N. J. *J. Phys. Chem. B* **2008**, *112*, 14168.

(131) Ostman, P.; Pakarinen, J. M. H.; Vainiotalo, P.; Franssila, S.; Kostiainen, R.; Kotiaho, T. *Rapid Communications in Mass Spectrometry* **2006**, *20*, 3669.

(132) Laughlin, J. B.; Cassady, C. J.; Cox, J. A. *Rapid Communications in Mass Spectrometry* **1997**, *11*, 1505.

(133) Lin, Y. S.; Chen, Y. C. *Anal. Chem.* **2002**, *74*, 5793.

(134) Chen, W. Y.; Chen, Y. C. *Anal. Chem.* **2003**, *75*, 4223.

(135) Chen, C. T.; Chen, Y. C. *Anal. Chem.* **2004**, *76*, 1453.

(136) Moulder, J. F. S., W. F.; Sobol, P. E.; Bomben, K. D. *Handbook of X-ray Photoelectron Spectroscopy*; Perkin-Elmer Corp: Eden Prarie, MN, 1992.

(137) Dewar, J. S. *Bull. Soc. Chim. Fr.* **1951**, *18*, C71.

(138) Mennig, M.; Schmitt, M.; Schmidt, H. *J. Sol-Gel Sci. Technol.* **1997**, *8*, 1035.

(139) Weaver, J. F.; Hoflund, G. B. *Chemistry of Materials* **1994**, *6*, 1693.

(140) Weaver, J. F.; Hoflund, G. B. *Journal of Physical Chemistry* **1994**, *98*, 8519.

(141) Kaspar, T. C.; Droubay, T.; Chambers, S. A.; Bagus, P. S. *Journal of Physical Chemistry C* **2010**, *114*, 21562.

(142) Hoflund, G. B.; Hazos, Z. F.; Salaita, G. N. *Physical Review B* **2000**, *62*, 11126.

(143) Schon, G. *Acta Chemica Scandinavica* **1973**, *27*, 2623.